fMRI-compatible Robotic Wrist Rehabilitation Manipulandum:

Design, Prototyping, and Implementation

By

Mohsen Khajoee

A Thesis submitted to the Faculty of Graduate Studies in

partial fulfillment of the requirements for the degree of

Master of Science

Department of Mechanical Engineering

Price Faculty of Engineering

University of Manitoba

Winnipeg, Manitoba, Canada

Abstract

Neurological rehabilitation is crucial for those with stroke or spinal cord injuries. These conditions often lead to upper extremity motor impairments. Such impairments make rehabilitation necessary for daily activities. Robotic rehabilitation devices come with engaging interfaces, showing promise in sustaining patient engagement. They offer encouragement for addressing upper extremity motor challenges.

The contributions of this thesis lie in developing an MRI-compatible three-degree-of-freedom (3-DOF) robotic manipulandum, designed for enhancing neurological rehabilitation exercises that focus on the wrist and forearm. Seamlessly integrated with an existing rehabilitation interactive computer game, the robotic rehabilitation device can dynamically provide assistance or resistance based on the control mode during the game play.

This robotic device prioritizes compatibility with functional magnetic resonance imaging (fMRI) as a core feature. fMRI enables brain scanning to provide insights into brain activity during rehabilitation exercises and potentially transform rehabilitation strategies. The device's 3D-printed mechanism, special sensors, and pneumatic actuators ensure MRI compatibility.

The developed robotic device underwent trial runs by ten healthy subjects to demonstrate its viability and identify potential areas for improvement, to enhance its effectiveness and fulfil its purpose more effectively in the future. The findings highlighted that two assistance modes notably enhanced user performance, whereas two resistance modes posed significant challenges. This work paves the way for practical deployment in real-world neurological rehabilitation scenarios, offering personalized and effective strategies for sustained patient rehabilitation.

Acknowledgments

First and foremost, I would like to thank Prof. Nariman Sepehri, my advisor, for his guidance and support throughout this thesis, Prof. Tony Szturm as well as Prof. Witold Kinsner. Their invaluable advice, assistance, patience, and knowledge were essential in my endeavors in undertaking my research. I would have not been able to complete it without their help.

Furthermore, my gratitude extends to Dr. Ehsan Jalayeri for his invaluable assistance in addressing any challenges that arose in the lab. I would also like to express my appreciation to Narges Ghobadi, Dr. Soleiman Hosseinpour, Michael Olynyk and the entire team at the Fluid Power and Telerobotics Research Laboratory for their unwavering support during my master's journey.

Finally, I am deeply thankful to my family whose encouragement served as a motivation whenever I felt overwhelmed. I am truly thankful to all those who played a role in this endeavor.

Table of Contents

LIST OF FIGURES

LIST OF TABLES

I. INTRODUCTION

1.1 Motivation

Many individuals encounter the need for neurological rehabilitation at different life stages, arising from conditions like strokes, spinal cord injury or developmental challenges. The aging population's increased vulnerability to such conditions raises concerns about the growing demand for neurological rehabilitation services [1]. Upper extremity motor impairment, a common outcome of neurological damage, affects both adults and children, impacting daily activities such as eating and leisure pursuits [2] [3]. Although substantial recovery often occurs within six months post-incident [4], the prolonged and challenging nature of neurological rehabilitation remains a significant obstacle.

Enriched rehabilitative exercises, incorporating interactive game activities with a robotically enhanced user interface, have shown a promise in promoting long-term engagement and yielding more effective results [5] [6] [7]. The success of rehabilitation hinges on consistent patient engagement. Traditional approaches often involve repetitive hand motions. Although effective to some extent [8], they may lack the necessary mental engagement for sustained participation.

It is essential to explore the integration of an MRI-compatibility of final products for functional magnetic resonance imaging (fMRI). The fMRI compatibility allows for a non-invasive exploration of engaged neural mechanisms during rehabilitation exercises. Therefore, clinicians and researchers can gain a real-time window into the brain's response to interactive activities and robotically assisted movements [9]. This dual-purpose approach not only targets the physical aspects of recovery, but also opens avenues for understanding the neural mechanisms involved, potentially revolutionizing neurological rehabilitation strategies.

1.2 Objectives

The primary objective of this thesis is to develop a three-degree-of-freedom (3-DOF) robotic manipulandum specifically designed for wrist and forearm movements. This

manipulandum is to be integrated with an existing rehabilitation interactive computer game [10] while ensuring compatibility with functional magnetic resonance imaging (fMRI).

Expanding upon this development, the intention is to broaden the utilization of this device and its accompanying computer game for neurological rehabilitative assessments and exercises. The robotic devices developed within this scope are expected to possess certain essential properties:

- Full compatibility with MRI scans without the use of electrical wires or circuits.
- Adaptability to the user's impairment or skill level, accommodating both digital adjustments through a computer game and physical interaction through different assistive and resistive control modes as well as passive mode.
- Accessibility for individuals with right- or left-hand dominance.
- Practical application or relevance to everyday life skills.
- Offer an enjoyable and engaging experience while also presenting a suitable challenge to the user.
- Ability to generate consistent and comparable patient data for analysis.

The ultimate goal of the project which this thesis forms a part, is the practical deployment of this newly developed manipulandum in real-world neurological rehabilitation scenarios.

1.3 Thesis Layout

Chapter 1 introduces the research background of this thesis. Chapter 2 reviews related concepts and topics, including current robotic rehabilitation equipment. Chapter 3 details the design and development of the robotic manipulandum from scratch as well as motion and force analysis. A detailed explanation of the rehabilitation software game as well as the features integrated into the computer game to provide real-time feedback from the game are covered in Chapter 4. This chapter presents the developed game interface, for use with the robotic manipulandum as well. Chapter 5 begins by outlining the test procedure of pilot studies, then presents both quantitative and qualitative evaluations: an analysis of the results is conducted and discussed and the feedback provided by test participants is considered. Chapter 6 provides conclusions derived from the project and outlines potential future improvements.

II. LITERATURE REVIEW

2.1 MRI-compatibility

MRI compatible devices are challenging to develop because there are strict limits to the materials, sensing and actuation requirement suited for use within an MRI room [11]. According to the ASTM F2503-20 standard [12], medical equipment can be classified as "MR unsafe", "MR conditional" or "MR safe". An "MR safe" device must be constructed entirely of materials that are non-metallic, non-magnetic, and non-conductive as determined solely by its material decomposition [13]. Moreover, the device should fulfill bidirectional compatibility to be suited for use in MRI environment, which means it should not generate any additional magnetic fields or radio frequency signals and neither should the device be affected by the strong magnetic field in an MRI room [11]. The following requirements must, therefore, be met by a system or device to be considered “MRI-compatible”. Firstly, safety must be assured for the system or device used in an MRI environment. Secondly, a high level of image quality must be maintained. Lastly, the electric and magnetic fields of the scanner should not affect the system or device [14]. Therefore, ferromagnetic materials are strictly prohibited because of the magnetic forces exerted on them.

Non-ferromagnetic metals, such as aluminum, titanium, brass, and composite materials, are acceptable alternatives [14] [11]. Similarly, any type of electric circuit or conductive material should be avoided, since the eddy currents developing on such materials cause noticeable noise, which manifests itself as shading, spatial distortion, and false positive activation artifacts in the resulting images. Aside from the material constraints, MRI machines also have a very narrow bore that creates dimension constraints. Conductive materials and electric currents are not suitable for the MRI room and could even pose danger to the patient, so an electromagnetic motor cannot be used as an actuator. Alternatively, MRI-compatible devices can use pneumatic, hydraulic, harmonic piezoelectric and non-harmonic piezoelectric actuators [15]. Hydraulic and pneumatic actuation systems tend to be intrinsically MRI compatible [14].

As the medium of transmission, pneumatic systems make use of pressurized air, which is readily available in hospitals and can deliver large distances without losing much pressure. Pneumatic actuators are suitable for systems that need MRI compatibility, nuclear power plants and systems where small, lightweight actuators are desirable, or pressurized air is already available. Dust, dirt, or magnetic fields will not affect the pneumatic drive's performance, even

under extreme operating conditions like extreme temperatures. Other advantages of pneumatic actuators are their low cost, low weight-power ratio, compact size, easy maintenance, and reliable operation. That is why pneumatic actuators are widely used in many applications including in MRI room [16].

2.2 Neurological Rehabilitation

According to the World Health Organization, rehabilitation is “a set of interventions needed when a person is experiencing or is likely to experience limitations in everyday functioning due to ageing or a health condition, including chronic diseases or disorders, injuries or traumas” [17]. Johns Hopkins Medical Organization describes Neurological rehabilitation as “a doctor-supervised program designed for people with diseases, injury or disorders of the nervous system with the overall goal to improve function, reduce symptoms and improve the well-being of the patient” [18]. In other words, neurological rehabilitation is a facet of medical rehabilitation that specifically concentrates on the brain rather than focusing on the muscles and skeletal structures of the body. Due to the complexity of brain functions, achieving optimal results requires a comprehensive approach that involves various aspects of medical care and therapy [19]. Some treatments involve undergoing invasive brain surgery or utilizing direct electrical neurological stimulation [20]. However, it is important to note that while this approach may be effective, it is generally not recommended to directly intervene and treat neurological issues. These techniques are considered high-risk treatment options and are typically reserved as a last resort, only implemented when all other alternatives prove ineffective or are impractical to implement.

Fortunately, there is a well-established approach for interacting with the neurological functions of the brain that does not require surgical intervention and is a part of everyone's daily experiences. This approach involves an individual's engagement and five senses used to perceive reality. The brain of an individual undergoes continuous changes and adaptations in response to the various stimuli encountered every day, both in childhood and adulthood, a phenomenon commonly referred to as neuroplasticity [21].

2.3 The Need for Rehabilitation Devices

A leading factor in physical impairment, stroke, inflicts neurological injuries that result in various physical disabilities like hemiplegia, paraplegia, paresis, speech impairments, limited physical capabilities, and challenges in grasping or holding objects [22]. Based on data from 1990

to 2019, stroke ranks as the second leading cause of death worldwide and the third leading cause of both death and disability on a global scale [23]. Stroke stands as a major contributor to upper extremity impairment, accompanied by other prevalent causes like trauma, spinal cord injuries, and neurological disorders. The crucial role played by the upper extremities in daily activities underscores the importance of optimal recovery for individuals with disabilities, enabling them to return to their regular lives. The rehabilitation process plays a pivotal role in expediting recovery for those dealing with upper extremity impairments. However, as the population of physically disabled individuals continues to surge, providing extensive physical therapy to this expanding group becomes increasingly challenging, especially with limited resources [24].

Traditional physical therapy, while effective, demands a considerable amount of time. Individual patients require extensive hours of one-on-one interaction with therapists to achieve complete recovery. Recognizing the need for innovative solutions, robot-assisted physical therapy has emerged as a progressive approach to address the rehabilitation needs of the growing population of individuals with upper extremity impairments. This technological advancement offers a fresh and promising way to provide effective and efficient physical therapy to a larger number of people facing challenges related to upper extremity impairment [24].

Furthermore, continuous advancements in techniques and cutting-edge equipment are consistently emerging to enhance the support provided to individuals navigating the challenges of neurological rehabilitation. Various strategies aimed at refining rehabilitative programs place a significant emphasis on the integration of computer-based assistance. An examination of ongoing developments in stroke rehabilitation, specifically in the context of hand function recovery, revealed that the incorporation of diverse forms of computer-based assistance, such as gaming, haptics, robotics and virtual reality, resulted in an overall enhancement of the effectiveness of exercises and the success of the recovery process [25]. This pattern is further supported and validated by additional studies exploring rehabilitation methods, highlighting robotics and gaming as potential effective approaches for rehabilitation [26]. Researchers are currently exploring ways to advance these techniques, aiming to enhance immersion and patient performance. This involves the development of devices as well as augmented virtual reality programs that integrate three-dimensional haptics for an even more comprehensive rehabilitation experience [27]. At the same time, robotic devices bring a new level of accuracy to gathering biomechanical data, giving

clinicians a consistent and measurable way to assess patients' impairments. This means that the information collected is more precise, offering a standardized approach to evaluating patients. By using robotic devices, clinicians can obtain detailed data that not only improve the accuracy of assessments but also, provide a more thorough understanding of patients' biomechanical conditions. This enhances the diagnostic process and creates opportunities for personalized and targeted interventions, pushing forward the field of biomechanical assessment in clinical practice [28].

Computer games play a crucial role in rehabilitation by providing an engaging platform that demands precise, accurate movements, which are essential for effective therapy. The interactive nature of these games ensures that patients remain motivated and can practice complex tasks in a controlled environment, enhancing motor skills and cognitive functions. This level of contact and precision in movement aids in faster recovery and better adaptation of rehabilitation exercises in daily life activities [29].

2.4 Current Rehabilitation Robots

Rehabilitation robots for human upper extremity can be categorized into two types: exoskeletons and end-effectors. Robotic exoskeletons emulate the structure of biological exoskeletons found in arthropods such as insects, spiders, and crabs. In the context of upper limb rehabilitation, exoskeletons feature a mechanical framework mirroring the anatomy of the human arm, with multiple connections to the user's upper extremity. These devices are designed to replicate the natural motions of the human arm's joints, allowing for targeted interaction with specific upper limb joints [24].

On the other hand, end-effector-based upper extremity rehabilitation robots incorporate an end-effector at the end of the serial link manipulator, engaging directly with the human upper extremity. Typically attached to the hand, wrist, or fingers, the end-effector moves in coordination with the attached part of the human arm, influencing the movement of other segments [24]. Some of the latest advancements in rehabilitation robots for the wrist and forearm movements are briefly described here.

WristBot, developed at the Italian Institute of Technology in Genoa [28], Italy, is a rehabilitation device specifically designed for the wrist and forearm. Featuring an impedance-

controlled manipulator powered by brushless motors, it can provide assistance or enable passive movement of the human wrist along three degrees of freedom. This encompasses six distinct movements, including flexion/extension (FE), abduction/adduction (AA), and pronation/supination (PS) as illustrated in Figure 1.

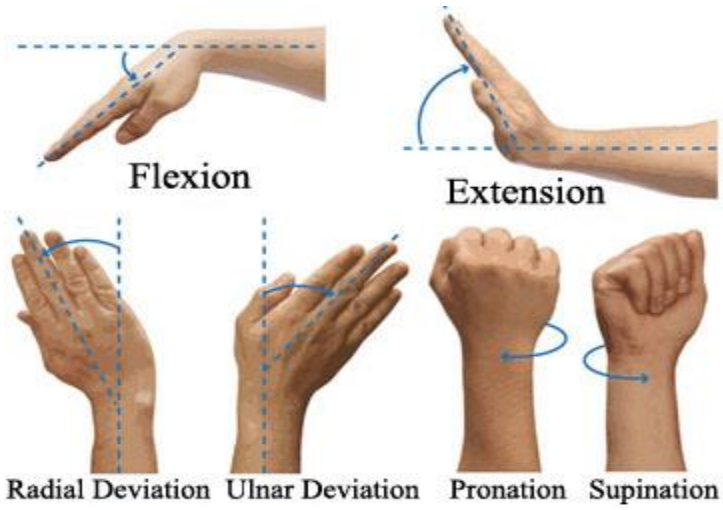

Figure 1: Wrist and forearm movements [30].

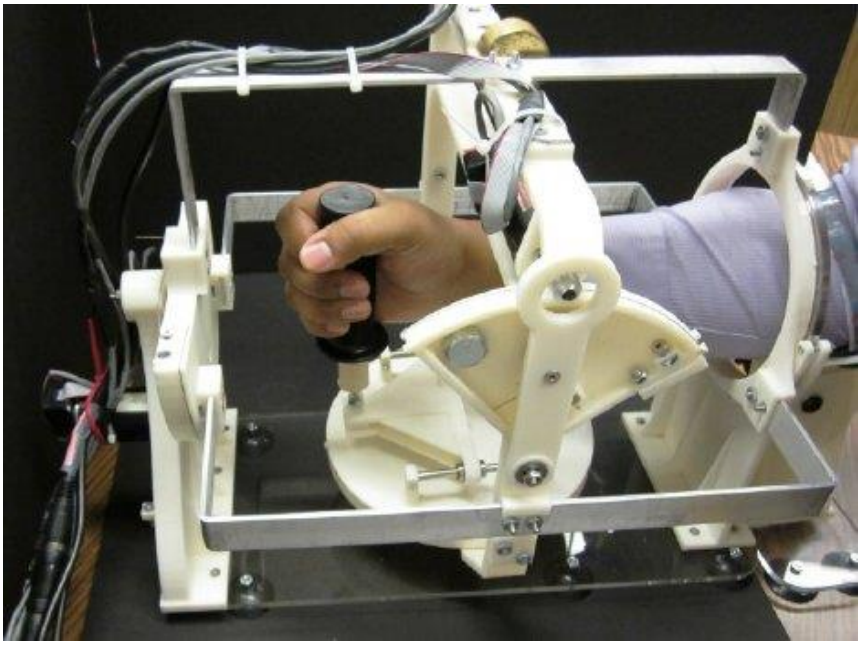

Figure 2: Wrist Gimbal: a forearm and wrist exoskeleton for stroke rehabilitation [31].

Wrist Gimbal [31] (see Figure 2) is crafted for post-stroke upper extremity rehabilitation. It comprises a serial kinematic structure with three revolute joints that facilitate forearm rotation,

wrist flexion/extension, and wrist abduction/adduction. Tailored for forearm and wrist rehabilitation, this three-DOF exoskeleton includes active DOFs aligned with pronation/supination, flexion/extension, and adduction/abduction joints. Additionally, two main control strategies, passive and resistive, have been integrated to enhance rehabilitation efforts.

OpenWrist (see Figure 3) is a forearm and wrist exoskeleton designed for pathology-agnostic rehabilitation in a standalone configuration. Utilizing a serial RRR mechanism, it facilitates manipulation of the user's wrist and forearm. Each actuated degree of freedom (DOF) is driven by a brushed DC motor. To gain a deeper insight into the rehabilitation process, this device enables a comparison between the wrist movement paths, as captured by the robot's encoders, and the motion tracked through passive markers [32].

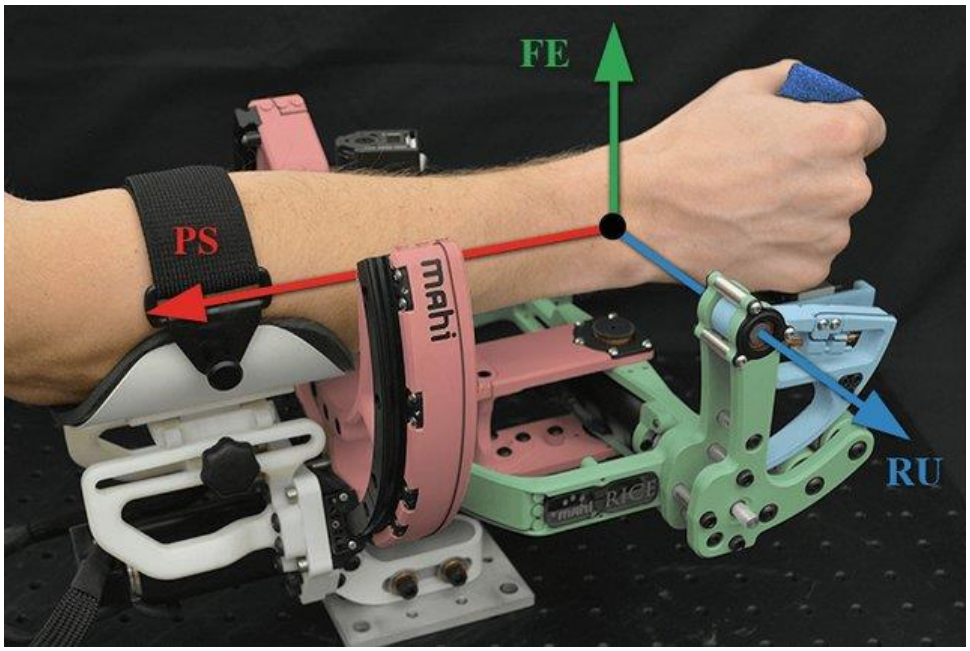

Figure 3: OpenWrist exoskeleton for pathology agnostic rehabilitation [32].

The Universal Haptic Drive is an end-effector-based rehabilitation robot featuring two modes: "ARM" mode and "WRIST" mode [33]. The transition between modes involves locking or unlocking a passive universal joint. The mechanical design includes an actuated bar connected to a spherical joint, which is fastened to a base plate. Serially coupled elements include a sliding mechanism for linear movement, a force sensor, a passive 2-degree-of-freedom universal joint that can be mechanically locked, and a handlebar. In "WRIST" mode, with the universal joint unlocked, the handlebar gains two degrees of freedom, allowing pronation/supination of the forearm and

flexion/extension. The robot employs a series-elastic-actuation mechanism, utilizing two sets of DC motors connected in series with elastic springs and connected to the actuated bar through wire ropes and pulleys.

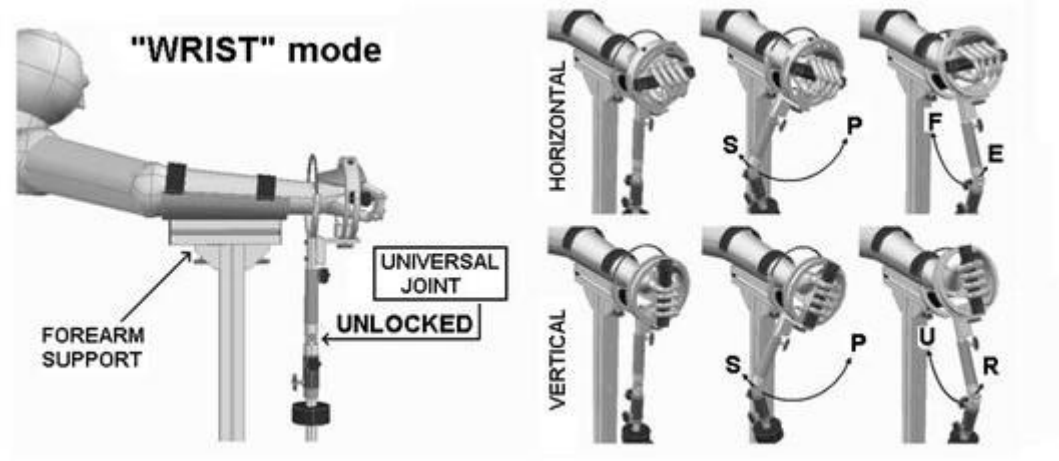

Figure 4: Universal haptic drive “wrist” mode [33].

Figure 5: CRAMER robot with a healthy subject [34].

Closed-chain robot for assisting in manual exercise and rehabilitation, CRAMER (see Figure 5), is a device developed by the University of California, Irvine to provide three degrees of freedom movements for forearm and wrist rehabilitation. This lightweight, portable, and cost-effective robot utilizes a parallel mechanism and incorporates a controller in its handle, allowing patients to engage in motion-based games during rehabilitation. The robot's guide rods, actuated by geared servomotors, control the handle's position. A trajectory optimization framework enables CRAMER to use appropriate motions for certain games, utilizing a 3-axis accelerometer. However, clinical testing of CRAMER has not yet been conducted due to interface-related issues [34].

2.5 Summary

This section discussed the challenges of MRI-compatible devices, emphasizing material restrictions and categorization criteria. While exploring neurological rehabilitation and the continuous adaptation of the brain through neuroplasticity, it emphasized the need for innovative solutions. Robot-assisted physical therapy, integrating computer-based assistance, gaming and virtual reality, emerges as a promising approach. Current rehabilitation robots for wrist and forearm movements, including Wrist Gimbal, OpenWrist, Universal Haptic Drive and CRAMER, address upper extremity impairments. However, there's a notable gap as no example were found of MRI-compatible robotic technology specifically focusing on neurological rehabilitative exercises with computer game integration. This highlights an opportunity for further development in this specific domain.

III. DESIGN AND PROTOTYPING OF DEVICE

3.1 Mechanical Framework Design

Accurate alignment of anatomical joint axes with device joint axes is a critical design consideration for exoskeletons, especially for wrist and forearm configurations where axes of all three degrees of freedom converge at the wrist centre. Misalignments may cause user discomfort and pain during movement [35]. Ensuring that the axes of rotation of the handle intersect precisely at the center of the user's wrist is imperative to mitigate such issues.

The human hand, wrist, and forearm collectively have 3 DOF. Figure 6 shows these distinct movements along with their corresponding rotation axes. In order to address all the motions of the wrist and forearm comprehensively, the proposed solution involves a three-degree-of-freedom serial mechanism featuring three revolute joints (RRR) illustrated in Figure 7. Each revolute joint corresponds to a distinct axis of rotation for the wrist and forearm. This design enhances flexibility and precision, ensuring precise alignment with the anatomical axes of the wrist and forearm. By employing a revolute joint for each axis, the mechanism aims to facilitate accurate alignment, thereby improving overall system functionality and performance. Furthermore, this design simplifies the process as each joint rotation corresponds directly to a specific axis movement. This simplification aids in measuring the state of the wrist and applying the necessary force. This is in contrast to an alternative mechanism, the Parallel manipulator design, where such correspondence can be more intricate and challenging.

Figure 8 presents the proposed RRR mechanism, along with a forearm support. Each link, joint and actuator within the mechanism is assigned a specific name, which will be consistently used for reference throughout the remainder of the thesis. A cylindrical handle is fixed at the end of the mechanism, enabling a secure grip. Its length allows users to adjust the grip height to their preference. The link connected the handle has a flat bottom surface, supporting the hand and maintaining wrist alignment. The handle's threaded bottom connects firmly to the threaded hole in the link (see Figure 9(a)). Also, there are two threaded holes on the link, allowing for potential adjustment of the handle position based on the forearm length if needed.

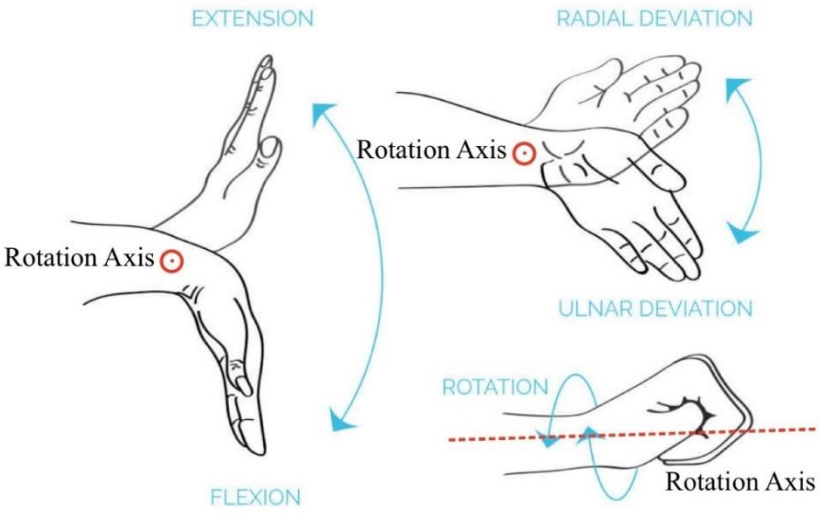

Figure 6: Axes of rotations for wrist and forearm [36].

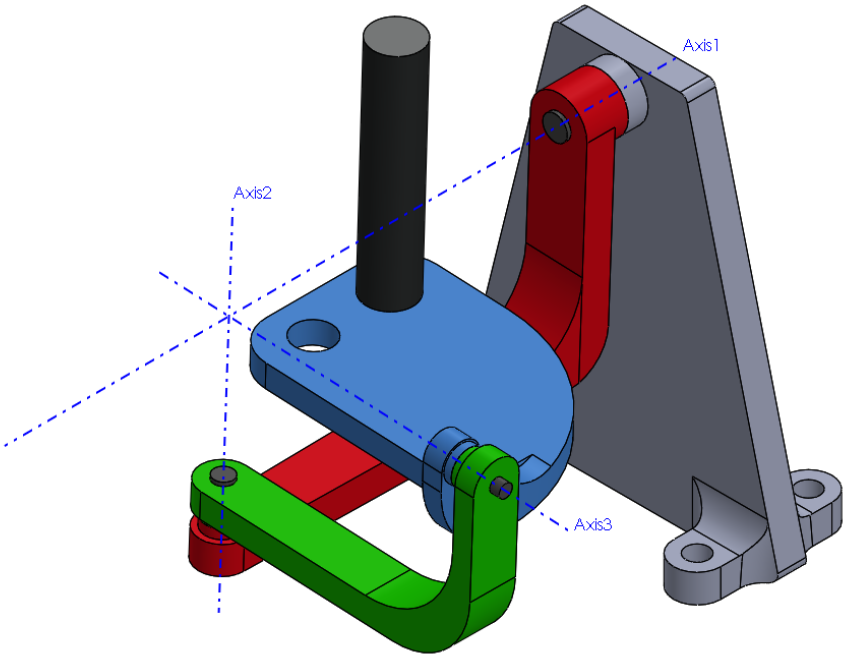

Figure 7: CAD model of the proposed RRR mechanism.

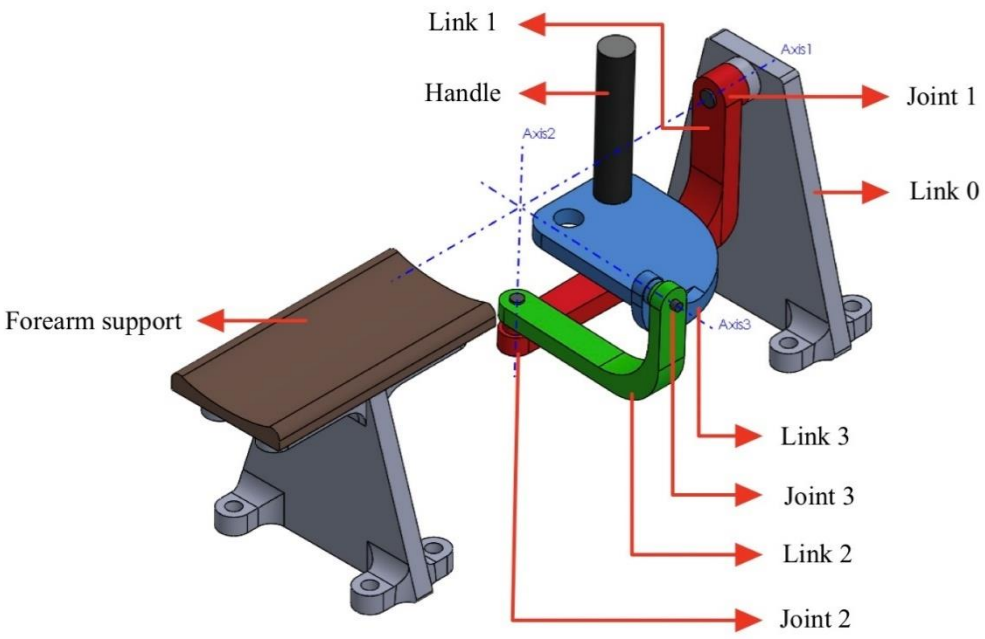

Figure 8: CAD model of the proposed RRR mechanism with the forearm support.

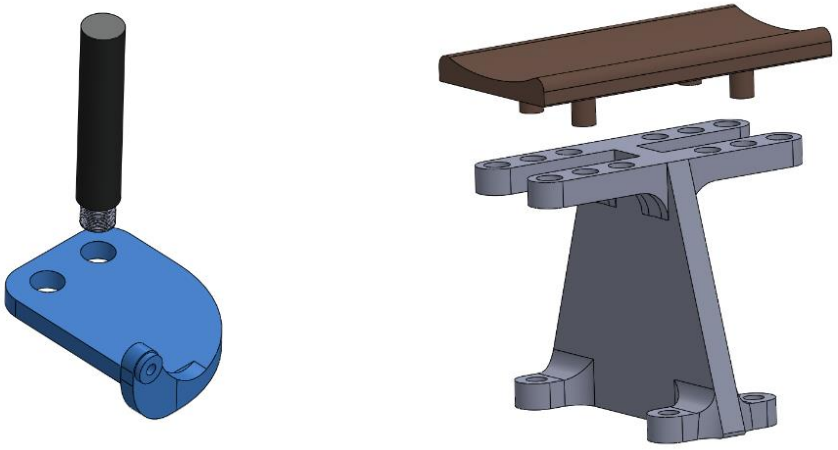

(a) (b)

Figure 9: Attachment mechanism and position adjustability of, (a) handle, (b) saddle-shape forearm support.

The forearm support is illustrated in Figure 8. This support is intended to bear the weight of the hand, facilitating ease of use, and directing attention to wrist movements. Its purpose is to eliminate the need to counteract gravity to stabilize the hand, allowing users to focus on their wrist movements without unnecessary strain. It can also be seen from Figure 9(b) that the saddle-shaped

support position is adaptable, allowing it to be moved closer or farther from the handle based on the user's forearm length.

The mechanism was prototyped utilizing 3D printing technology with PLA filament using a Creality Ender 10S-Max 3D printer. This approach facilitated the rapid development of prototypes, enabling prompt feedback from rehabilitation experts and patients who utilized the mechanism. Crucially, it ensured the MRI-compatibility of the mechanical structure. During this phase, an Inertia mouse, shown in the Figure 10, was attached at the top of the handle. This arrangement allowed the movement of the handle to be translated into corresponding cursor movements on the computer monitor. Consequently, users could engage in various computer games compatible with a standard computer mouse by manipulating the handle, performing wrist or forearm movements. The versatility of the system was enhanced by the ability to change the orientation of the inertia mouse, thereby enabling different combinations of three rotations to be selected for mapping into horizontal and vertical movements of the cursor.

From the above explanation, it is understood that the initial design of the mechanism was without considering actuators or sensors. In order to convert the linear motion of the actuators into rotations, adjustments were made to the design to include attachment points for the actuators, and considerations were given to integrating sensors. This resulted in a more detailed design for each link, making it easier to attach actuators and sensors.

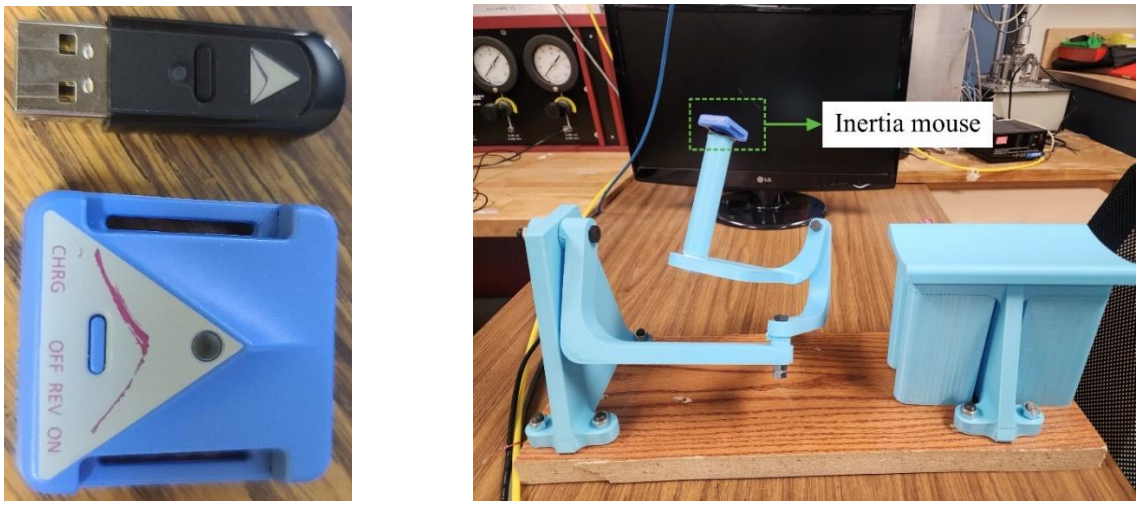

(a) (b)

Figure 10: (a) Inertial mouse and accompanying USB wireless dongle [37], (b) inertial mouse mounted on the handle.

Initially, the links were designed as single parts for simplicity and to reduce backlash. However, since the links were 3D printed, even small changes, such as adjusting the clearance of the encoder shaft housing, required reprinting the entire link. This process was time-consuming and inefficient in terms of prototyping time and material use. Therefore, a decision was made to break down each link into smaller parts, connected using 3D printed screws and nuts, which made the modification process more efficient.

In Figure 11 the complete assembly of links, air cylinders and encoders are displayed. In this assembly, link 0 is fixed to a base with screws and nuts. It provides support for the whole serial links. Figure 12(a) shows link 0. The circular structure at the top right facilitates the attachment of the encoder body. The yoke (see Figure 12(b)) is essential for converting the linear motion of actuator 1 to rotation. Figure 13 shows the rotation mechanism of joint 1.

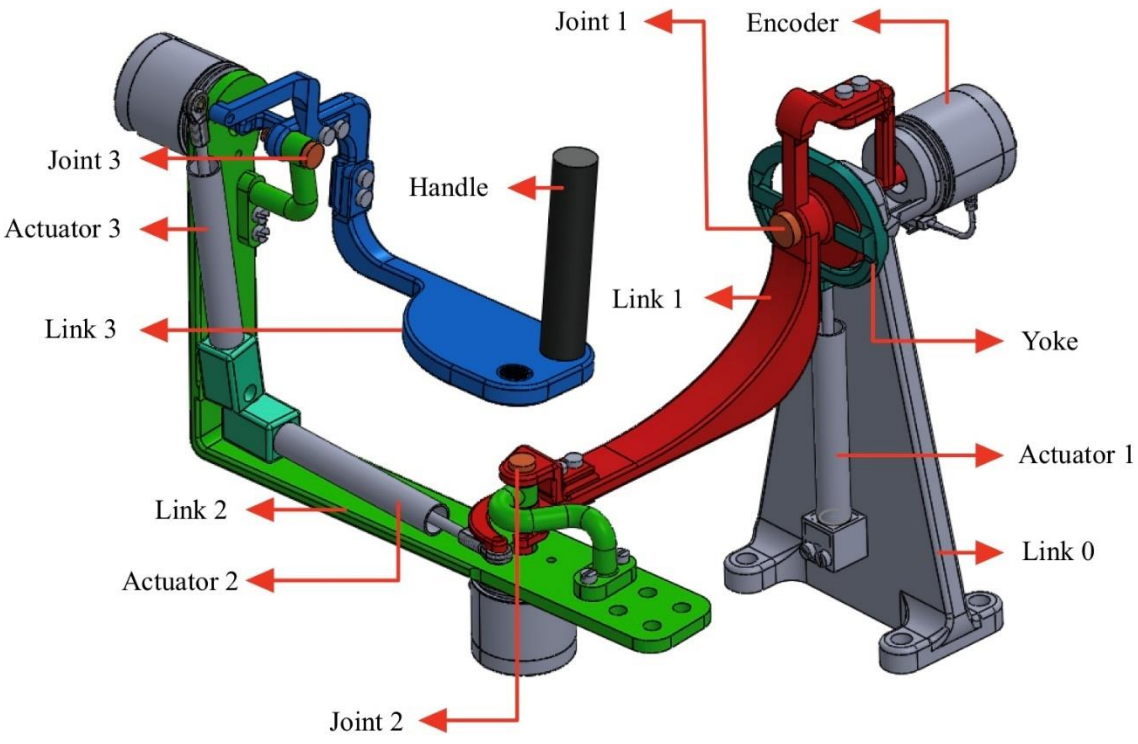

Figure 11: Assembly of the links with the actuators and encoders.

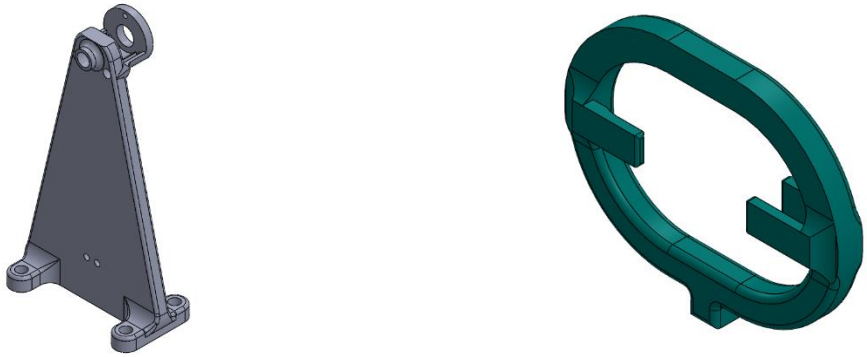

(a) (b)

Figure 12: (a) Link 0 supporting serial links, (b) yoke.

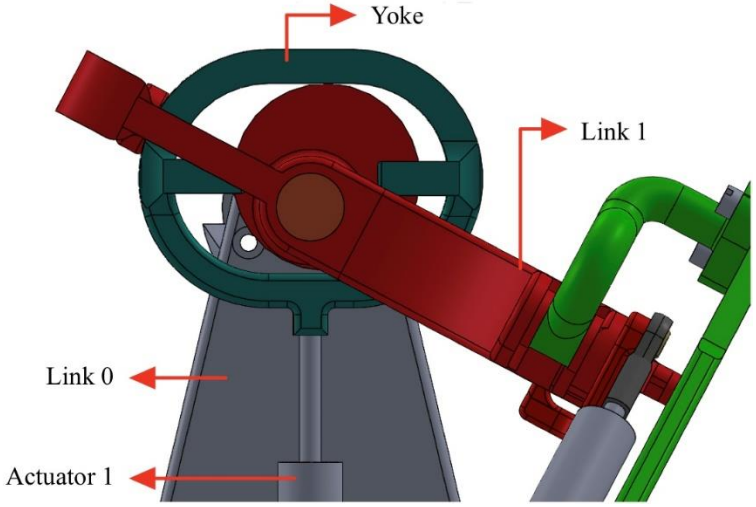

Figure 13:Assembly of joint 1.

Figure 14 to Figure 16 show the assembly and exploded view of link 1, 2 and 3 respectively. Each link is composed of different parts and fixed using screws and nuts. Moreover, Figure 15 illustrates how the encoders are assembled to link 2.

The assembly of joints 2 and 3 can be seen in Figure 17. For joint 2 (see Figure 17(a)), actuator 2 rod is connected to link 1 at point A, while the base of actuator 2 is connected to link 2. With the configuration shown, the expansion and retraction of actuator 2 rotates link 2 around point B, where joint 2 is located. Similarly, with reference to Figure 17(b), actuator 3 is connected to link 3 at point A and the base is connected to link 2. Therefore, the expansion or retraction of actuator 3 leads to rotation of link 1 around point B.

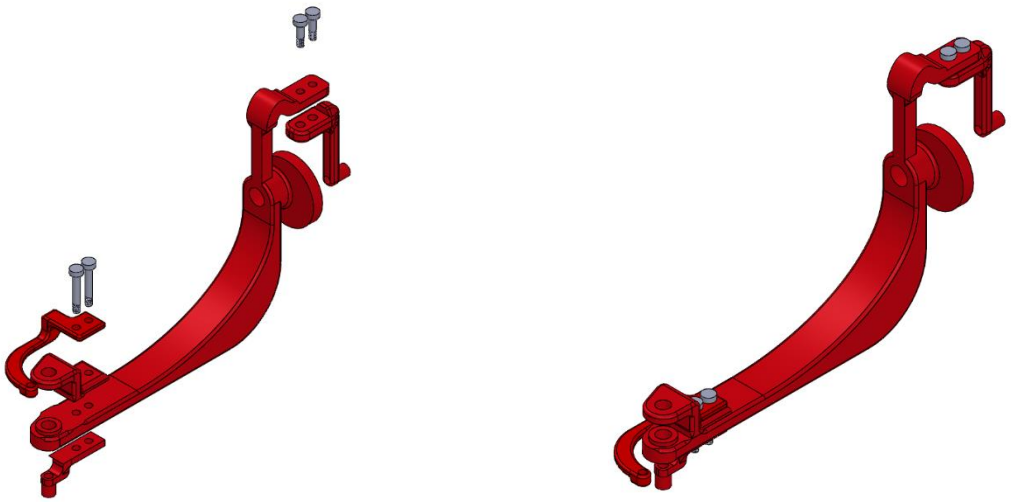

(a) (b)

Figure 14: Link 1, (a) exploded view, (b) assembled view.

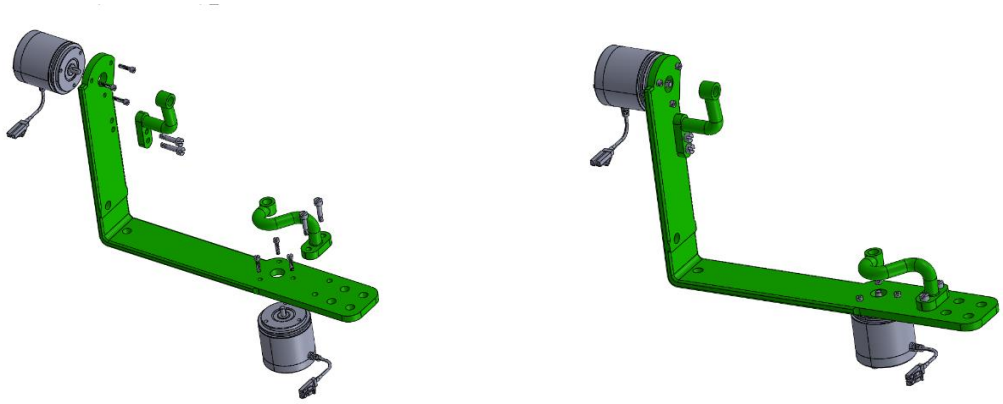

(a) (b)

Figure 15: Link 2, (a) exploded view, (b) assembled view.

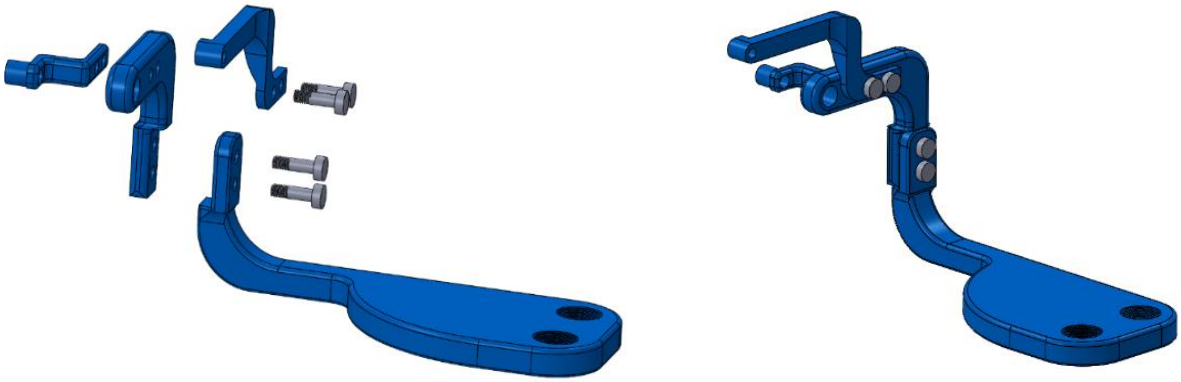

(a) (b)

Figure 16 : Link 3, (a) exploded view, (b) assembled view.

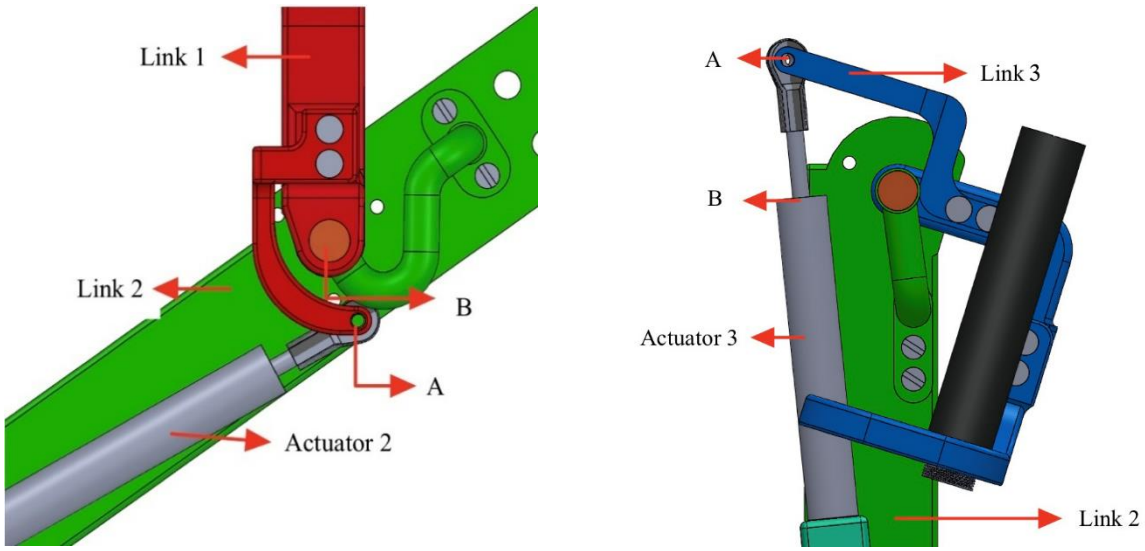

(a) (b)

Figure 17: Assembly of, (a) joint 2, (b) joint 3.

3.2 Bearings

Instead of employing metallic ball bearings, Iglide bearings made from advanced high-performance plastics designed for MRI environments have been utilized. These bearings are self-lubricating and exhibit exceptionally low friction, making them well-suited for application of wrist manipulation. These bearing are used in the revolute joints as well as the joints between the actuators rod and the links reducing friction and providing smooth rotations.

(a) (b)

Figure 18 :Iglide plastic bearings, a) rod end bearing with female thread, b) J sleeve bearing with flange [38].

3.3 Sensors

To accurately capture the state of the mechanism, and therefore the state of the user's wrist, the utilization of sensors becomes imperative. While three rotary encoders prove effective in measuring the angles of individual joints, conventional sensors are unsuitable for magnetic resonance imaging (MRI) due to the adverse impact of the strong magnetic field on electrical signals. Consequently, fiber optic encoders are employed as an alternative. Specifically designed for functional MRI (fMRI), Micronor's MRI-compatible fiber optic incremental position sensor, MR340-1 [39], is non-metallic and MRI-safe (see Figure 19). This sensor, with a resolution of 360 pulses per revolution (ppr) equivalent to 1 degree, is used to measure the angular position of the links.

Figure 19: MR340-1incremental encoder controller [39].

When powered, the encoder receives optical pulses from a converter and transmits the resulting data back to the converter in optical form via a fiber optic cable. The converter shown in Figure 20, is placed outside the MRI room, and converts this optical data to electrical digital pulses. This convertor outputs two phase-shifted digital signals with 1 kHz frequency. Depending on the direction of the shaft rotation, the phase shift is either +90° or -90°, this signal is referred to as the quadrature signal. The time plot of two encoded quadrature signals can be seen in Figure 21.

Figure 20: MR340-1 incremental encoder converter [39].

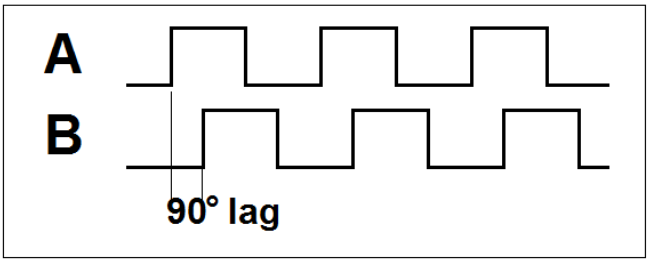

Figure 21: Quadrature signal, incremental encoder converter output [39].

3.4 Actuation System

Actuators are essential for generating the requisite force or torque to facilitate user interaction by offering assistance or resistance. However, the strong magnetic field within the MRI environment renders electrical motors unsuitable. Conversely, hydraulic actuators, requiring a pump and oil reservoir, pose challenges such as potential oil leakage and are designed for applications demanding substantial forces (unnecessary for the current mechanism).

In light of these considerations, pneumatic actuators emerge as a favorable choice due to their lightweight, compact nature and, most importantly, compatibility with MRI environments. AC 13270-4 Airpel pneumatic cylinders [40] have been used for this purpose. These cylinders feature a 2-inch stroke and are constructed from materials such as brass, borosilicate glass, carbon graphite, silicone rubber, and plastic. Moreover, they operate within a pressure range from full

vacuum to 50 psi. Three actuators have been used in the device, with one specifically for each joint. This configuration grants the device a three-degree-of-freedom actuation capability.

Figure 22: AC 13270-4 Airpel pneumatic cylinder [40].

Figure 23: SMC ITV0050 3UM electro-pneumatic regulators [41].

In order to control the air pressure in the chambers of each actuator to adjust the forces, SMC ITV0050 3UM electro-pneumatic regulators have been used (see Figure 23). They can regulate the pressure between 0.145 to 130.534 psi by adjusting the analog voltage input within 0 to 10 V DC [41]. Since these pressure regulators operate with 0-10 DC voltage and the control system used is not able to produce analog voltages, a PWM to analog convert is required. For this

purpose, 6 Globeagle PWM to voltage 0-10V adjustable digital analog signal converter modules [42] have been incorporated into the controller, receiving a PWM signal from the microcontroller. The PWM to analog converter is shown in Figure 24. Since each actuator requires two pressure regulators, one for each chamber, a total of six pressure regulators and six PWM to analog converters have been used.

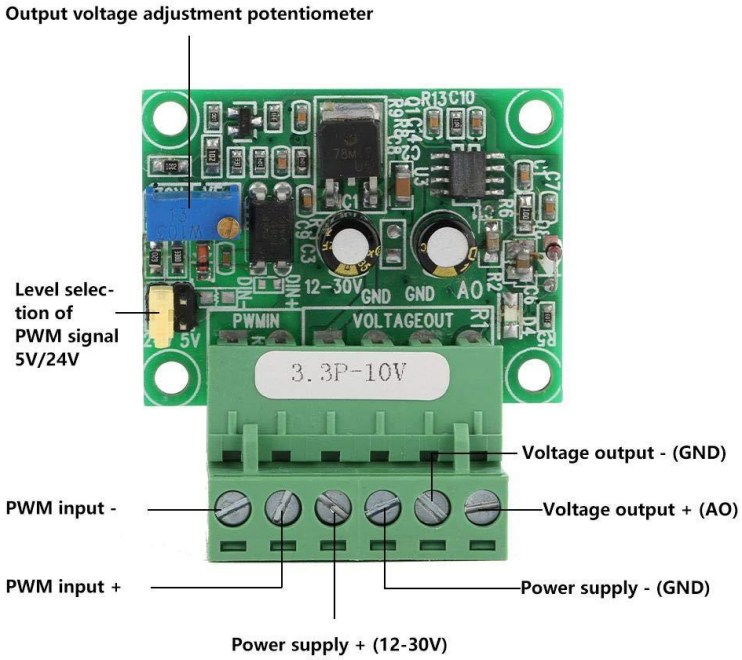

Figure 24: PWM to voltage 0-10 v adjustable digital to analog converter module [42].

3.5 Microcomputer

For data acquisition and implementing different control algorithms that adjust the assistive or resistive forces accordingly, a processing unit is necessary. A Raspberry Pi Pico W has been selected for this purpose, and has been programmed in CircuitPython. It features a dual-core ARM Cortex-M0+ processor and a wide range of GPIO (general purpose input/output) pins [43] for collecting input signals and generating outputs, making it well-suited for this project.

It is the main component for obtaining input signals and generating output signals. An advantageous feature of the Raspberry Pi Pico is its ability to store multiple files and codes in its

memory. This allows users to effortlessly switch between different codes and facilitates the storage of data in file formats, such as text files. This thesis utilizes the Pico W's capacity to store multiple files and codes in its memory. This capability is specifically employed to record actuators' forces in a text file.

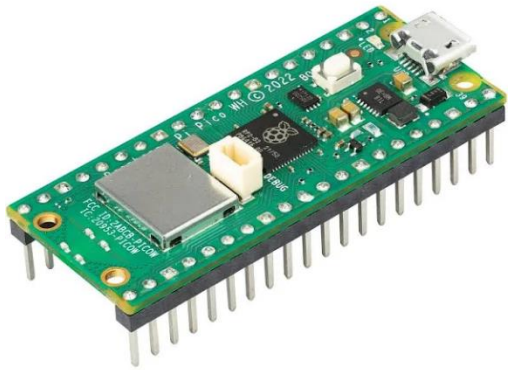

Figure 25: Raspberry Pi Pico W based on the RP2040 microcontroller [43].

3.6 Electrical Layout

No electrical components are allowed in the MRI environment. Therefore, all these components are placed in a 3D-printed box and must be placed outside the MRI room. The designed box is shown in Figure 26.

The electrical circuit design of the device, centres around the Raspberry Pi Pico for data acquisition and actuator control. It details how critical components are interconnected. Below the key components are listed (see Figure 27):

- Raspberry Pi Pico: The central processing unit responsible for generating PWM signals for the actuators and receiving encoder position signals and executing the algorithms.
- Encoder Converters: Devices converting encoder optical signals to a format readable by the Raspberry Pi Pico, providing real-time position feedback.
- Pressure Regulator Valves: The system to control the air pressure within the actuators chambers to adjust the force based on the input voltage.

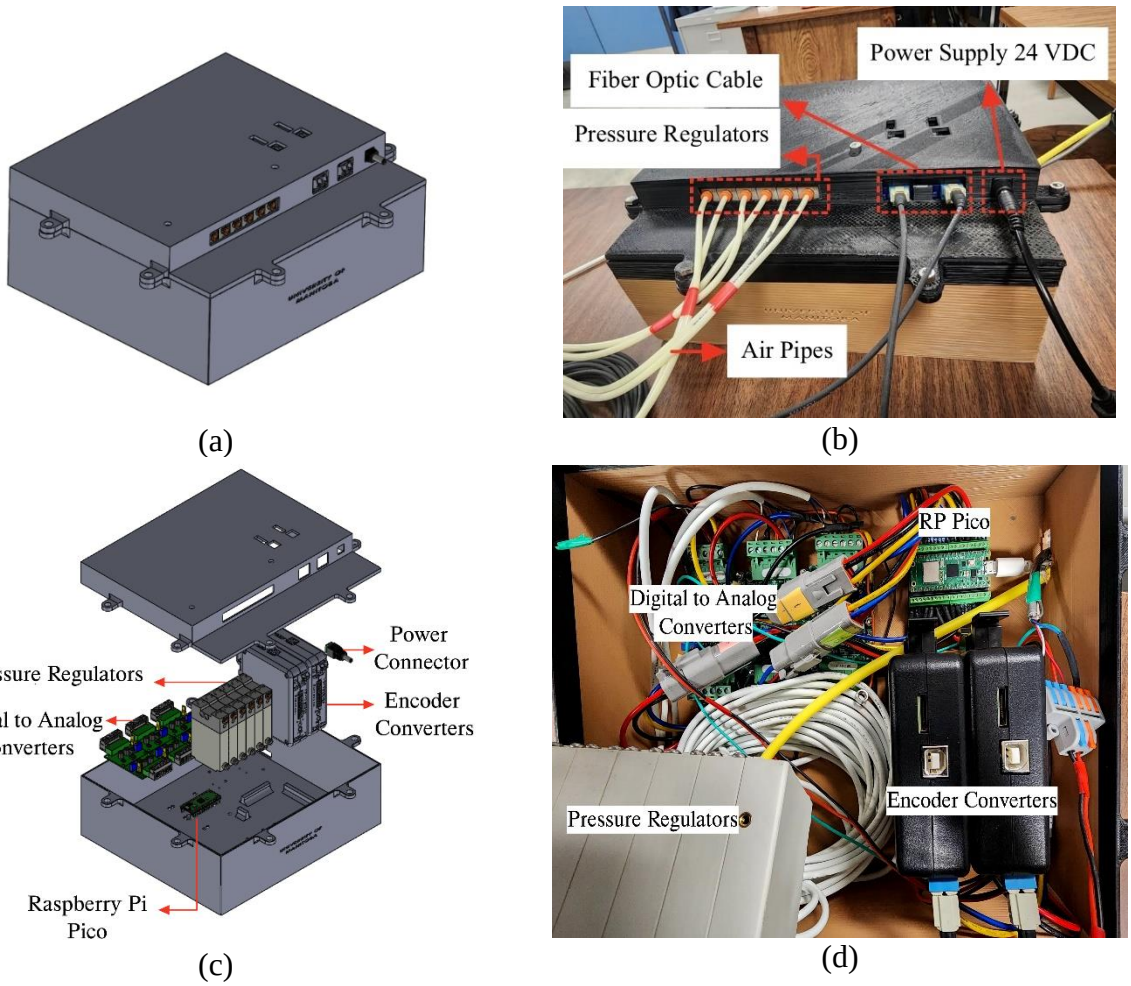

Figure 26: Box containing the electrical components of the device, (a) assembled box CAD view, (b) assembled 3D-printed box, (c) exploded view, (d) inside view.

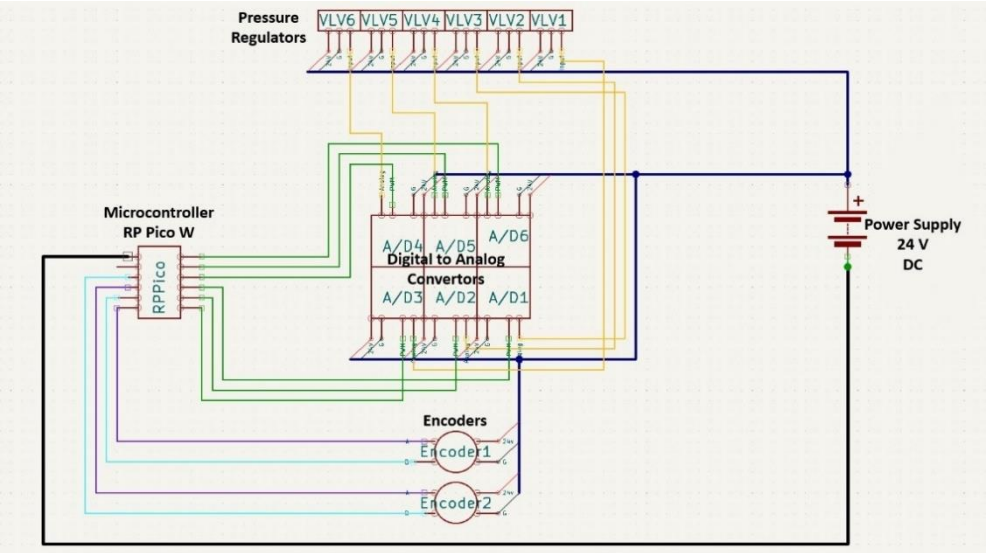

Figure 27: Electrical layout.

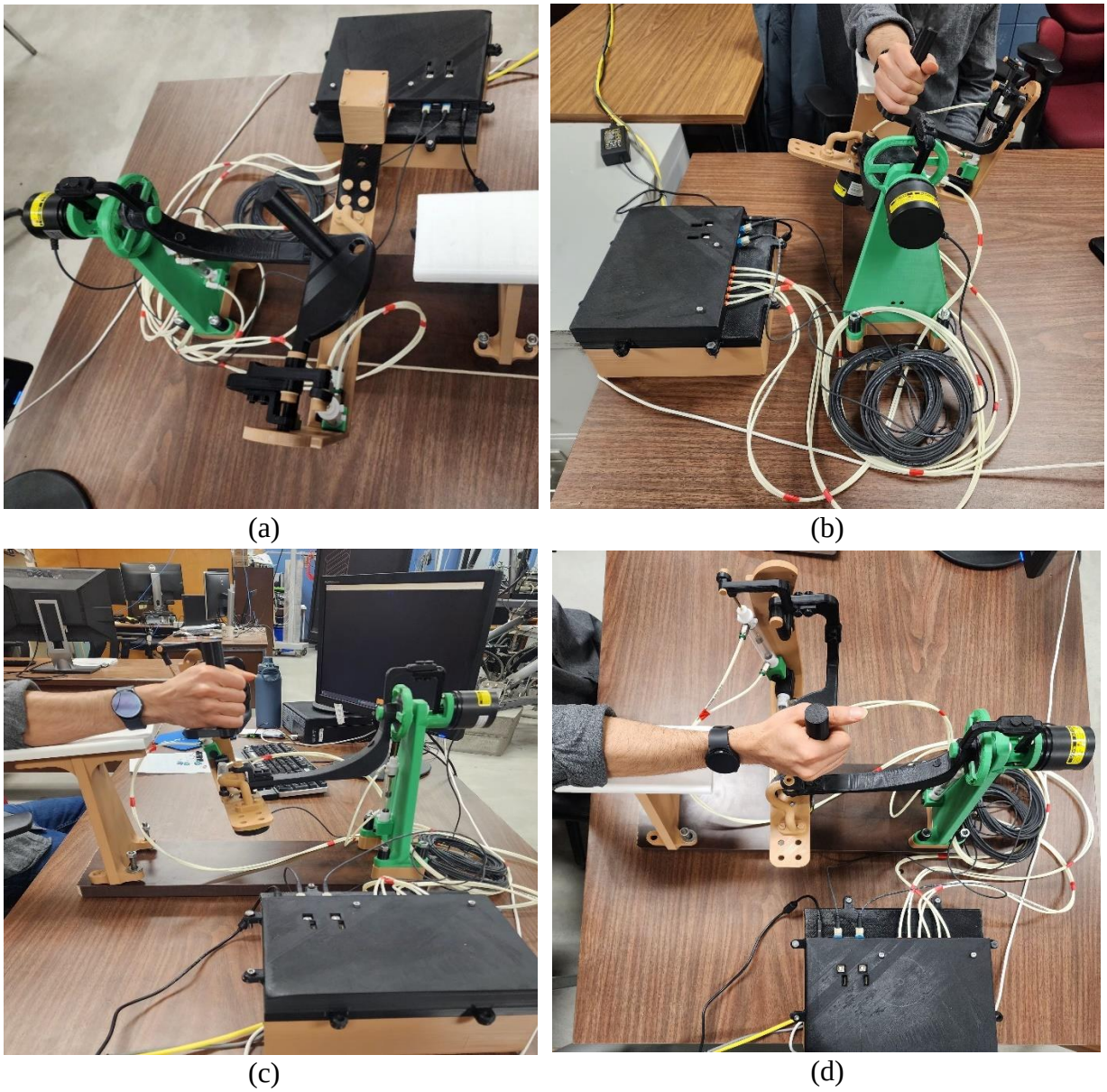

(a) (b)

(c) (d)

Figure 28: (a) Developed prototype, (b) user holding handle, front view, (c) side view, (d) top view.

- PWM to Analog Converters: Components converting digital PWM signals from the Raspberry Pi Pico into analog signals to drive pressure regulator valves.
- 24-Volt Power Supply: Common power source providing energy to the encoders, pressure regulator valves, and PWM to Analog Converters. The Raspberry Pi Pico is powered by a computer system through a USB cable. However, a common ground ensures proper electrical continuity between the Raspberry Pi Pico and other components.

Figure 27 illustrates the electrical layout of the device. The microcontroller, Raspberry Pi Pico, is connected to the encoder converters, receiving positional feedback. PWM signals from the Raspberry Pi Pico are sent to the PWM to Analog Converters. The PWM to Analog Converters then generate analog signals, regulating the voltage for the pressure regulator valves. A common ground ensures proper electrical continuity between all components.

The Raspberry Pi Pico serves as the central hub, orchestrating communication between encoders, actuators, and converters. Encoders provide real-time feedback, allowing the Raspberry Pi Pico to adjust PWM signals in real time.

Figure 28 illustrates the assembled prototype of the device. The wires were intentionally selected to be longer to facilitate positioning the box outside the MRI room when needed.

3.7 Motion Analysis

The motion analysis of the device is done using MATLAB 2023b Simulink software in Simscape Multibody package for kinematic analysis. Given that each joint corresponds to a specific rotation in the wrist and forearm, the range of motion of each joint is examined separately.

3.7.1 Joint 1

Figure 29 shows the block diagram of the movement mechanism of link 1 which translates the linear motion of actuator 1 into rotational movement around joint 1 axis using a yoke and eccentric circle of link 1. The 3D visualization of this simulation is seen in Figure 30. As it can be seen in Figure 31, the angle of rotation of joint 1 can be adjusted by varying the pneumatic actuator stroke. As the actuator stroke changes from 0 to 19.7 mm, link 1 rotates from -80° to 80° which matches the functional range of motion for the pronation (80°) and supination (80°) movements [44]. At zero angle the hand is in neutral position and zero stroke refers to the fully retracted position of the actuator.

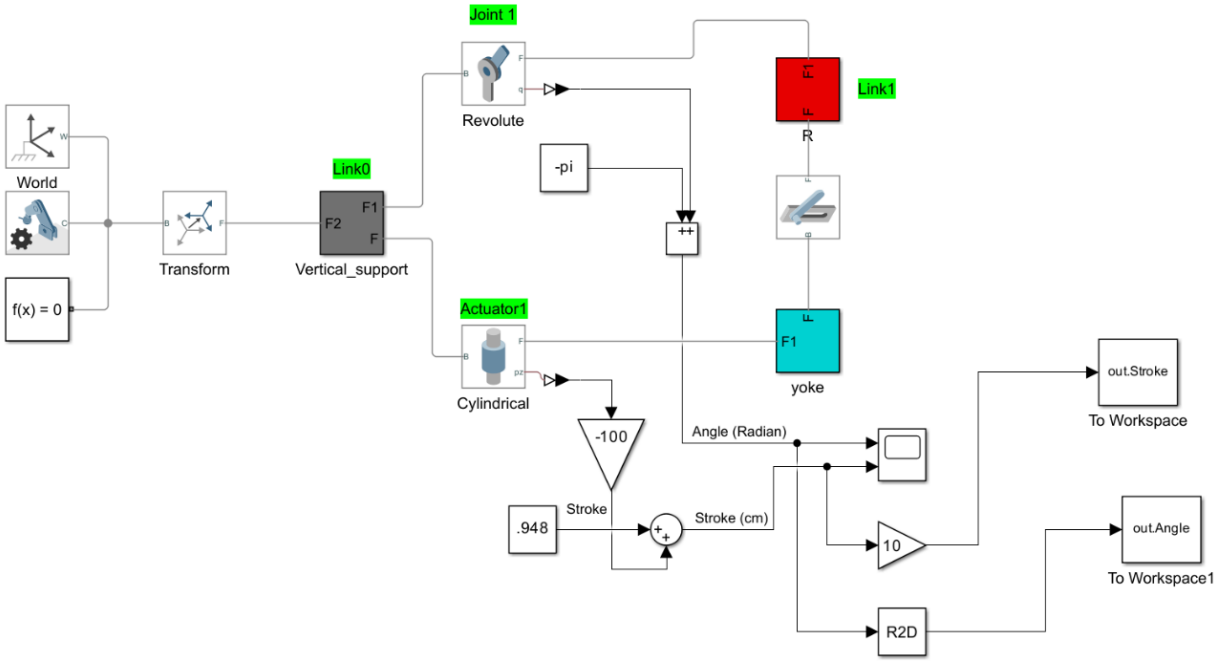

Figure 29: Block diagram of kinematic analysis of the first joint of the mechanism.

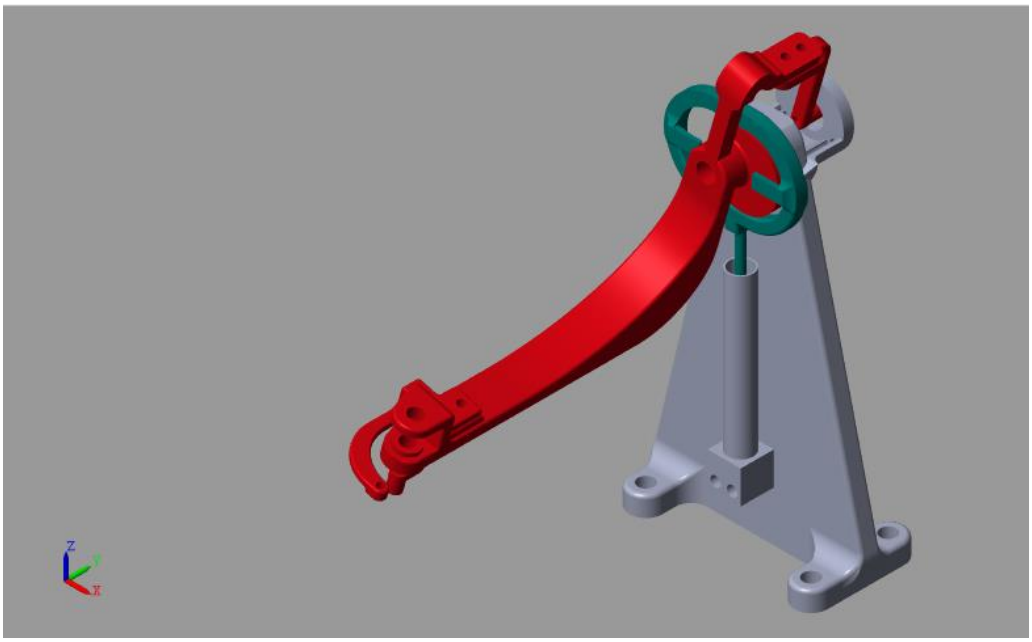

Figure 30: 3D visualization of kinematic analysis of joint 1 in Simscape.

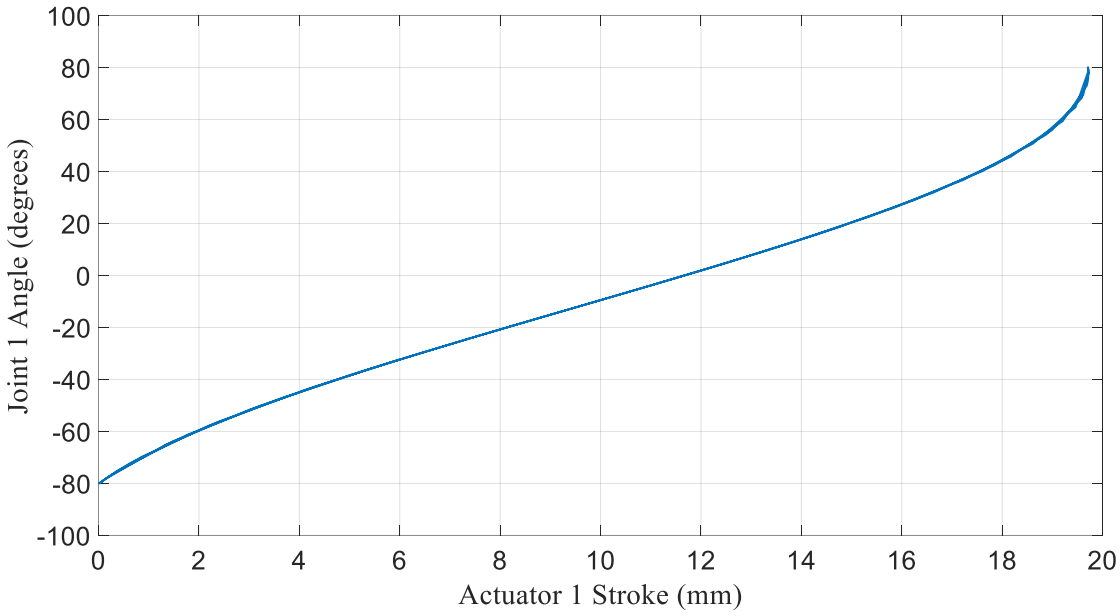

Figure 31: Joint 1 angle variation with actuator 1 stroke.

3.7.2 Joint 2

Figure 32 shows the block diagram of the movement mechanism of link 2 which translates the linear motion of actuator 2 into rotational movement around joint 2 axis. The 3D visualization of this simulation can be seen in Figure 33. As the actuator stroke changes from 0 to 53 milometers, link 2 rotates from -66.8° to 70°, corresponding to 66.8° of flexion and 70° of extension. This range of motion is enough for the wrist extension, 50°, and flexion, 45° during activities of daily living [45].

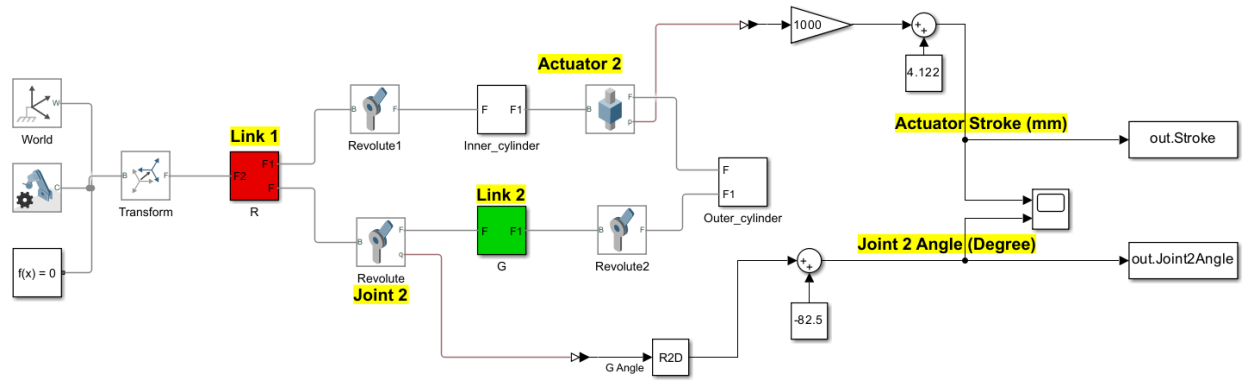

Figure 32: Block diagram of kinematic analysis of the second joint of the mechanism.

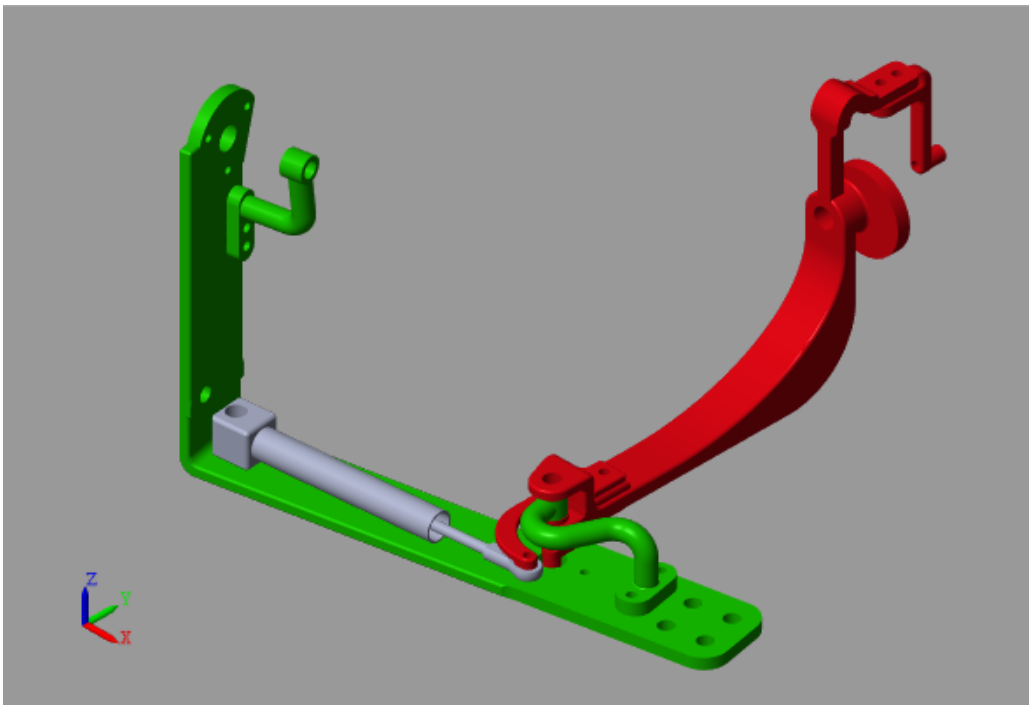

Figure 33: 3D visualization of kinematic analysis of the second joint of the mechanism.

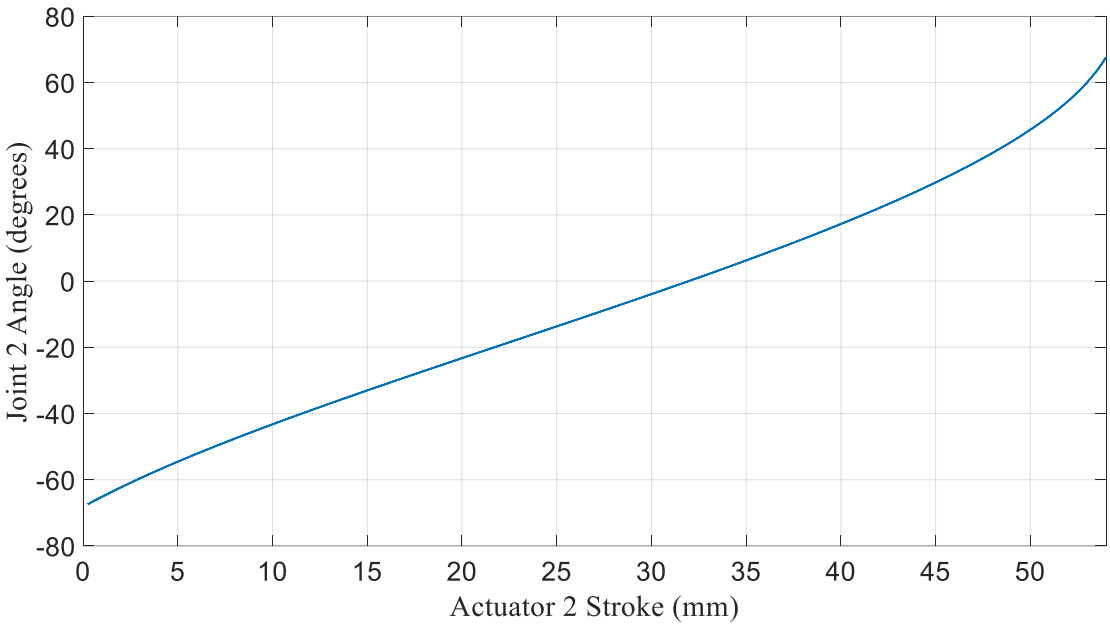

Figure 34: Joint 2 angle variation with actuator 2 stroke.

3.7.3 Joint 3

The linear motion of actuator 3 also is converted to rotational movement around joint 3 axis. The 3D visualization of this simulation can be seen in Figure 35. As it can be seen in Figure 36, as the actuator stroke changes from 0 to 53 mm, link 3 rotates from -47° to 27°. This rotation corresponding to 47° of ulnar and 27° of radial deviation, covering the functional motion range of 40° for ulnar and 15° for radial deviation [45].

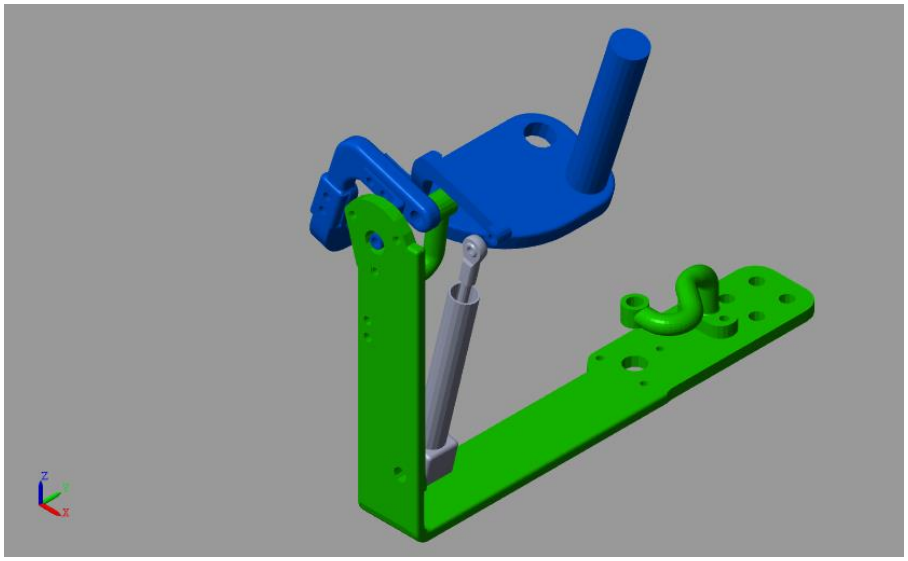

Figure 35: 3D visualization of kinematic analysis of the third joint of the mechanism.

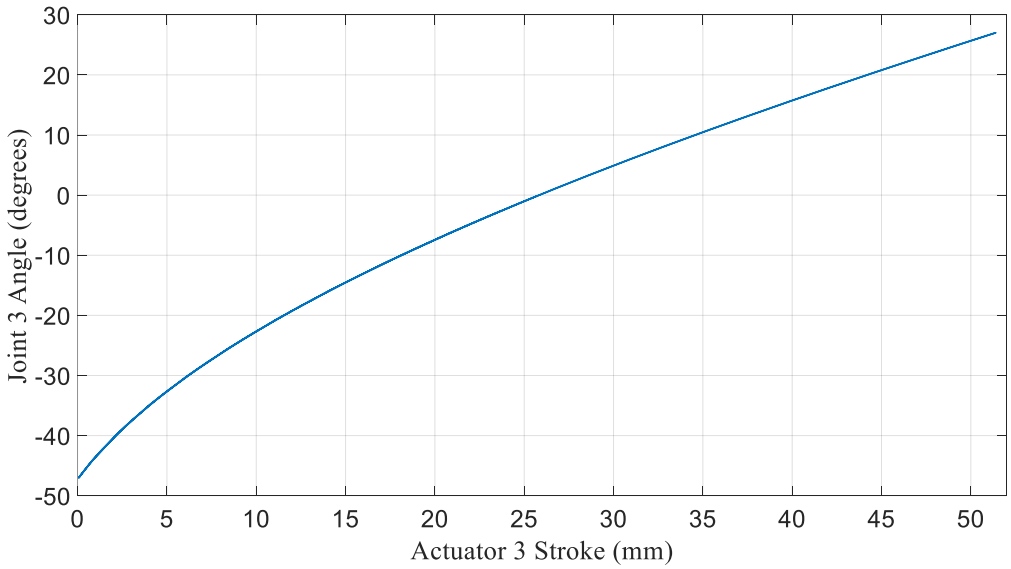

Figure 36: Joint 3 angle variation with actuator 3 stroke.

3.8 Force Analysis

Force analysis of this device has been done using MATLAB Simulation software, Simscape Multibody package for dynamic analysis. To simplify the analysis process, each joint is analyzed one at a time due to the torques being independent and decoupled in this device. Given that each joint corresponds to a specific rotation in the wrist and forearm, the maximum torque of each joint is examined separately.

The force generated by a two-chamber pneumatic actuator is a function of the air pressure applied and the effective piston area in each chamber. The force of the actuator is calculated as follows:

$$F = P_a A_a - P_b A_b \tag{1}$$

where F is the actuator force, P_a and P_b are the pressure inside each of the two chambers and A_a and A_b are the corresponding pneumatic piston's effective areas. In this study, only one actuator chamber is pressurized at any given moment, according to force direction, while the other chamber maintains at atmospheric pressure.

For the pneumatic actuators that has been used on this device the maximum pressure is 50 psi. Also, A_a and A_b are 0.093 and 0.105 in^2, respectively. To ensure that the calculated force is achievable in both retraction and expansion, the smaller piston area is used to calculate the maximum force.

$$F = 50\ psi\ \times\ 0.093\ in^2 = 4.65\ lbf\ \equiv\ 20.6\ N \tag{2}$$

The calculated force is used in the simulations below to see the resulting torque for each joint.

3.8.1 Joint 1

Figure 37 shows the block diagram of the torque mechanism of link 1 which converts the force of the linear actuator into torque around joint 1 axis using a yoke.

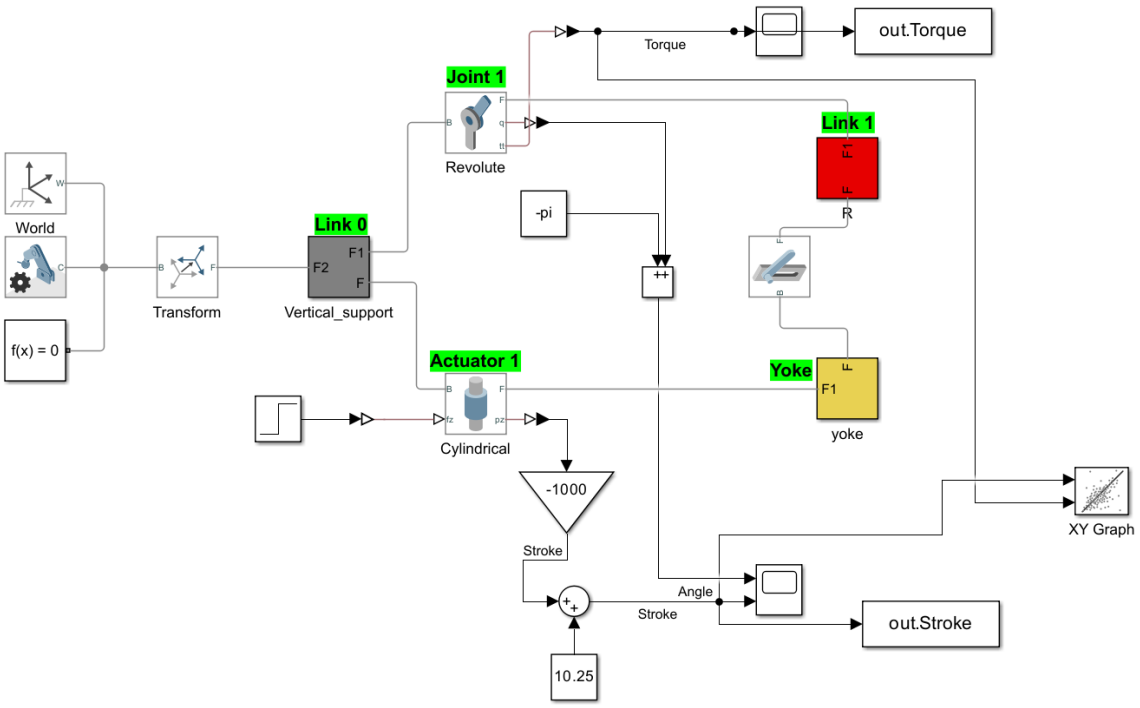

Figure 37: Block diagram of dynamic analysis of joint 1 of the mechanism.

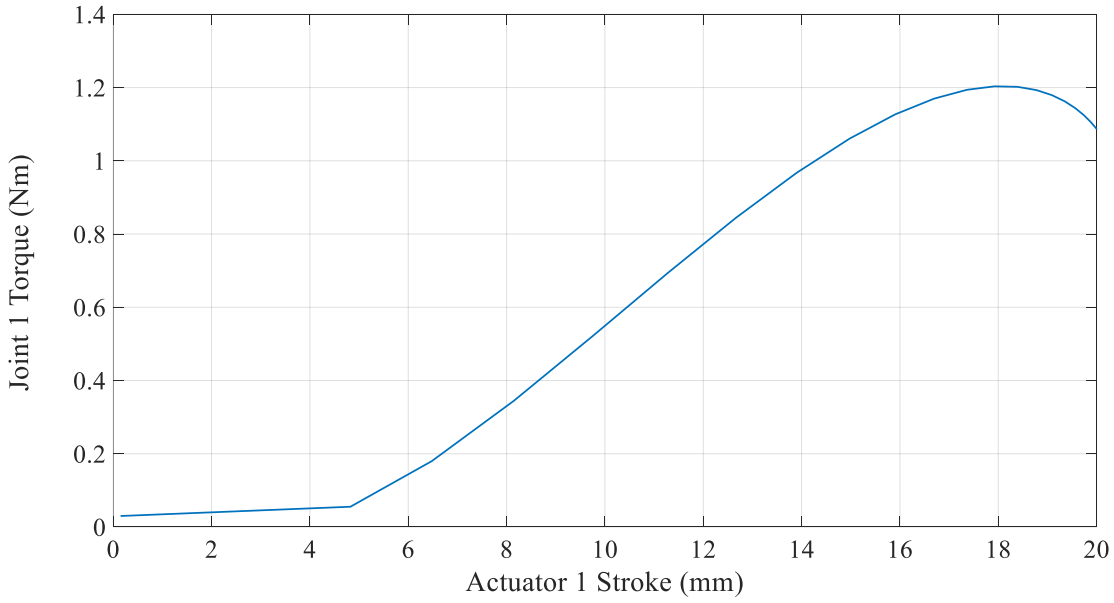

Figure 38: Joint 1 maximum torque variation with actuator 1 stroke.

It can be seen in Figure 38, the torque of joint 1 changes by varying the pneumatic actuator stroke. Studies indicate that pronation and supination movements require a torque of 0.72 Nm

during ADLs. Even though the torque reaches a peak of 1.2 Nm for this joint, in lower strokes the torque is less than 0.72 Nm. To accommodate this, a custom actuator with a larger diameter can be ordered and higher pressure can be used. The custom actuator can still be integrated into the design.

3.8.2 Joint 2

As it can be seen in Figure 39, the torque of joint 2 changes by varying the pneumatic actuator stroke. The torque value for flexion and extension movements during activities of daily living (ADLs) is 0.21 Nm [46]. The stroke changes from 5 to 45 mm to cover the functional range of motion. Within this range of stroke, the maximum torque is above the value of 0.21 Nm.

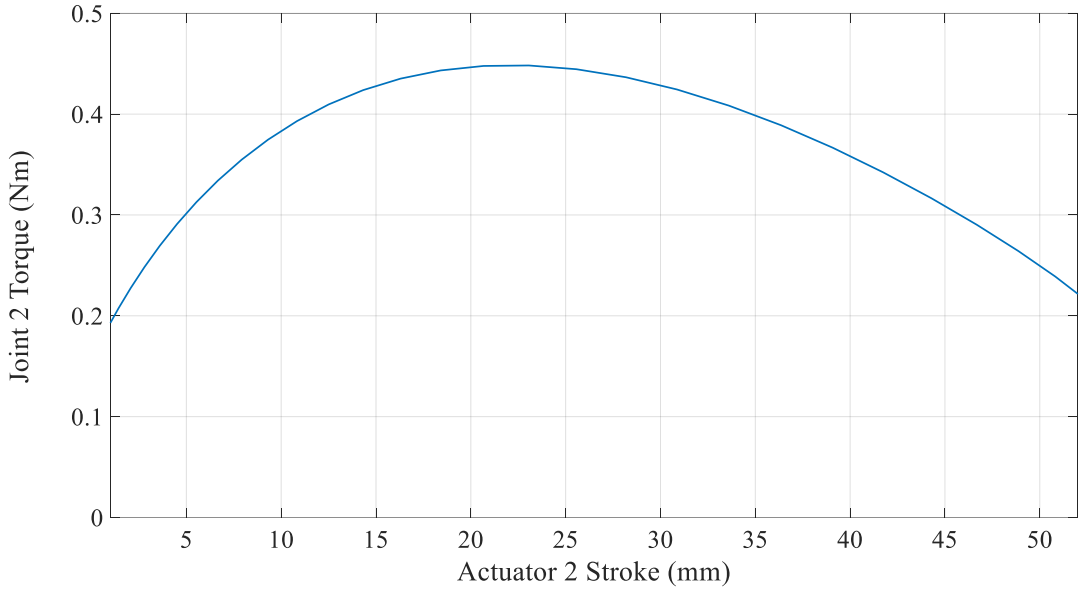

Figure 39: Joint 2 maximum torque variation with actuator 2 stroke.

3.8.3 Joint 3

During ADLs, for ulnar and radial deviation, 0.25 Nm torque is required [46]. Figure 40 shows that the resulting maximum torque of joint 3 is greater than 0.25 Nm for the whole stroke range.

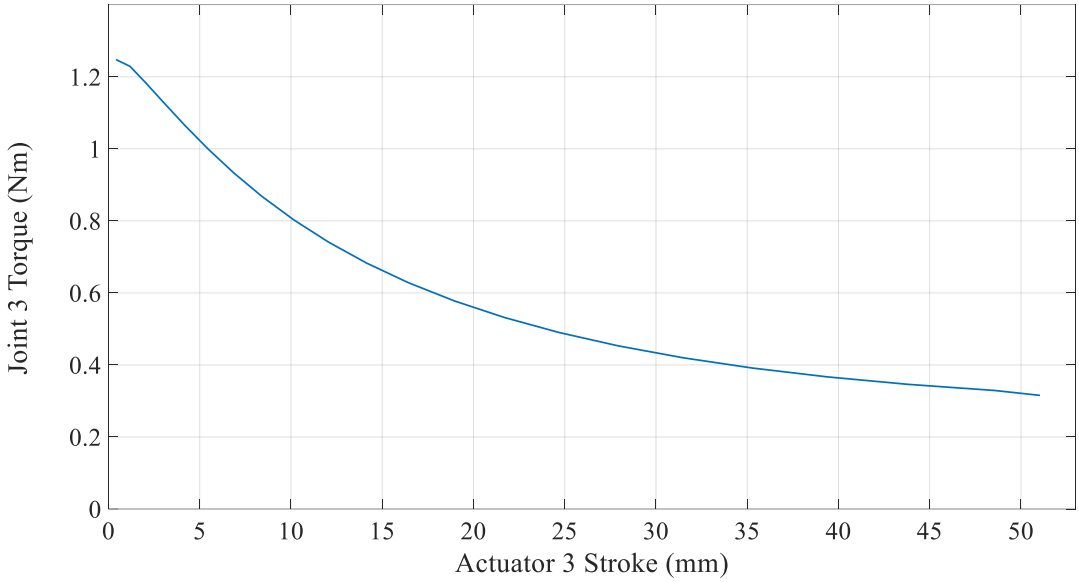

Figure 40: Joint 3 maximum torque variation with actuator 3 stroke.

3.9 Summary

This Chapter focused on the development of a mechanical framework for a newly designed 3-DOF device for wrist and forearm rehabilitation. The device employs three revolute joints to align with the anatomical axes of wrist and forearm, providing comfort and precision. The CAD model illustrated the design, featuring a cylindrical handle to grip, forearm support, and an adjustable attachment mechanism.

The mechanical structure was prototyped using 3D printing technology. An Inertial Mouse was initially integrated for physical and neurological therapy exercises. The initial design emphasized simplicity but lacked details on actuators and sensors. The design evolved to accommodate MRI compatible actuators and sensors. Links were designed using divided smaller parts to facilitate replacement. Bearings made from advanced high-performance plastics designed for MRI environments were used. Fiber optic encoders were chosen for compatibility with MRI, and pneumatic actuators were selected for their lightweight nature and MRI compatibility. The actuation system, controlled by a Raspberry Pi Pico, utilizes pneumatic cylinders and pressure regulators.

Motion and force analyses were conducted using MATLAB Simscape Multibody toolbox. Focusing on each joint separately, the torque and force ranges for each joint were calculated based on the mechanisms and actuator characteristics.

This chapter provided a comprehensive overview of the mechanical design, including considerations for alignment, modularity, materials, actuators, sensors, and control systems. The iterative prototyping process and attention to MRI compatibility demonstrate a systematic approach to developing a versatile and effective rehabilitation device. The chapter concludes with an electrical layout diagram illustrating the integration of key components for data acquisition and precise control of actuators, followed by motion and force analysis.

IV. GAME INTERFACE

4.1 RTP Game

The RTP game [47] is a computer game software based on repetitive task practice (RTP). This computer-based rehabilitation software has been specifically designed to assist in the recovery of individuals with neurological impairments. The core gameplay involves using a paddle to catch a falling target ball, a mechanism aimed at enhancing motor skills through repetitive and targeted movements.

The user controls a paddle at the bottom of the screen, utilizing the mouse cursor, which can move laterally across the entire span of the screen. The singular goal of the game is to “catch” the target ball with the paddle before they disappear at the bottom of the screen, with any contact between the paddle, either the top and sides, and object counting as a successful “catch”. A successful catch will cause the object to “explode”, disappearing with a burst of colour, as demonstrated in Figure 41 in the bottom left corner, accompanied by a popping sound. After a pre-determined amount of time has elapsed, during which objects are continually generated, the game will abruptly come to an end and the words “Game Over!” will appear on the now motionless screen. Meanwhile, as the user is attempting to catch the falling objects, the program is keeping track of the players gameplay performance.

Figure 41 displays the graphical interface of the RTP game with four different targets. The yellow rectangle at the bottom of the screen is the paddle controlled by the user, the soccer ball is the target that needs to be captured by the paddle. On the top centre of the screen the remaining time of the game is shown.

After initializing the program, the user is presented with a prompt window, such as the one displayed in Figure 42, which allows to adjust the settings to change the difficulty of the game. This customization ensures that the game meets the specific needs and capabilities of each user, making it a versatile tool for a wide range of patients.

There are a number of parameters directly influencing gameplay, shown in Figure 42 that can be adjusted to accommodate varied skill levels.

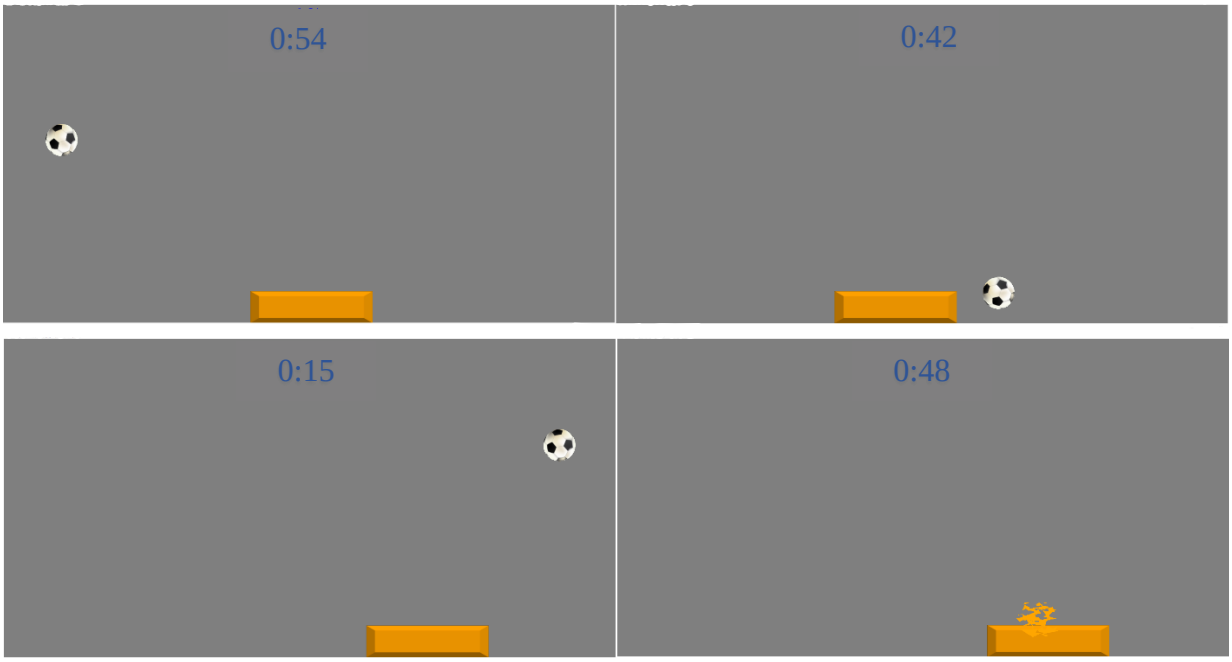

Figure 41: Graphical interface of the RTP game and successful interception during gameplay.

- Speed of moving targets can be adjusted (the range of adjustment is enough that most skill levels can be accommodated by either speeding up or slowing down the target movement).
- Frequency of target appearance can be changed in the game settings.
- Sensitivity of the user-controlled paddle can be adjusted for both the X and Y axes individually as needed.
- Paddle size can be adjusted from 50% to 300% of the default paddle size.
- Movement direction can be specified to coincide with the selected joint movement. This can be achieved by selecting one-dimensional-axis movement for horizontal (East–West) or vertical (North–South) configurations.
- Length of time for a gaming session is adjustable ranging from 15 seconds to 3 minutes.

These additional options, displayed in Figure 42 alongside the new game window, allow for the mouse sensitivity to be adjusted as well as the size of the paddle. Overall, difficultly experienced by the user can then be set to a level to challenge the users while still being within their abilities to complete. The final two windows of possible settings, as depicted in Figure 43, allow for both cosmetic and non-cosmetic changes to gameplay. These options allow the

appearance of the falling objects to change, (dotted spheres or soccer balls), as well the size and speed at which these objects move on the computer screen. These options are meant to better cater to the needs of each individual user.

The RTP game integrates an assessment tool for analyzing paddle movements. This assessment considers various metrics, including the success rate, response time, movement time, and absolute error, allowing for a comprehensive evaluation of the player's motor abilities. The assessment screen is shown in Figure 44. The output graph and features will be described in Chapter 5.

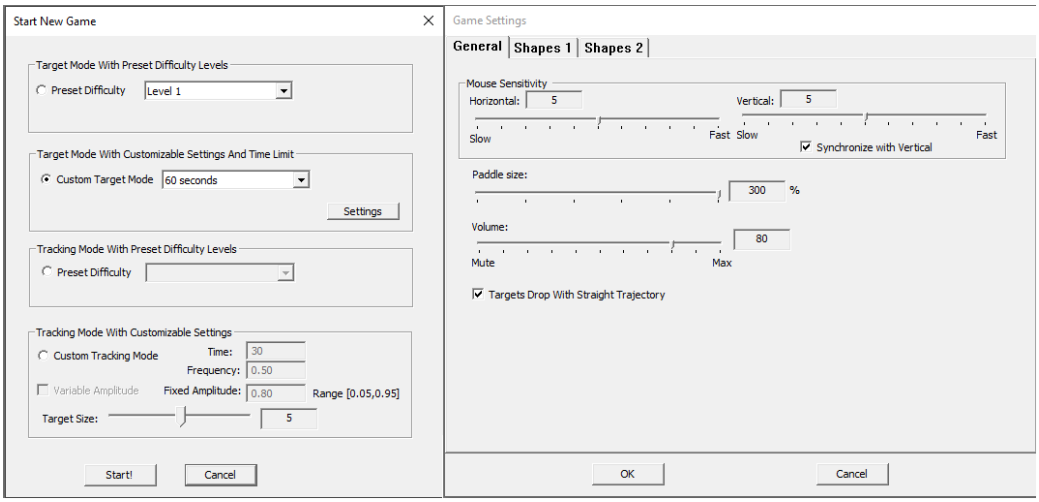

Figure 42: Game prompts and general game settings of the RTP game.

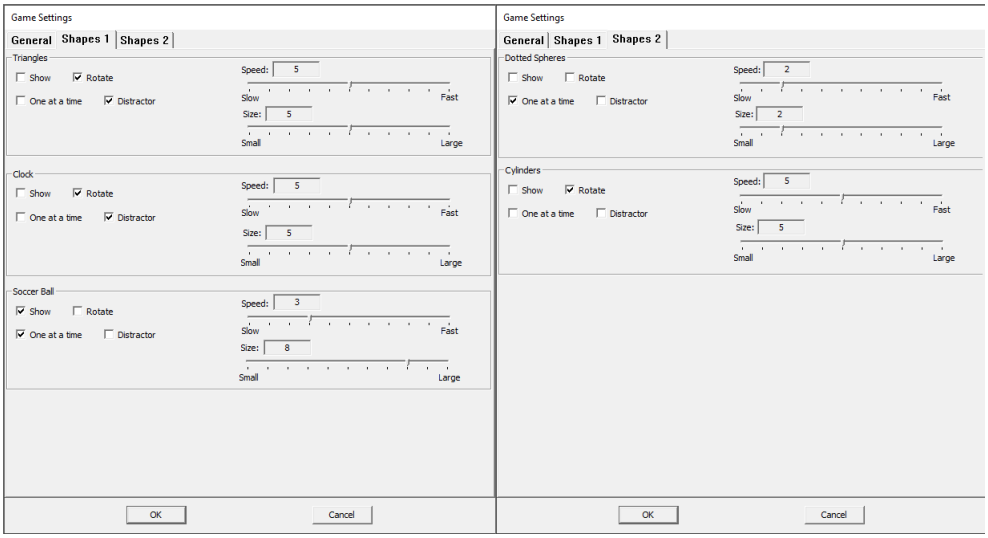

Figure 43: Shapes game settings of the RTP game.

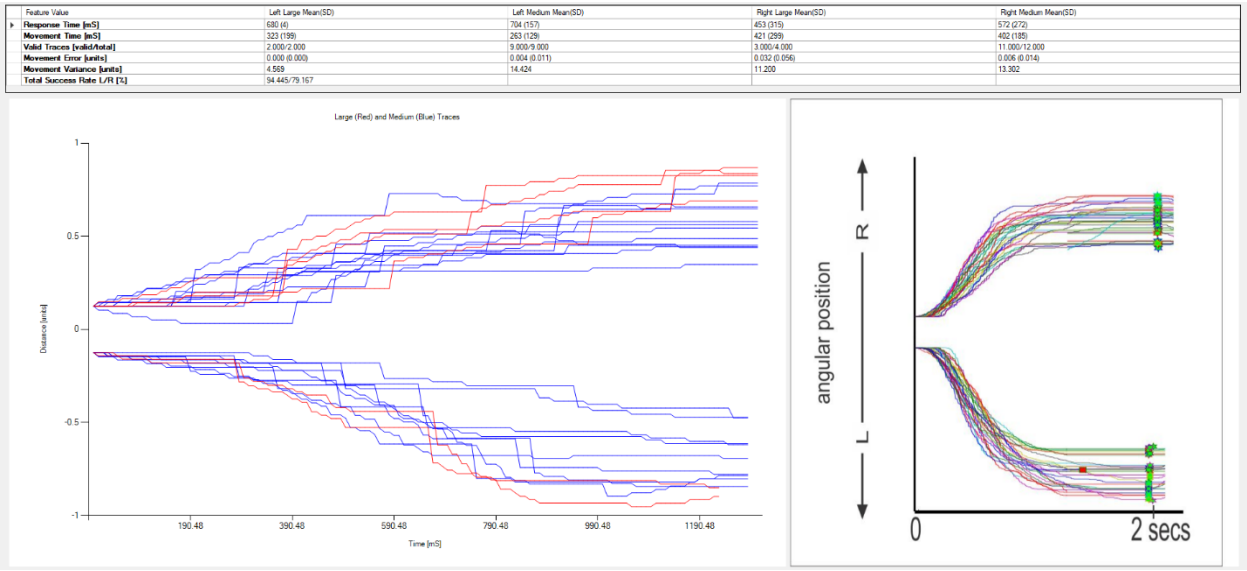

Figure 44: Game assessment screen of the RTP game.

The game records several statistics for each individual interaction event, which includes any movement of the paddle between the moment an object is generated until the same object disappears. These values include if an object is successfully intercepted or not, the time it takes for the user to react to the generation of a new object, the time it takes for the user to move the paddle to the interception point and the amount and direction by which the object is missed, when appropriate. The program processes these measurements and produces a table of average values, a graph along with the settings of the relevant session. These values, along with the accompanying graph, will be used by healthcare professionals to monitor and assess the rehabilitative progress of patients.

The source code of the RTP game has been modified to include a new feature in this thesis. This feature enables the game to send the "position difference" data, which represents the distance between the target ball and the paddle, along with its direction to the serial port. This information is sent every 10 ms, allowing the microcontroller to read and process it. Given this information, the controller can provide assistance by assisting the user in catching the ball or applying resistance in the opposite direction if needed. This modification enhances user experience by providing real-time assistance or resistance.

4.2 Development of Game Interface

Along with the newly developed physical interface, an accompanying set of software programs must be created. This is necessary for the proper functioning of the device for both the purposes of testing as well as for the proper utilization in the rehabilitative work undertaken by various healthcare professionals. The developed physical game interface required a unique program, which was developed as a single script in CircuitPython. CircuitPython is an open-source programming language designed for microcontrollers, which are small, single-board computers often used for embedded systems and electronics projects. It is a variant of the Python programming language that is optimized for ease of use and accessibility in the context of hardware development. The script is run on Raspberry Pi Pico W, which allows for real-time communication between the hardware and its corresponding software on an attached computer.

Note that although all the tasks are written in a single file program, the code consist of different sections and algorithms which are explained in the following.

4.2.1 Data Acquisition

In order to determine the state of the robotic manipulandum, encoders are utilized to measure the angles of each joint. These joint angle measurements enable controlling the movement of the mouse cursor on the computer screen, given the handle's motion. To accurately recreate the original analog signal from these discrete signals, ensuring a close match without missing any peaks or troughs, it is necessary for the sampling rate to exceed a certain value. The following calculation establishes the minimum required sampling rate.

The maximum frequency at which the human hand and wrist can move during high-speed sports activities, such as martial arts or certain types of drumming, is 5 Hz. This means the users can move the handle at a maximum frequency of 5 Hz. The cut-off frequency is defined as the upper limit of movement frequency that the system needs to detect and accurately reproduce. Frequencies beyond this threshold either do not occur under normal conditions or are not significant for analysis purposes in this case. Therefore, the cut-off frequency for these movements is established at 5 Hz. The Nyquist rate for this case is calculated in Equation (3).

$$Nyquist\ rate = 2f_c = 10\ Hz \tag{3}$$

Consequently, the sampling rate must be greater than or equal to the Nyquist rate to prevent aliasing.

A critical case happens when the cut-off frequency dominates the signal. Under such conditions, angular position of each link, θ, its derivative as well as its maximum derivative are presented in Equations (4), (5) and (6) respectively:

$$\theta(t) = \frac{FS}{2} sin(2\pi f_c t) \tag{4}$$

$$\frac{d\theta(t)}{dt} = FS\pi f_c\, cos(2\pi f_c t) \tag{5}$$

$$max\left(\frac{d\theta(t)}{dt}\right) = FS\pi f_c \tag{6}$$

where FS (Full Scale) is the amplitude of the signal. The calculation of the aperture time, T_a, is derived from Equation (7) [48]. To achieve a seamless interaction between the manipulandum and the game, quantization step, Q, must adhere to $Q = \frac{FS}{50}$. This quantization step ensures that game is responsive to the movements as small as two percent of the range of motion. Consequently, the sampling frequency, $f = \frac{1}{T_a}$, must be no less than the value expressed in (8).

$$T_a \leq \frac{Q}{max\left(\frac{d\theta(t)}{dt}\right)} = \frac{\frac{FS}{50}}{FS\pi f_c} = 1.27 \times 10^{-3}\ s \tag{7}$$

$$f \geq \frac{1}{7.64 \times 10^{-3}} = 785.4\ Hz \tag{8}$$

Since the data is acquired with the maximum output frequency of the sensors, i.e., 1 kHz, the required sampling frequency satisfies Inequality (8) and the Nyquist rate. Therefore, the analog input signal can be reconstructed with a small quantization error.

4.2.2 Emulating a Computer Mouse

The developed manipulandum emulates a computer mouse. By moving the handle, one can move the mouse cursor on the screen. It measures the angle of the joints and maps them into the linear motion of the mouse cursor within the computer monitor screen. Each joint angle can be mapped into cursor vertical or horizontal movement. For the third joint of the mechanism for example, it moves the mouse cursor vertically within the screen because it changes by ulnar and radial deviation, which is similar to a vertical movement making it more intuitive. In the program by choosing the joint which the user is going to use to play the game, the horizontal or vertical movement is chosen automatically. Moreover, the sensitivity will be adjusted based on the range of motion of that joint.

The manipulandum can also be used to play two-dimensional games. In this scenario, two encoders are read simultaneously: one maps to horizontal cursor movements, and the other to vertical movements. By manipulating the handle, it is possible to move the cursor in a straight diagonal line.

4.2.3 Receiving the Position Difference

The RTP game sends the position difference to the controller via serial communication through the serial port. The controller checks the serial port for reading the position difference. As soon as the position difference is sent to the serial port, it starts reading it character by character. The game sends the position difference with “enter”, “/n”, as the last character showing that the data package has ended. Therefore, as soon as the microcontroller reads “/n” it finds that the data package has ended and starts to reconstruct a number representing the position difference.

The position difference message is a signed number. In the horizontal mode, if it is positive, it means that the ball is on the right side of the paddle and when it is negative, it means the target ball is on the left side of the paddle. In the vertical mode, the positive position difference means the balls is higher that the paddle and vice versa. The position difference indicates the distance between the target ball and paddle as the percentage of the screen width in the horizontal mode and screen height in vertical mode. It ranges from -100 to 100. The position difference is 100 when the ball appears on the right edge of the screen and the paddle is on the left edge in the horizontal mode.

4.2.4 Monitoring and Control Algorithm

After receiving the position difference from the computer game, the microcontroller sends the necessary signals to the pressure regulators to adjust the pneumatic actuator forces, responsible for providing assistance or resistance based on the received position difference. Since in control theory, the difference between the desired output and the current output is called error, the term error is used instead of the position difference in the control algorithms. Different control modes that have been used with this device is described below.

A) Passive Mode:

No actuation force is required in this mode.

B) Assistive Mode:

The assistive modes are designed to help players in playing the game by applying force in right direction to help capturing the target ball.

I) Proportional Assistance:

$$F = k_p\, e \tag{3}$$

where F is actuation force. k_p is a constant proportional gain and e is the error or position difference received from the RTP game.

II) Proportional Assistive with threshold:

If the absolute value of the error is greater than a threshold, then a proportional assistive force is applied. Otherwise, the force will be zero.

$$\begin{cases} if\ \ abs(e) \leq threshold \ \rightarrow\ F = 0 \\ if\ \ abs(e) > threshold \ \rightarrow\ F = k_p\, e \end{cases} \tag{4}$$

where $abs(e)$ and $treshold$ are the absolute value of the error and a constant positive number chosen as the threshold, respectively.

III) Assistive with threshold:

If the absolute value of the error is greater than a threshold, then apply assistive force. This mode is different from proportional assistive with threshold, as it correlates not

directly with the error, but with the difference between the error and the threshold. This mode provides a continuous force, avoiding abrupt changes when the error exceeds the threshold in magnitude, unlike the previous mode.

$$\begin{cases} if\ \ abs(e) \leq threshold\ \rightarrow\ F\ =\ 0 \\ if\ \ abs(e) > threshold\ \rightarrow \begin{cases} if\ e > 0 \rightarrow F\ =\ k_p\ (e - threshold) \\ if\ e < 0 \rightarrow F\ =\ k_p\ (e + threshold) \end{cases} \end{cases} \quad (5)$$

IV) Assistive as needed:

If the absolute value of the error is greater than a threshold and the error is increasing, a proportional-derivative assistance force is applied. This assistive mode let the user to play the game and helps the user only when the magnitude of the error is increasing i.e. the paddle is not moving in the right direction.

$$\begin{cases} if\ \ abs(e) \leq threshold\ \ \rightarrow\ F\ =0 \\ if\ \ e > threshold\ \ and\ \ \dot{e} > 0\ \rightarrow\ F\ =\ k_p\ (e - threshold) + k_d\ \dot{e} \\ if\ e < -threshold\ and\ \ \dot{e} < 0\ \rightarrow F\ =\ k_p\ (e + threshold) + k_d\ \dot{e} \end{cases} \quad (6)$$

where $\dot{e}$ is the error derivative and k_d is a constant derivative gain.

C) Resistive Mode:

The resistive modes function in contrast to the assistive modes. They introduce a deliberate challenge to the gameplay by applying force in opposite direction to make it harder to capture the target ball.

I) Constant unidirectional force:

Regardless of the error a constant force (in an arbitrary direction) is applied, the value of which is determined by the user.

$$F = constant \quad (7)$$

II) Constant value resistive:

A constant force is applied in the opposite direction of the correct movement. The goal is to make it challenging to play the game by moving the paddle farther away from the ball.

$$\begin{cases} if\ abs(e) \leq threshold \ \rightarrow \ F = \ 0 \\ if\ e > \ +threshold \ \rightarrow F = +constant \\ if\ e < -threshold \ \rightarrow F = \ -constant \end{cases} \quad (8)$$

III) Inverse Proportional Resistive:

The force of this resistive mode is proportional to the inverse of the error, i.e. it increases as the paddle gets closer to the target. Since this can result in an extremely large force being applied when the error becomes negligible, a saturation filter is used to maintain the force value in a limited range. Also, adding a threshold, prevents applying very large forces if the error is too small to be noticeable.

$$\begin{cases} if\ abs(e) < threshold \quad \rightarrow \quad F = \ 0 \\ if\ e > \ +threshold \ \rightarrow F = k_p \left(\frac{1}{e - threshold}\right) \\ if\ e < -threshold \ \rightarrow F = k_p \left(\frac{1}{e + threshold}\right) \end{cases} \quad (9)$$

IV) Random disturbance force:

In this mode a random force will disturb user movement with the frequency of 10 Hz.

The above algorithms calculate the actuation force ranging between -100 and 100. This number represents the percentage of the maximum actuators force. Therefore, if the formulas calculate a force greater than 100 it will be substitute with 100 because the actuator cannot make larger forces. This percentage is used to produce PWM signals for the PGIO pins connected to digital to analog convertors. The Digital to analog convertors produce analog voltages according to the PWM signals. These analog voltages then activate the pressure regulators changing the pressure inside each chamber of the actuators and therefore adjusting the actuators force. The PWM digital to analog converters can distinguish changes as small as 0.1% in PWM signal levels. This sensitivity allows the converter to have a minimum increment of input PWM that changes the output voltage by 0.1%, resulting in 1000 distinct levels. This corresponds to a resolution of approximately 10 bits (since $2^{10} = 1024$). Therefore, the voltage and force resolution can be calculated as in Equation (15) and (16) respectively.

$$Voltage\ resolution\ = \frac{Vmax}{Number\ of\ levels} = \frac{10\ V}{1000} = 0.01\ V \quad (10)$$

$$Force\ resolution = \frac{F_{max}}{Number\ of\ levels} = \frac{4.65\ lbf}{1000} = 0.00465\ lbf \quad (11)$$

This resolution and granularity is enough to have precise control over pressure and force for this project.

Based on the direction of the calculated force, only one of the actuator chambers is pressurized at a time, while the other chamber remains at atmospheric pressure. It is also worth noting that the output of these control modes is saved in a text file with the corresponding time. This enables recording the exerted force and observing its effect on the user's performance.

4.3 Summary

This chapter described the development of the software components crucial to the functionality of the proposed rehabilitation device. It outlined two main components: The RTP game, a pre-existing interactive computer program and, the microcontroller program developed for the Raspberry Pi Pico W.

The RTP game, designed for diagnostic and rehabilitative purposes at the University of Manitoba's College of Rehabilitation, serves as an interactive therapeutic exercise tool. The game involves catching falling objects with a player-controlled paddle, allowing for customizable difficulty levels and user movement tracking. Insights into the game settings, showcasing screenshots and illustrations were provided. Emphasis was placed on the recording and analysis of gameplay performance statistics, offering valuable data for healthcare professionals to monitor patients' rehabilitative progress.

The microcontroller program, implemented on the Raspberry Pi Pico W, has been written in CircuitPython, an open-source language designed for microcontrollers. The program is segmented into various sections, each serving specific tasks.

- Emulating a Computer Mouse: The microcontroller emulates a computer mouse, translating handle movements into cursor movements on the computer screen. Sensitivity adjustments can be made based on the selected joint for gameplay.
- Reading the Position Difference: The program reads position difference sent by the RTP game through the serial port. The position difference, representing the distance between the target ball and the paddle as well as the direction, is used for subsequent control adjustments.
- Control Algorithm: The microcontroller employs different control modes, including passive mode, assistive modes with various strategies, as well as resistive modes with constant, proportional, or random disturbance forces. These modes aim to provide assistance or resistance for the user while playing the RTP game.

The chapter concludes by highlighting the interconnectivity between the software and hardware components. It underscores the critical role of the microcontroller in reading position difference, processing control algorithms, and regulating actuators to provide tailored assistance or resistance during gameplay. Additionally, the interface records the exerted force for further analysis, contributing to a comprehensive understanding of the device influence on the user performance.

V. PILOT STUDIES

5.1 Testing Procedure

The prototype of the robotic manipulandum can be seen in Figure 45. The design involves the development of a robotically enhanced user interface for a pre-existing program (RTP game), that has been utilized in current neurological rehabilitative activities. As the design is eventually meant to be used by individuals with limited physical abilities, the usability of the developed design needs to be verified before its introduction to actual patients undergoing treatment. The best way to confirm usability for the design is to test it with individuals who are not undergoing rehabilitative treatment, recording and examining their performances and making notes of suggestions offered or issues noticed during use. Therefore, the developed device incorporating different control modes was tested by multiple subjects. Relevant data were gathered as well as any notable observations or comments.

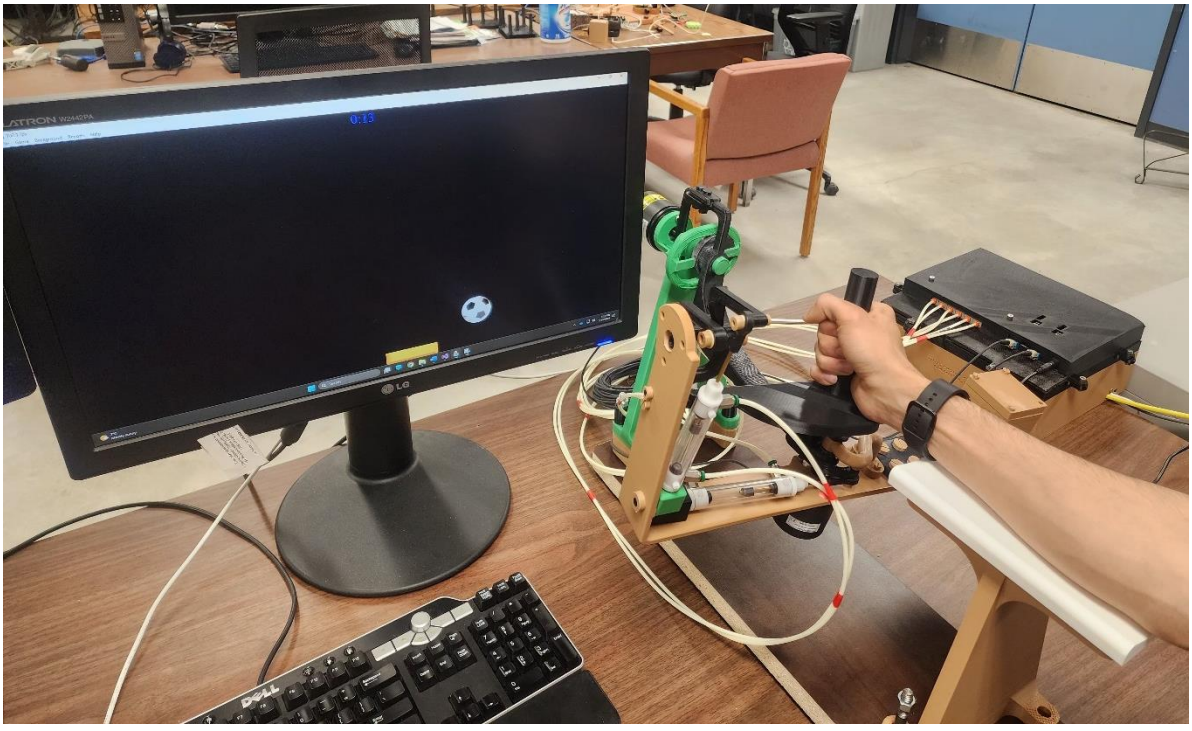

Figure 45: Wrist robotic manipulandum integrated with RTP game.

Data logs taken during these trial runs performed with 10 participants were then plotted into a series of graphs. None of these participants were undertaking or in need of any neurological

rehabilitative therapy. All participants were right-handed, consisting of 2 females and 8 males. Each participant played the RTP game once with the device, testing each control mode across all three joints. Except for joint 1, pronation/supination, only passive, proportional assistive and constant resistive modes were tested. The actuation modes sequence for each user was assigned randomly. These trials aimed to evaluate the device's effectiveness on user performance.

Since the RTP game is a one-dimensional game, the tests were done by only activating one joint at a time. The users played the game with one joint corresponding to the paddle movement at a time. The following table shows the RTP game settings for each joint.

Table 1: The RTP game settings for each joint.

	Joint1	Joint 2	Joint 3
Movement	Pronation/Supination	Extension/Flexion	Ulnar/Radial deviation
Mouse sensitivity	5	5	5
Paddle size	75%	75%	125%
Target speed	6	6	6
Target size	3	3	7
Time	60 s	60 s	60 s
Target trajectory	Straight	Straight	Straight
Paddle movement	Horizontal	Horizontal	Vertical

The tests were conducted with the parameters set as follows: $k_p = 100$, $k_d = 5$, $\text{constant} = 3$, and $\text{threshold} = 0.15$. The value of threshold has been chosen arbitrarily here and can be determined based on key performance indicators in future.

5.2 Results and Discussion

5.2.1 Qualitative Analysis

The plot depicted in Figure 46 shows a set of typical paddle traces for a user without an impairment playing the RTP game. This graph is displayed alongside each new graph in the RTP game, serving as a reference for comparison. Each line represents the paddle displacement from the moment the ball appears on the screen until it disappears either hitting the paddle or being

missed. The speed of the game remained constant throughout the entire gameplay, resulting in similar durations of movement for the balls, with some exceptions for the slightly longer movements of the lost balls which move until the end of the screen.

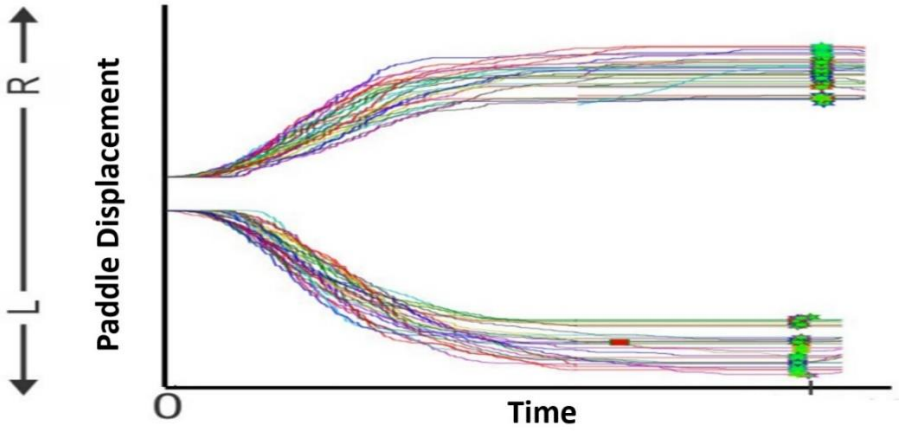

Figure 46: Typical paddle traces shown in the RTP game.

The game data and performance of the player are stored in a text file. Also, the force data is stored in a text file within the Raspberry Pi Pico Memory. MATLAB was used to read the output text files, compute and plot the outcomes of the RTP game as well as the forces.

The traces are classified into three groups of large, medium, and small movements in The RTP game. If the distance between the ball and the paddle, the moment the target ball appears is greater than 66% of the screen size, the paddle trace is considered a large trace. If this number is between 20% and 66%, it is a medium trace any number smaller than 20% is considered a small trace.

Since the movement in large and medium traces is long enough to analyze, the focus is placed on those movements in this thesis. In addition, there are only a few large traces in each gameplay and most of the traces are medium. Therefore, analyzing the medium traces is of great importance compared to the large and small traces. Typical large and medium traces of the paddle in various control modes for wrist extension/flexion, played by a subject (subject 3) are plotted. The following figures provide overlay plots of game movement responses in each direction for each game trial by subject 3.

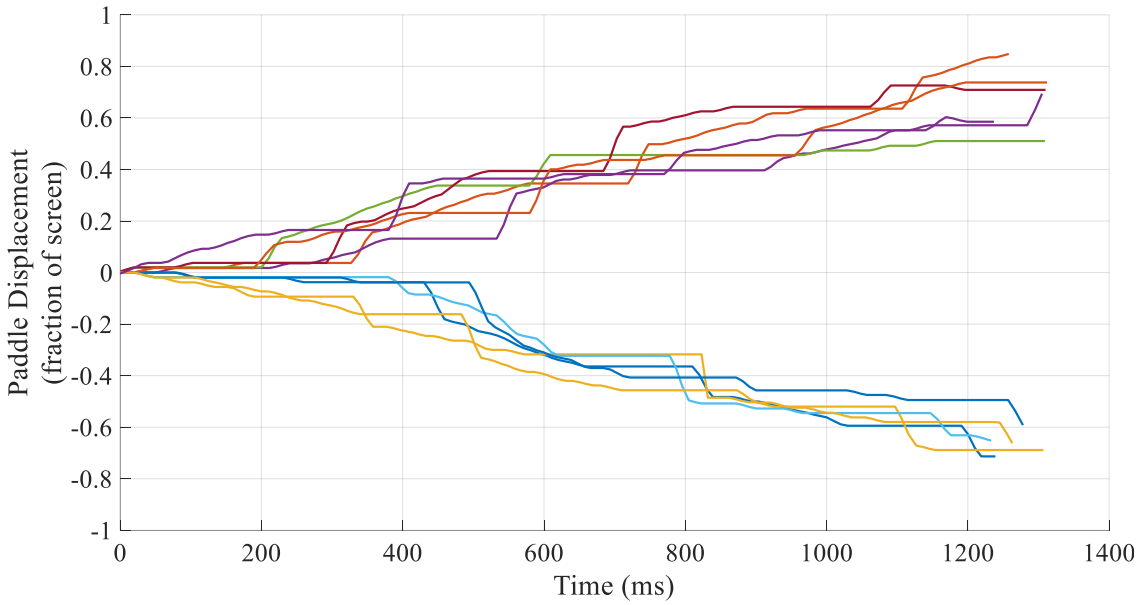

Figure 47: Normalized game traces- passive mode – second joint – extension/flexion – subject 3.

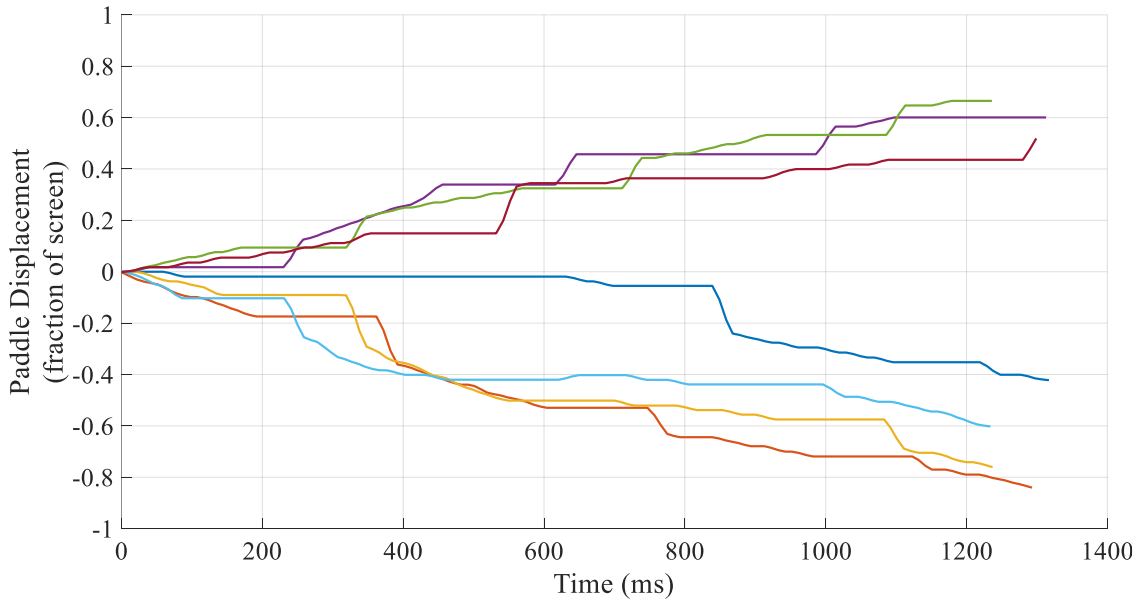

Figure 48: Normalized game traces – constant resistive with threshold force mode – second joint – extension/flexion – subject 3.

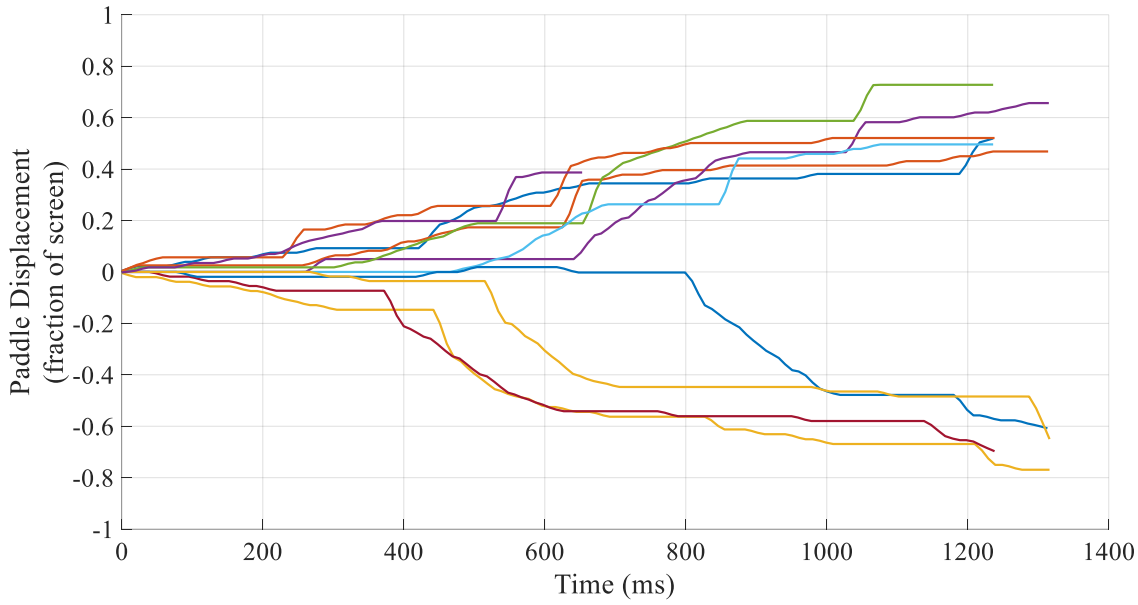

Figure 49: Normalized game traces – inverse proportional resistive force mode – second joint – extension/flexion – subject 3.

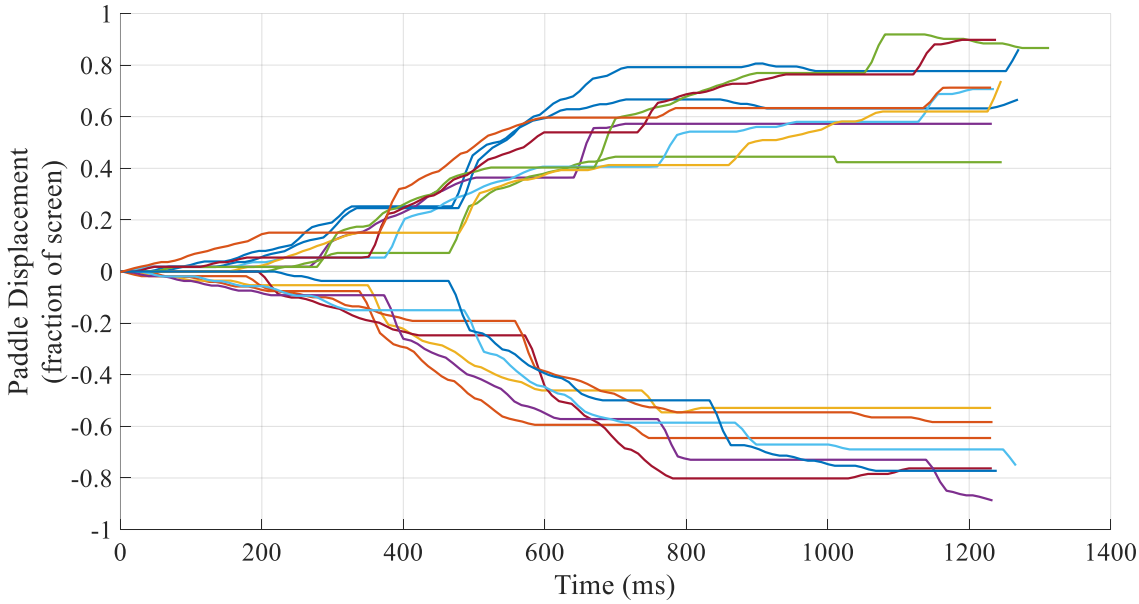

Figure 50: Normalized game traces – proportional assistive with threshold force mode – second joint – extension/flexion – subject 3.

Figures 52 to 56 show the corresponding position differences pertaining figures 47 to 51. They represent the difference between the position of the target ball and the paddle during large and medium paddle movements as in (15). The samples are for subject 3 data log.

$$Position\ Difference = X_{target} - X_{Paddle} \quad (12)$$

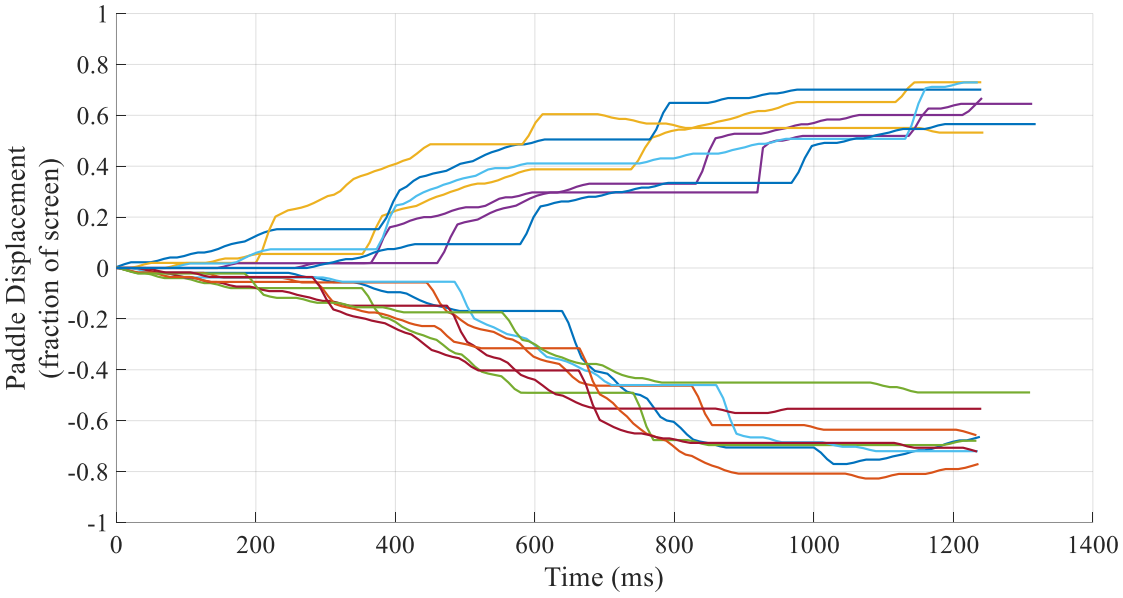

Figure 51: Normalized game traces – assistive as needed force mode – second joint – extension/flexion – subject 3.

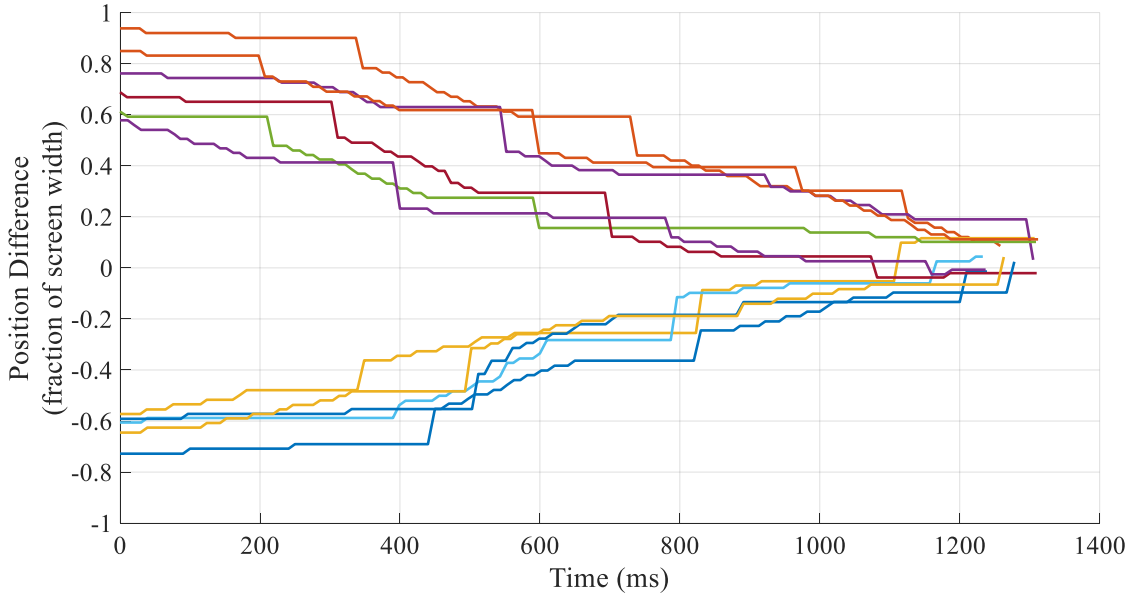

Figure 52: Normalized game position difference – passive mode – second joint – extension/flexion – subject 3.

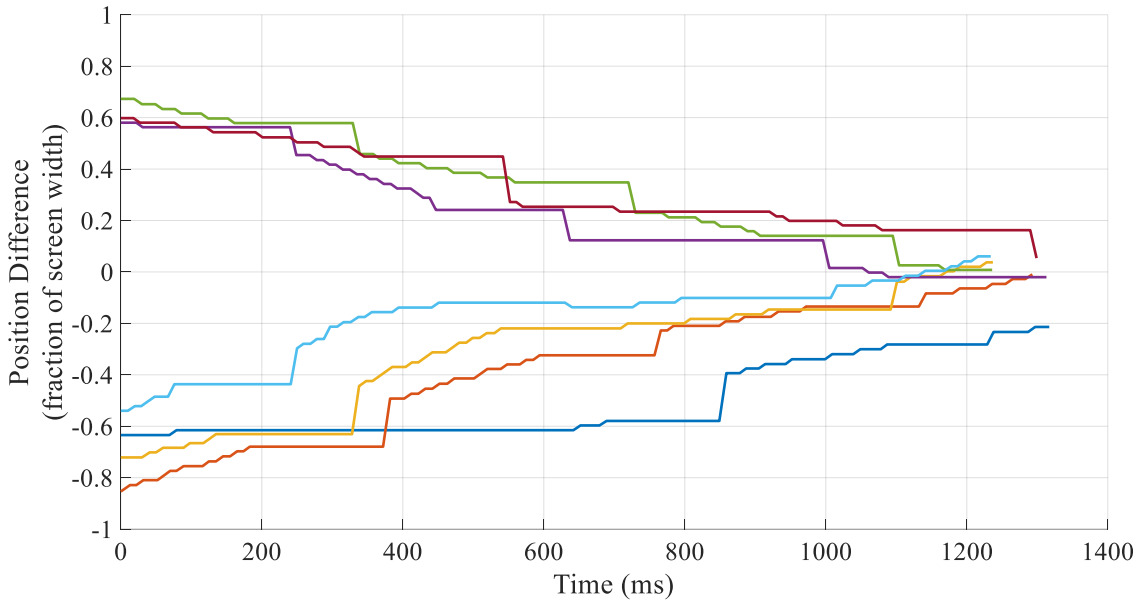

Figure 53: Normalized game position difference – constant resistive with threshold force mode – second joint – extension/flexion – subject 3.

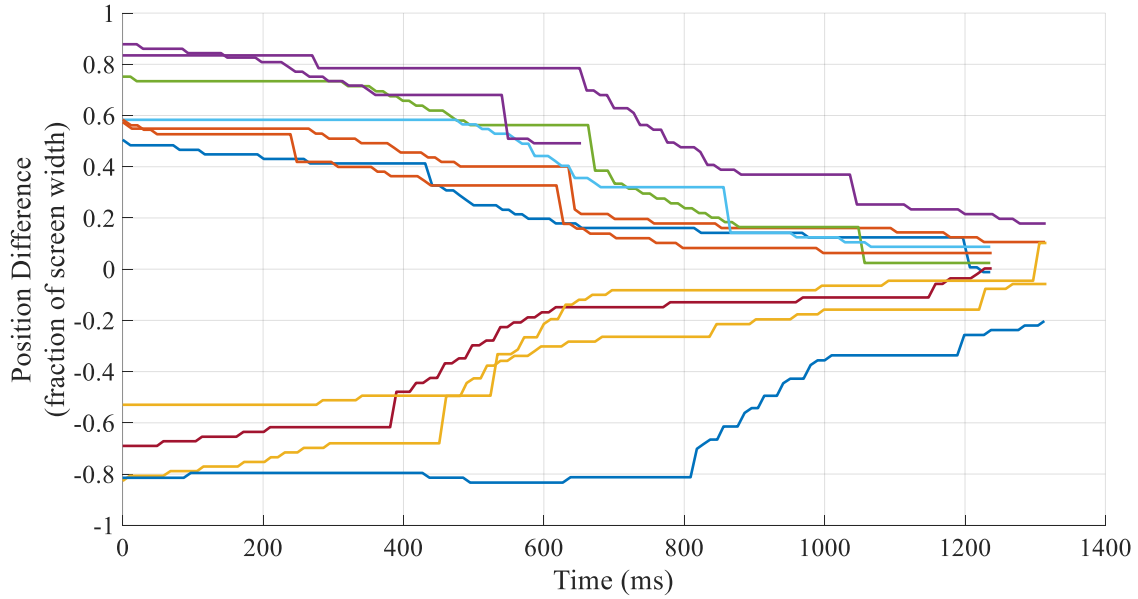

Figure 54: Normalized game position difference – inverse proportional resistive force mode – second joint – extension/flexion – subject 3.

From the shown figures, it is observed that, the position difference for different targets converge to zero eventually. However, by comparing the passive mode in Figure 52 with resistive modes shown in Figure 53 and Figure 54, it is seen that in the resistive modes, it took longer for the position difference to converge to zero compared to the passive mode.

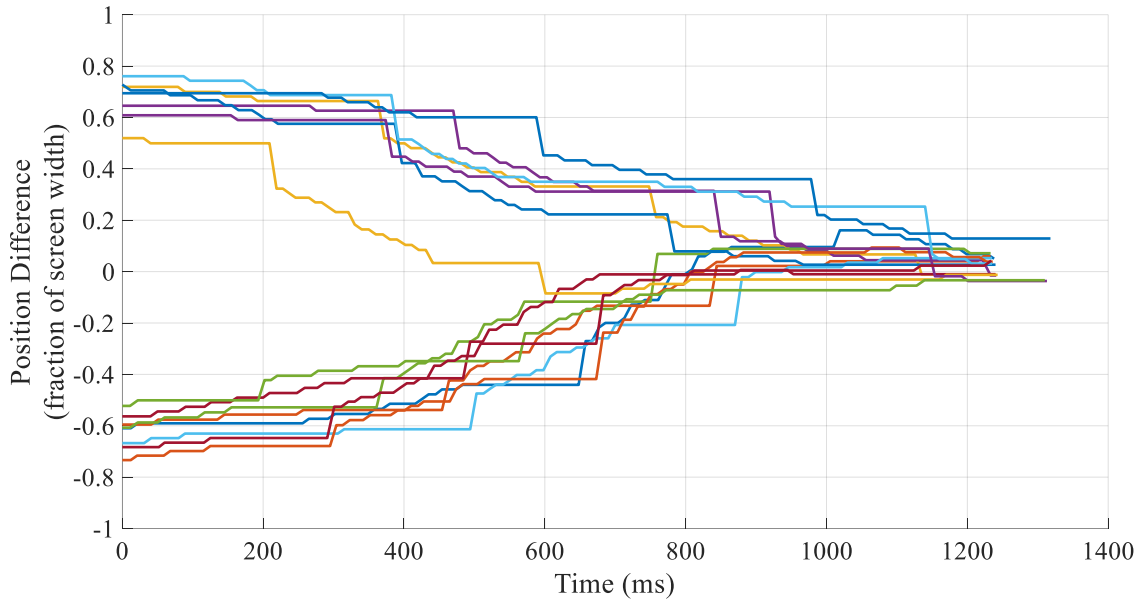

Figure 55: Normalized game position difference – proportional assistive with threshold force mode – second joint – extension/flexion- subject 3.

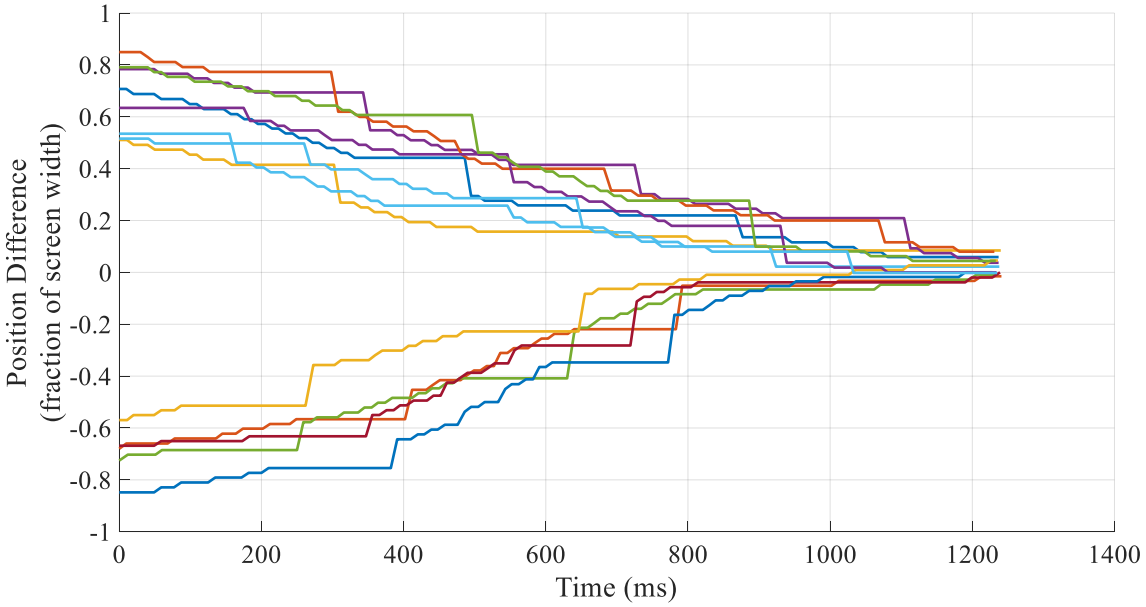

Figure 56: Normalized game position difference – assistive as needed force mode – second joint – extension/flexion – subject 3.

On the other hand, the assistive modes, shown in Figure 55 and Figure 56 helped the user to minimize the position difference more quickly compared to the other modes. The resistive and assistive forces, alongside the position difference or the error for subject 3 during the wrist extension/flexion activities in each actuation mode, are presented in Figure 57 to Figure 64.

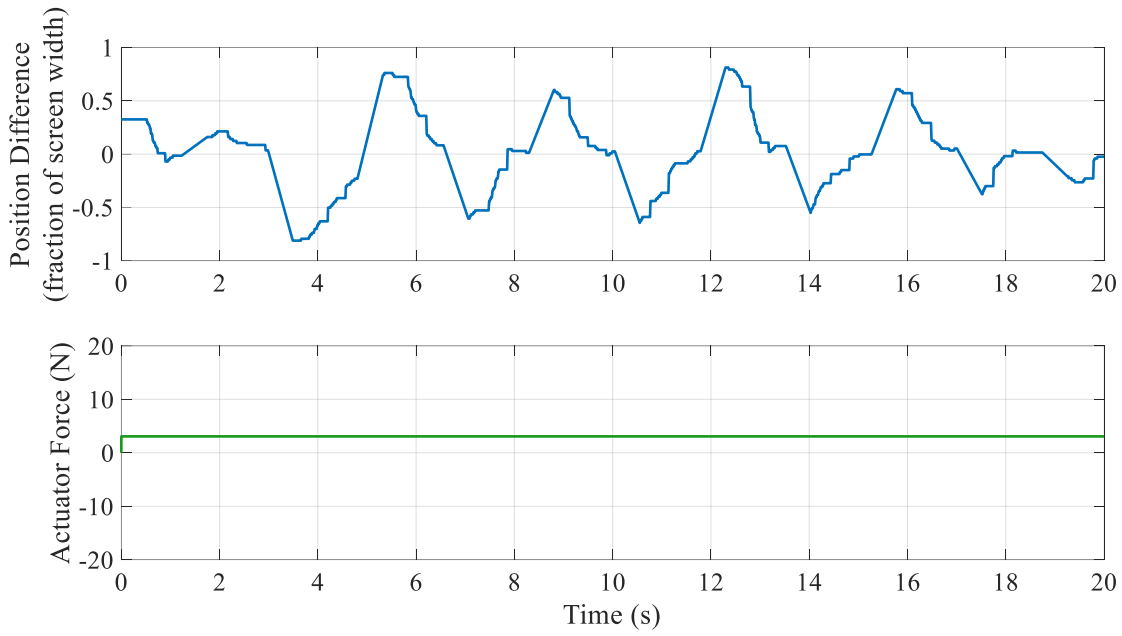

Figure 57: Actuator force and normalized position difference – unidirectional mode – second joint – extension/flexion – subject 3.

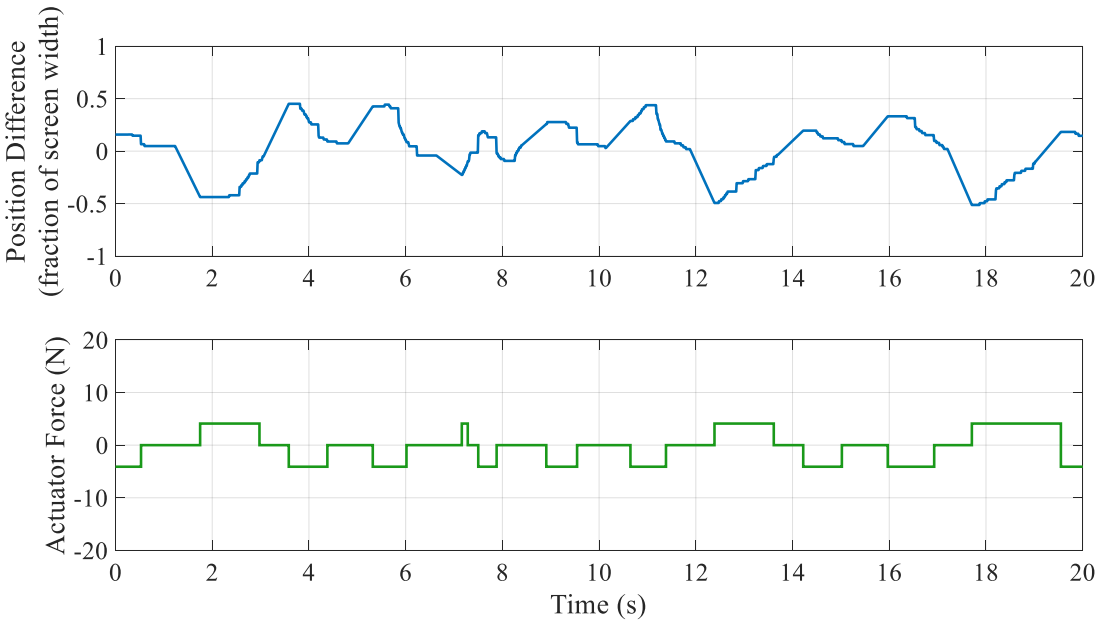

Figure 58: Actuator force and normalized position difference – constant resistive mode – second joint – extension/flexion – subject 3.

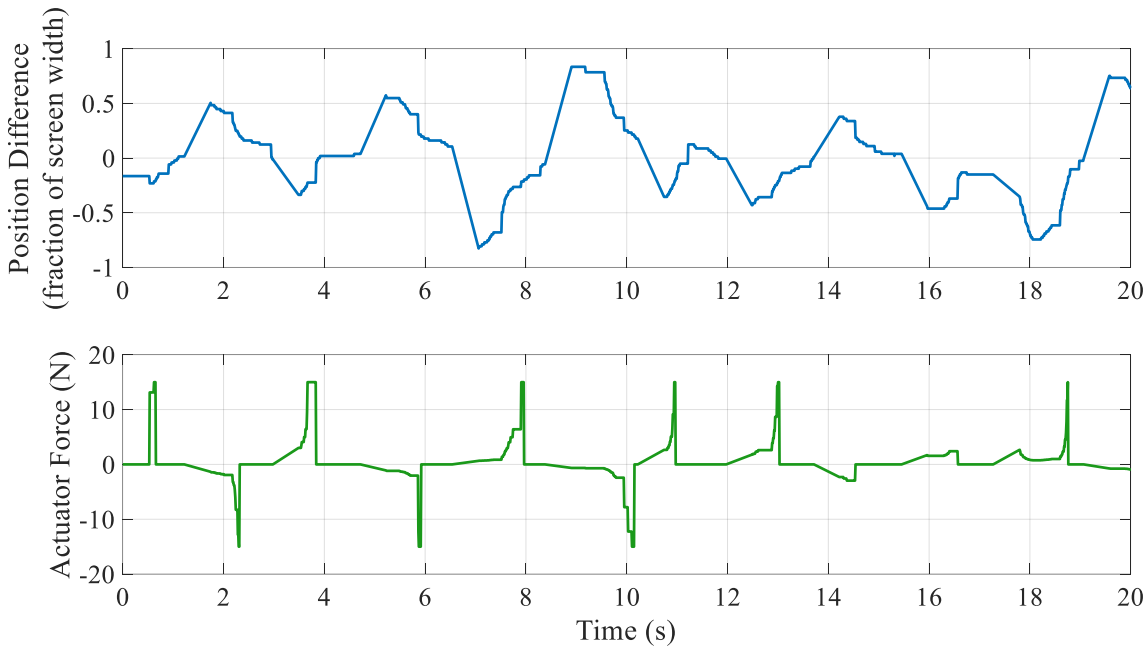

Figure 59: Actuator force and normalized position difference – inverse proportional resistive mode – second joint – extension/flexion – subject 3.

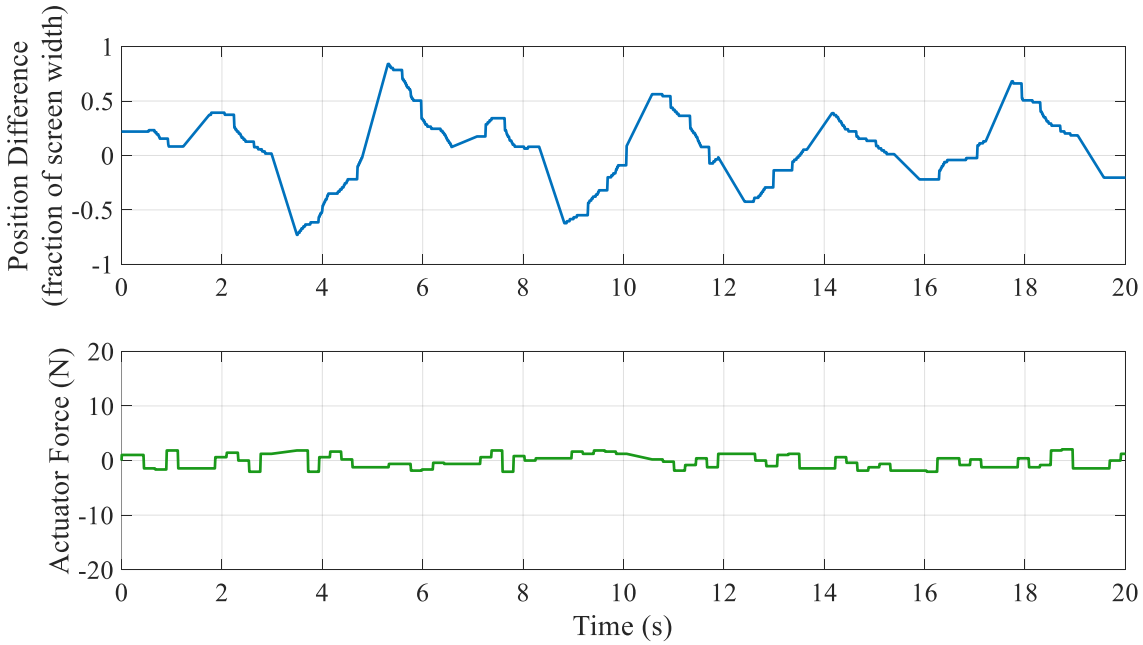

Figure 60: Actuator force and normalized position difference – random disturbance mode – second joint – extension/flexion – subject 3.

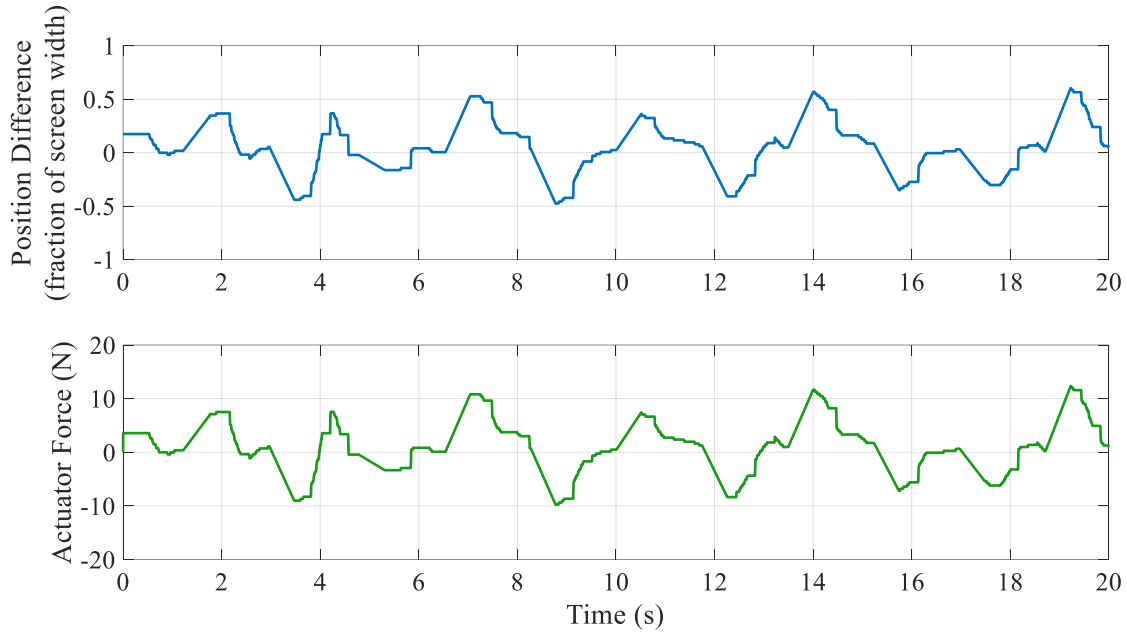

Figure 61: Actuator force and normalized position difference – proportional assistive mode– second joint – extension/flexion – subject 3.

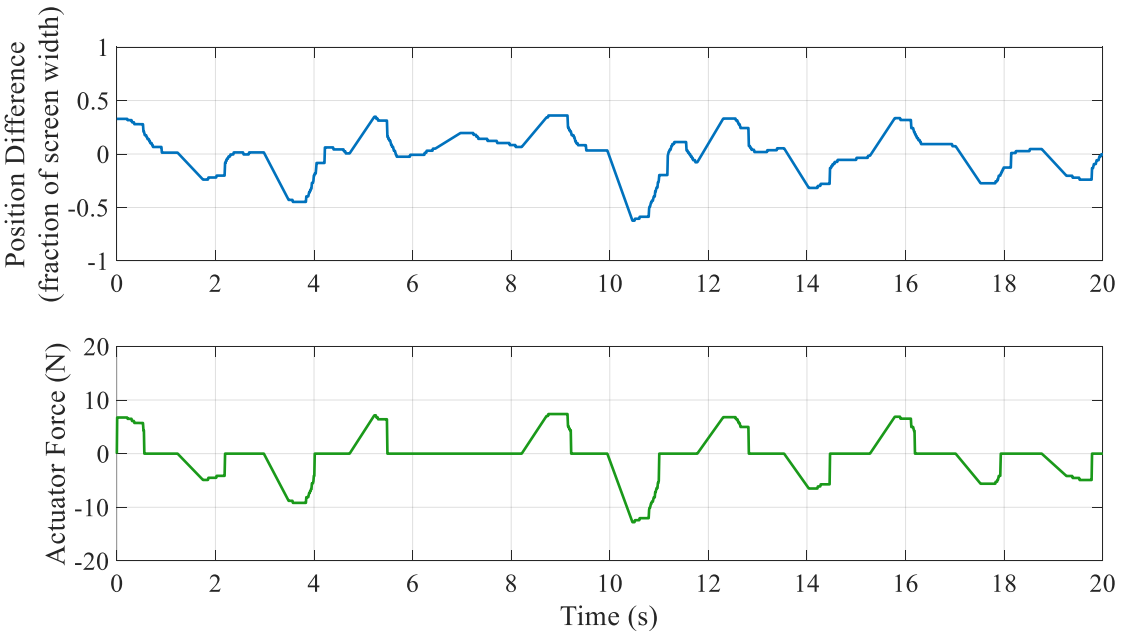

Figure 62: Actuator force and normalized position difference – proportional assistive with threshold mode – second joint – extension/flexion – subject 3.

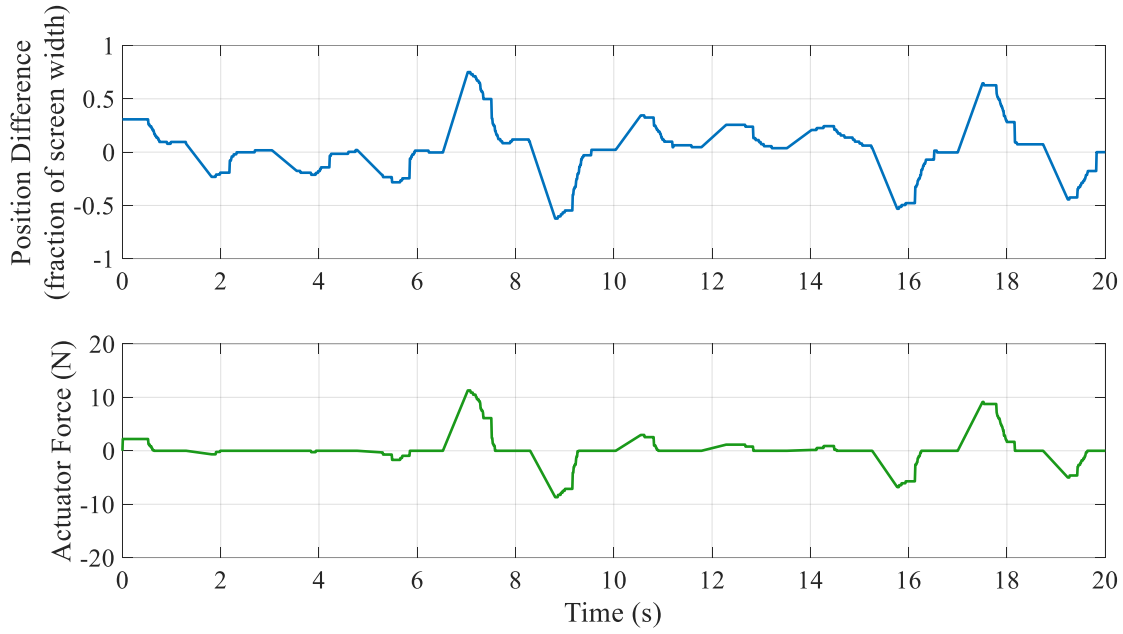

Figure 63: Actuator force and normalized position difference – assistive with threshold mode – second joint – extension/flexion – subject 3.

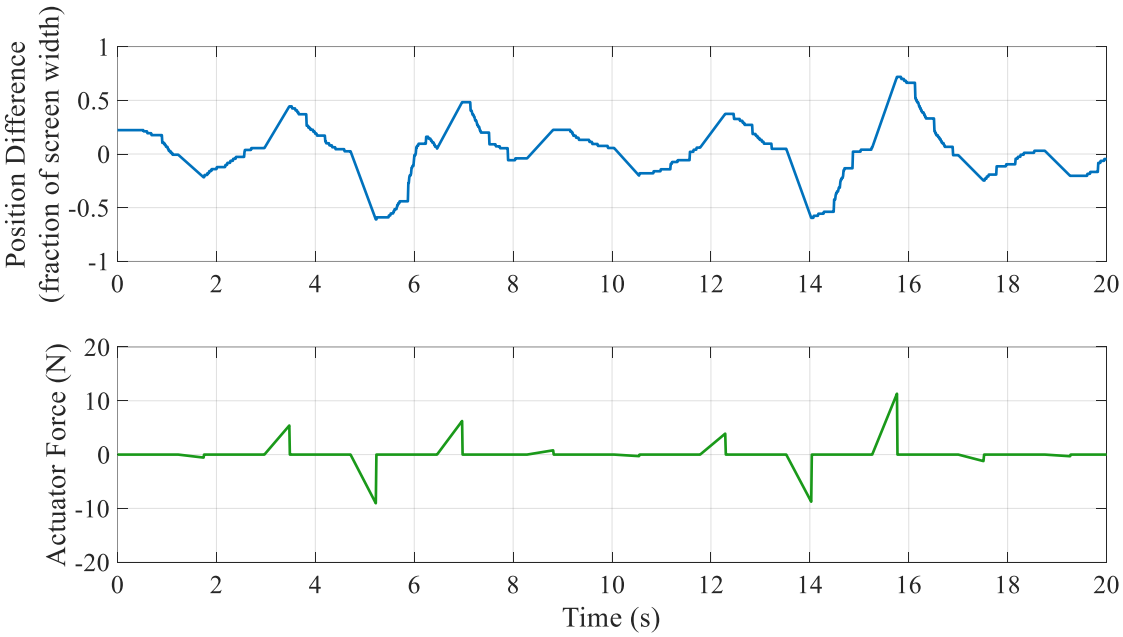

Figure 64: Actuator force and normalized position difference – assistive as needed mode – second joint – extension/flexion – subject 3.

5.2.2 Quantitative Analysis

The subjective nature of game performance poses challenges when attempting to compare the performance of different subjects. Such comparisons can be highly subjective, making it challenging to derive meaningful data. A more suitable approach involves comparing the average performance across all subjects. However, this requires multiple datasets obtained from various control modes and users over an extended period of time to ensure objectivity in the analysis. In order to study the users' performance more in depth in different control modes, the following performance measures were quantified:

- Success Rate: It is the percentage of the total number of target objects that were caught by the paddle in one game trial.
- Response Time: It is the time from target appearance to the start of the game paddle movement. Values for response time are determined for each game movement response, and then the average is computed over the group of game movement responses for each direction.
- Movement Time: It is the time from the start of the game paddle movement to the moment the distance between the target ball and paddle reaches 10 % of the initial distance. Values for response time are determined for each game movement response, and then the average is computed over the group of game movement responses for each direction.
- Average Absolute Error: It is the average of distances between the target ball and the paddle when the target ball disappears hitting either the bottom, in the horizontal mode, or the left in the vertical mode. These distances are presented in percentage of screen width or height. This is a good measure of performance as it considers how close the user could get to the target even though the target ball was missed, whereas the success rate only shows how many targets ball the player has caught.

The following graphs, show plots of the average response time, the average movement time, average success rate and average absolute error for data collected when using the developed robot and game interface.

Figure 65 to Figure 70 depict the average response time and movement time, derived from data collected during the game interface testing. Separate calculations were performed for the

averages across all assistive and resistive modes. The illustrations provide insights into the overall performance metrics in various gaming scenarios. It is worth noting that for any of the joints, the direction of the movement is very important, and the paddle traces have to be separately analysed as movement in each direction involves different sets of muscles and neurons.

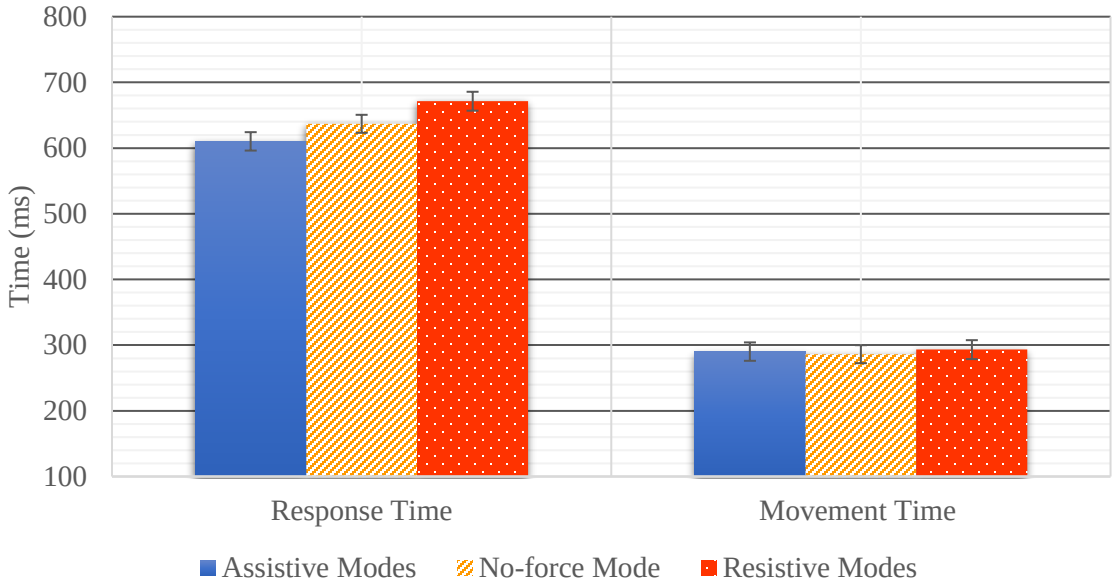

Figure 65: Average response and movement time – joint 1 – pronation.

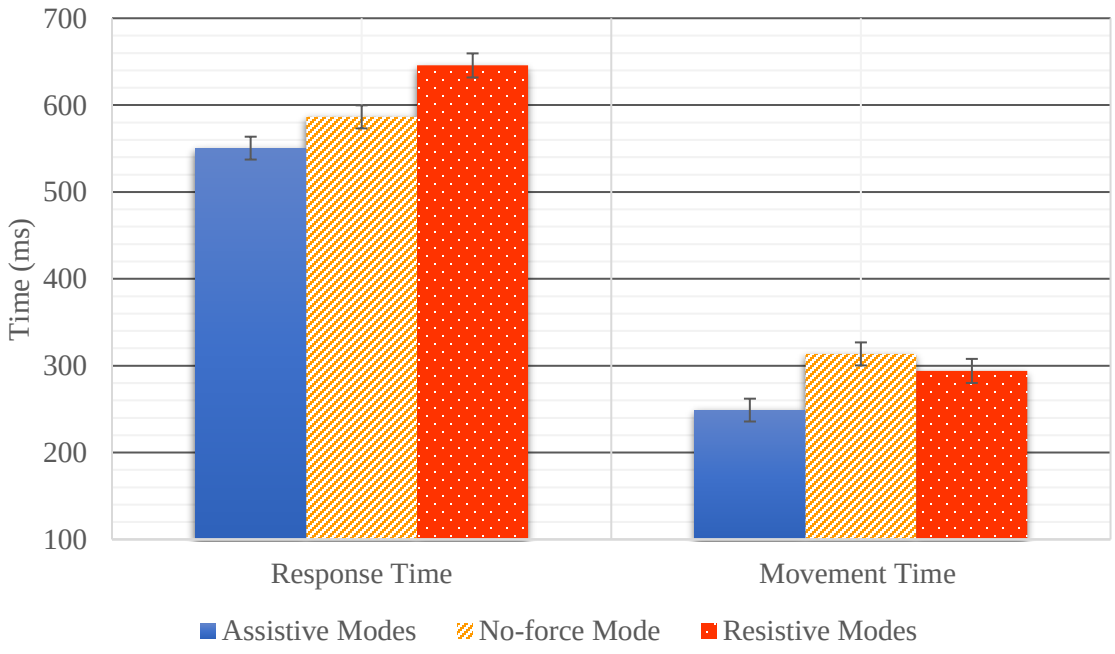

Figure 66: Average response and movement time – joint 1 – supination.

As it can be seen in Figure 65 the average response time over all the assistive modes for pronation were smaller than the mode without actuation. Moreover, the average response time over all the resistive modes for pronation was larger than the other two modes. The actuation force in the assistive mode helps the user to move the paddle towards the target ball and in the resistive modes it challenges the user by exerting force in the opposite direction of the right movement. Therefore, the actuation force helps to move the handle faster and in the assistive modes and slower in the resistive mode compared to the case when there is no actuation. Also, the average movement time over all assistive modes is slightly smaller the passive mode. The corresponding number in the resistive modes is slightly higher.

In Figure 66, the same pattern of smaller average response time and movement time in assistive modes can be observed for supination. However, the average movement time for the resistive modes is slightly smaller than the passive mode. On the other hand, average response time in the resistive modes is greater than the passive mode, making the sum of response time and movement time larger for the resistive modes. The same pattern of shorter response and movement time for assistive modes and longer times for resistive modes compared to the passive mode is observed for join 2 and joint 3, wrist flexion/extension and ulnar radial deviation.

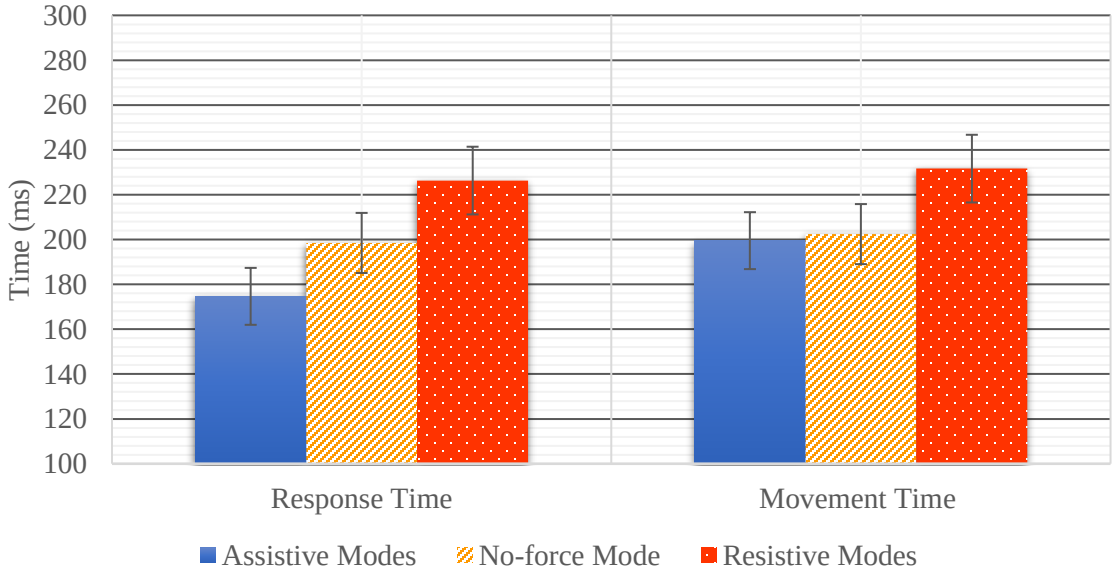

Figure 67: Average response and movement time – joint 2 – extension.

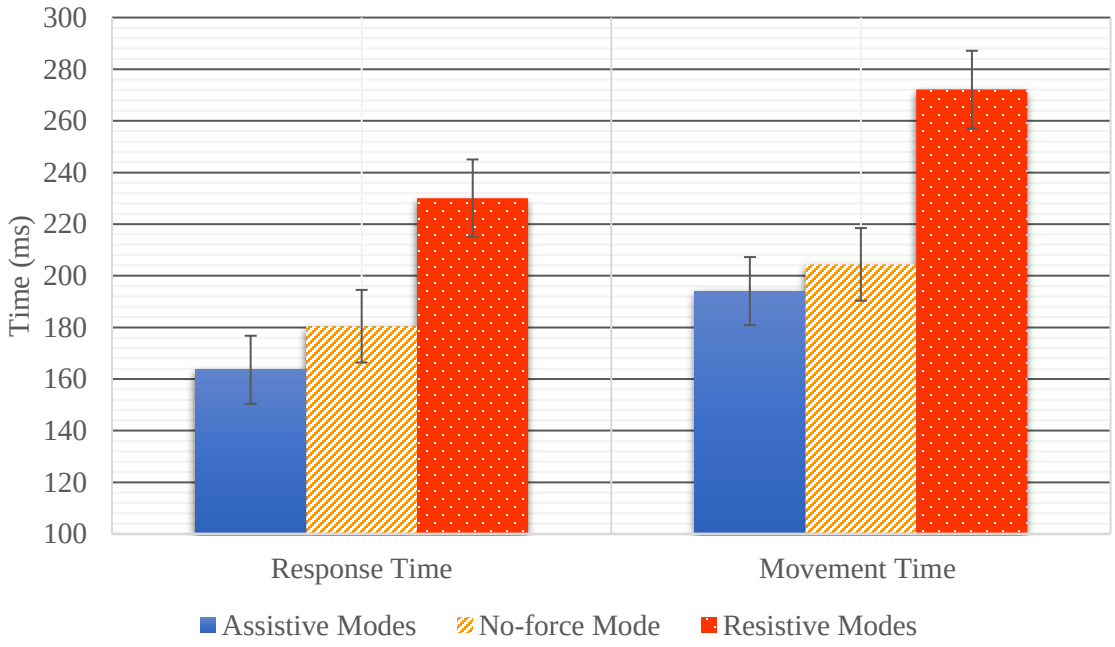

Figure 68: Average response and movement time – joint 2 – flexion.

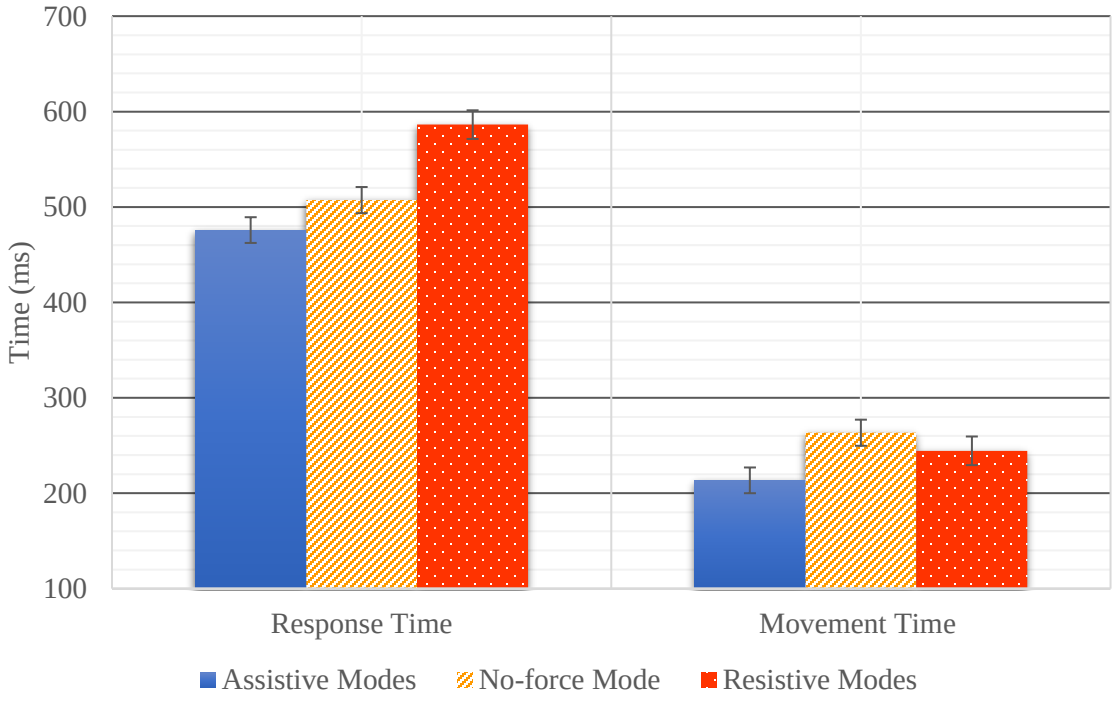

Figure 69: Average response and movement time – joint 3 – ulnar deviation.

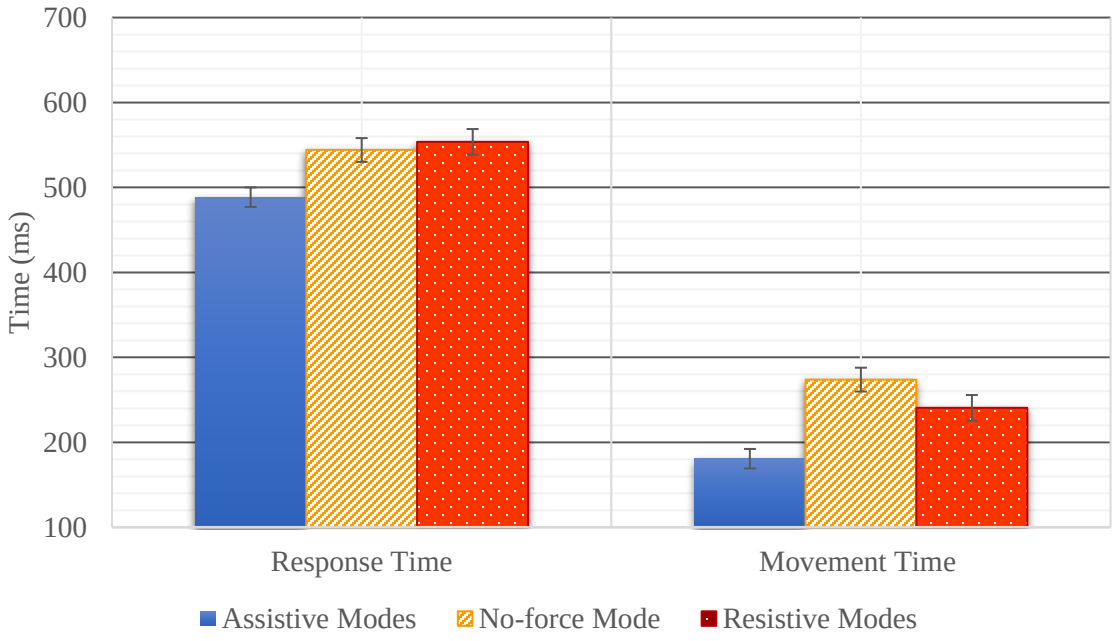

Figure 70: Average response and movement time – joint 3 – radial deviation.

Figures 67 and 68 show, the success rate and absolute error for joint 1 trials, respectively.

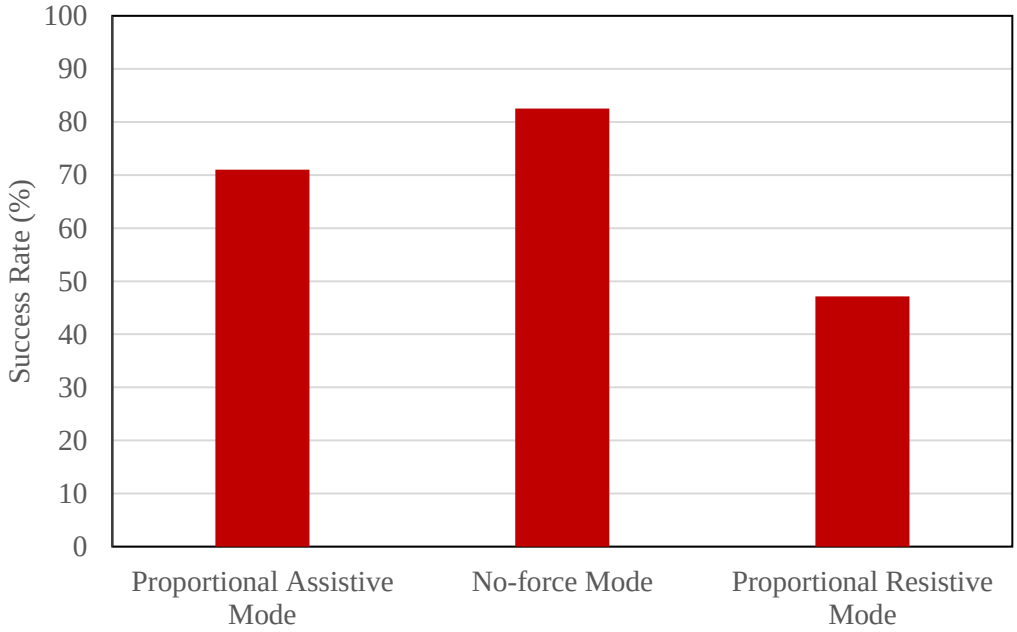

Figure 71: Average success rate – joint 1 – pronation.

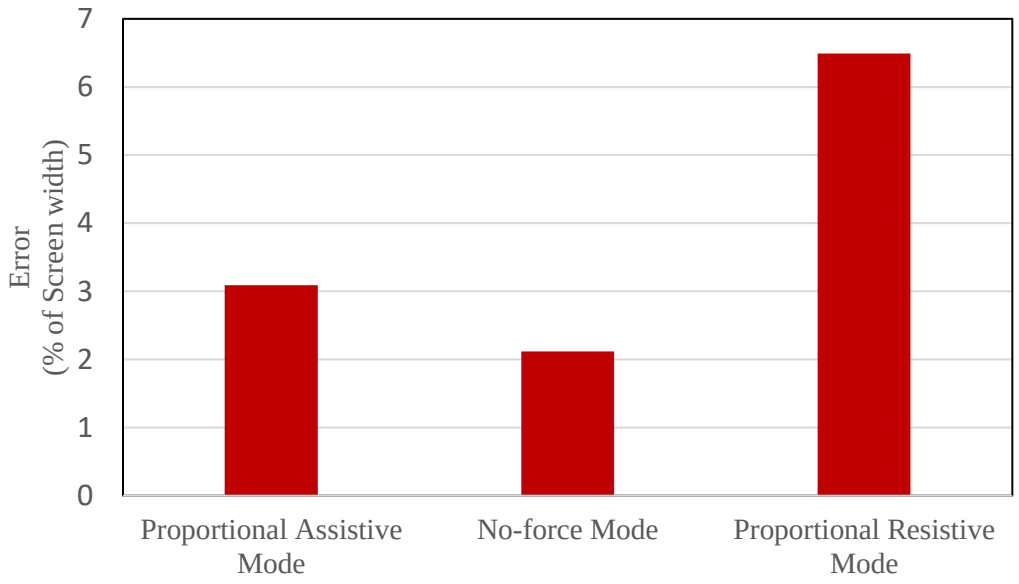

Figure 72: Average absolute error – joint 1 – pronation.

As it can be seen in Figure 71, the success rate for the proportional assistive mode was slightly lower than the mode without force. That is because of the overshoot caused by the proportional controller. The subject has to manage the overshoot which was rather challenging compared to the normal mode without force. However, the proportional resistive reduced the success rate significantly, proving that this mode has been effective and challenging the user compared to the normal mode. The average absolute error for joint 1 for the same reasons shows similar results.

In order to compare the effects of different control algorithms, the average success rate and absolute error are plotted for each assistive and resistive mode separately. Figures 69 to 72 show the success rate and absolute error for wrist extension with different control modes.

With reference to Figure 73, the proportional assistive mode exhibits the lowest success rate, primarily attributed to the overshoot produced by this control mode. Users encountered difficulty in suppressing the overshoot in this mode. Introducing a threshold, wherein the position difference is less than 15 percent of the screen width or height for horizontal and vertical modes, respectively, helped mitigate this issue.

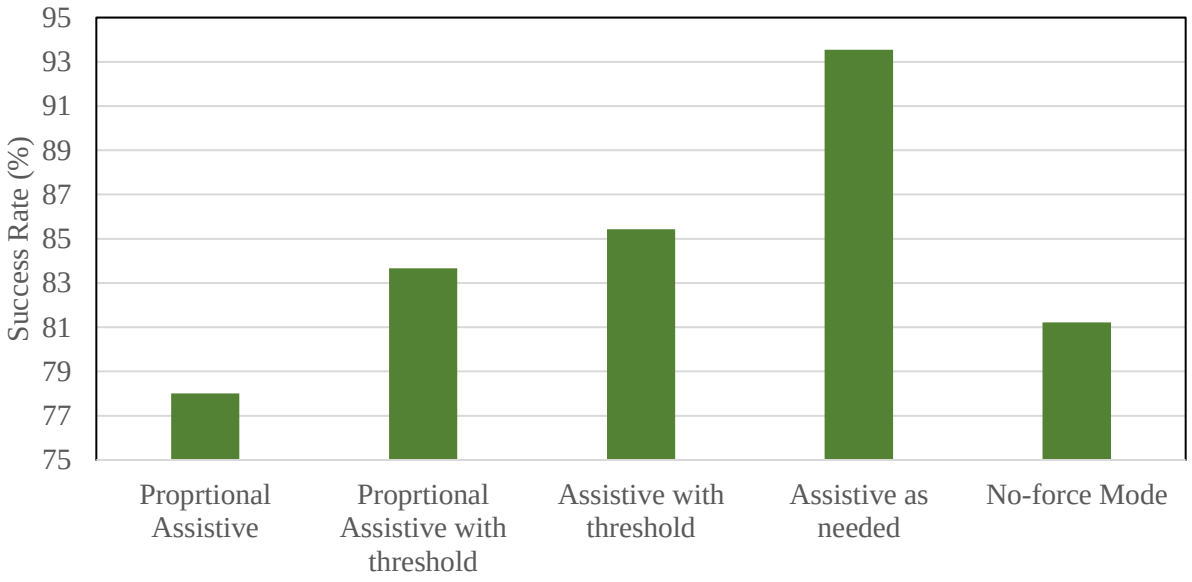

Figure 73: Average success rate in assistive modes – joint 2 – wrist extension.

The subsequent mode, which boasts an even higher success rate, is the assistive with threshold mode. This mode is akin to the previous one, with the key distinction being that the force is proportional to the difference between the position difference and the threshold, rather than the position difference itself. This resulted in a smaller force and further reduction in overshoot.

In the assistive as needed mode, the algorithm has been employed that allows the user to play the game independently. It intervenes only when the paddle is not moving towards the target i.e. either moving in the opposite direction or remaining stationary. The system assists the user in moving the paddle towards the target, ceasing assistance as soon as it starts moving in the correct direction. Normal subjects found this mode to be the most straightforward, as it eliminates the need for assistance in moving their forearm and wrist.

It is noteworthy that the proportional assistive with threshold, assistive with threshold, and assistive-as-needed modes exhibit higher success rates compared to the passive mode.

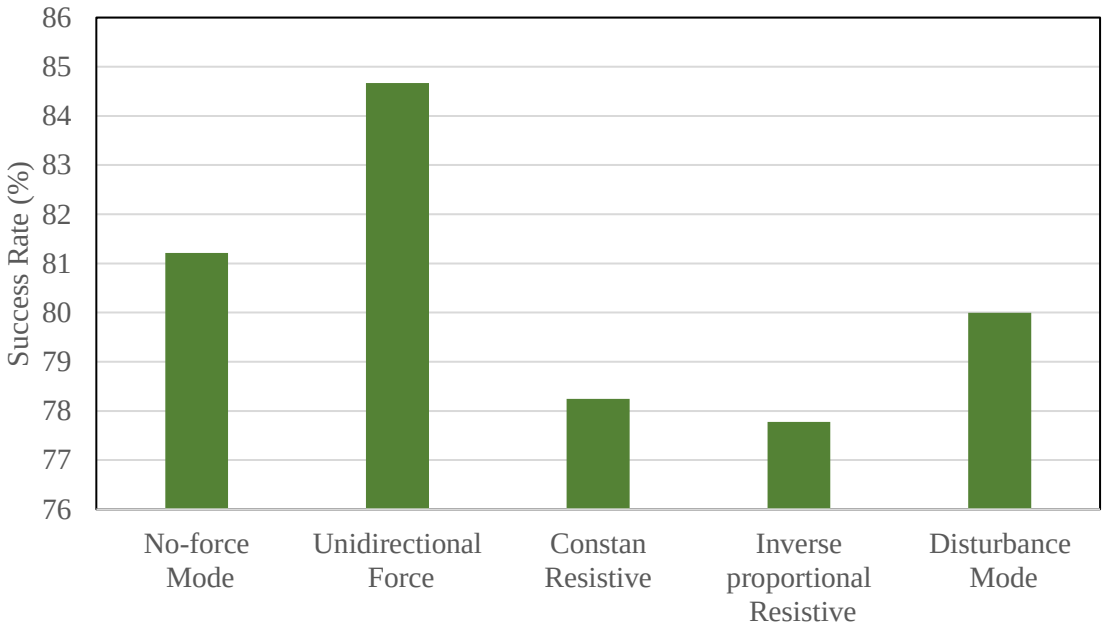

Figure 74: Average success rate in resistive modes – joint 2 – wrist extension.

Figure 74 illustrates the average success rate of all subjects in different resistive modes for wrist extension. Notably, the inverse proportional resistive mode exhibits the lowest success rate, signifying that subjects found this mode to be the most challenging. In this mode, the resistive force increased as the user moved the paddle towards the target, making it difficult for them to overcome the substantial force. Moreover, when the paddle is in close proximity to the target, the resistive force provided by the actuator suddenly becomes zero while the user continues to push the handle, resulting in overshooting and causing occasional misses of the target ball.

An intriguing observation in the Figure 74 is that unidirectional force positively influenced average performance. This is attributed to the assistance provided in one direction and resistance in the opposite direction. The predictability of the force aids users in performing better, particularly when moving in the opposing direction at a slower pace, enhancing their overall control. The same pattern of results can be observed in Figure 75 and Figure 76 for absolute error.

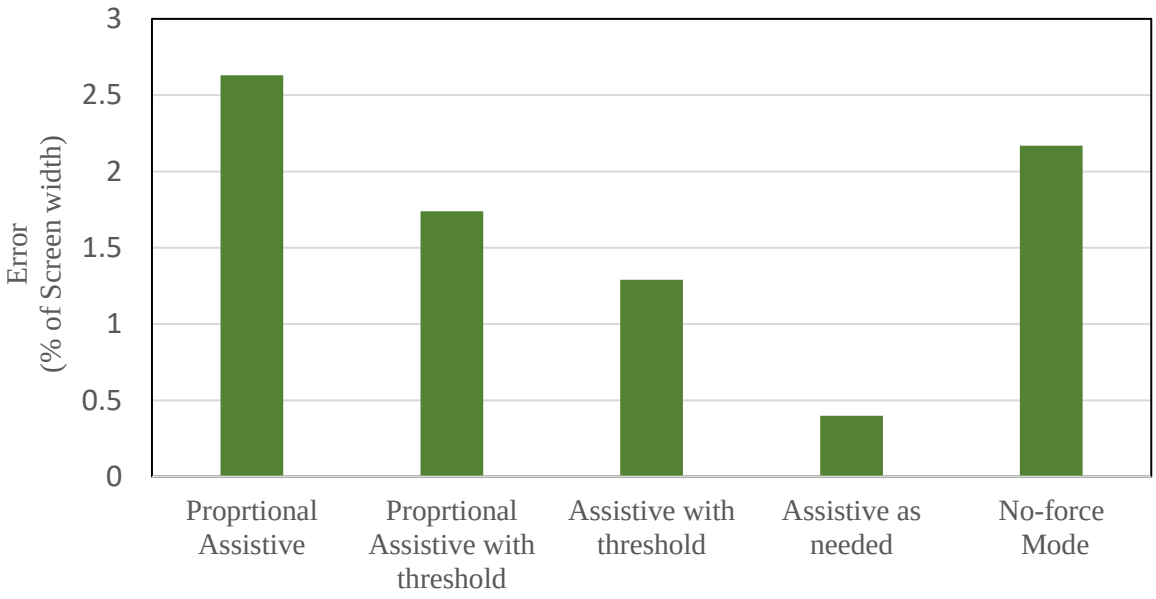

Figure 75: Average absolute error in assistive modes – joint 2 – wrist extension.

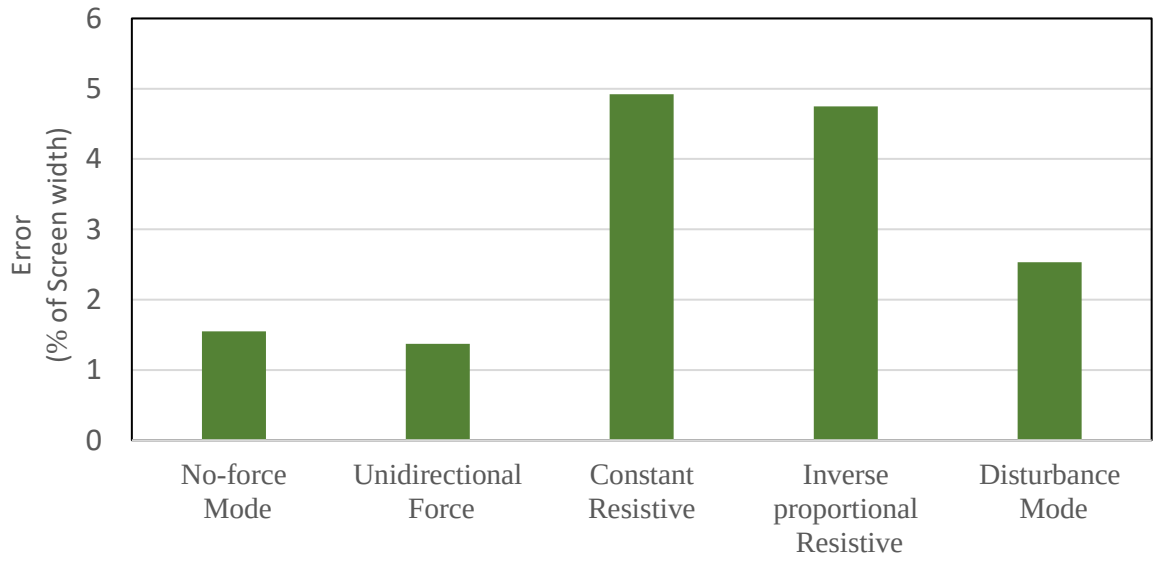

Figure 76: Average absolute error in resistive modes – joint 2 – wrist flexion.

Figures 73 to 76 depict success rate and the average absolute error when the target ball disappears in assistive and resistive modes, for joint 3 respectively.

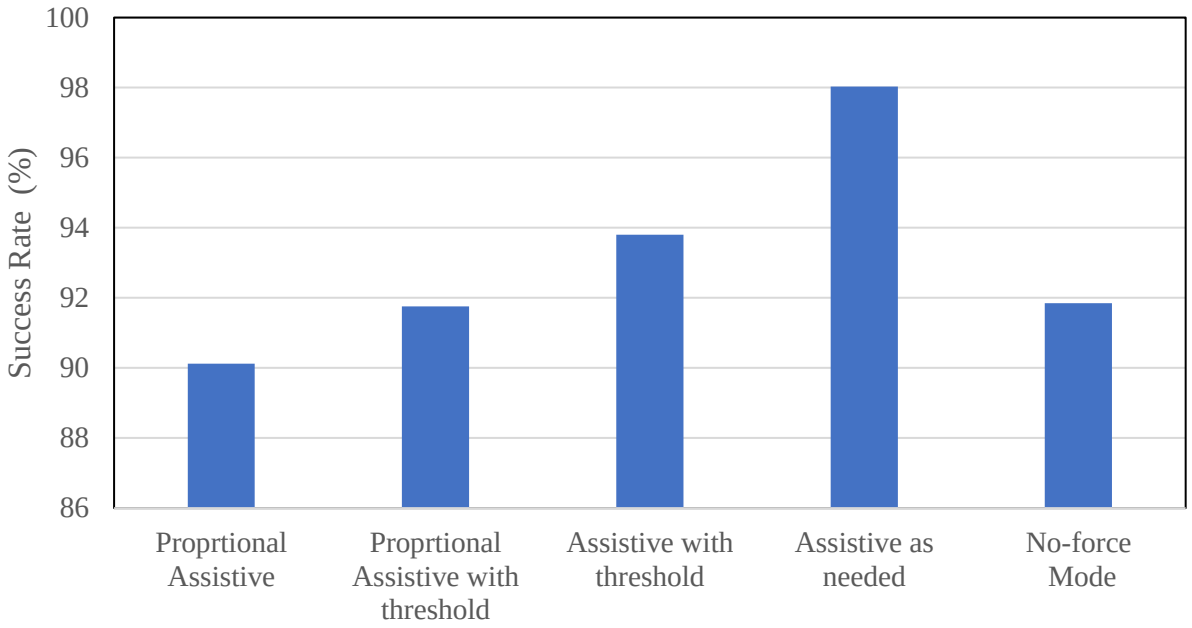

Figure 77: Average success rate in assistive modes – joint 3 – radial deviation.

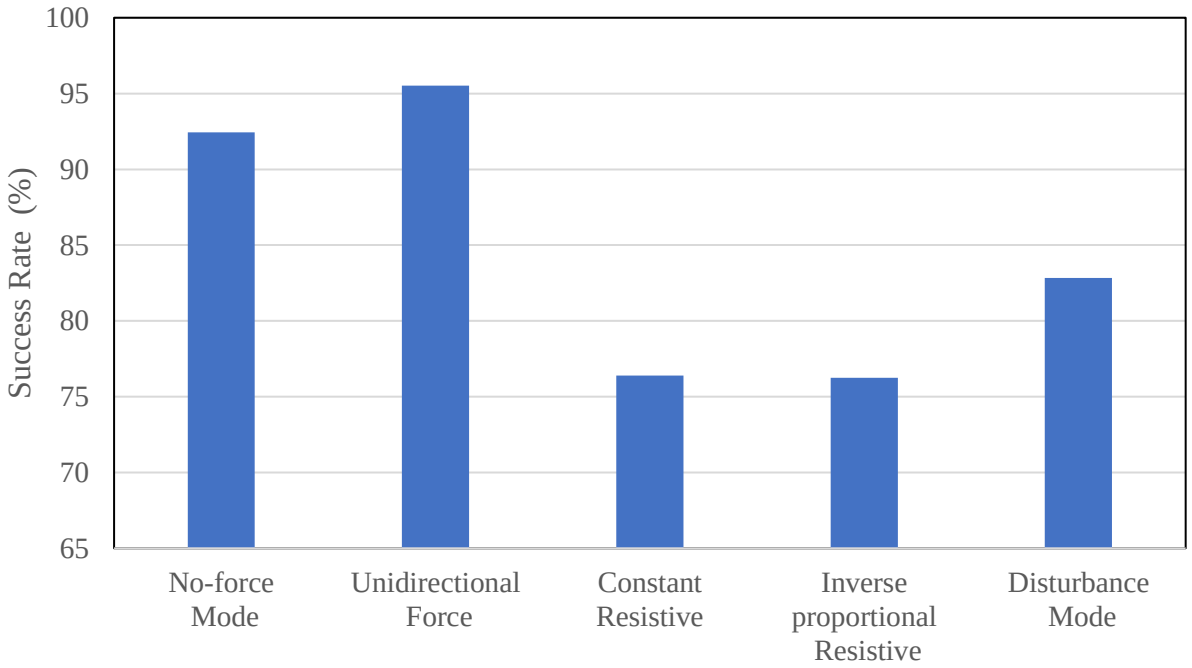

Figure 78: Average success rate in resistive modes – joint 3 – ulnar deviation.

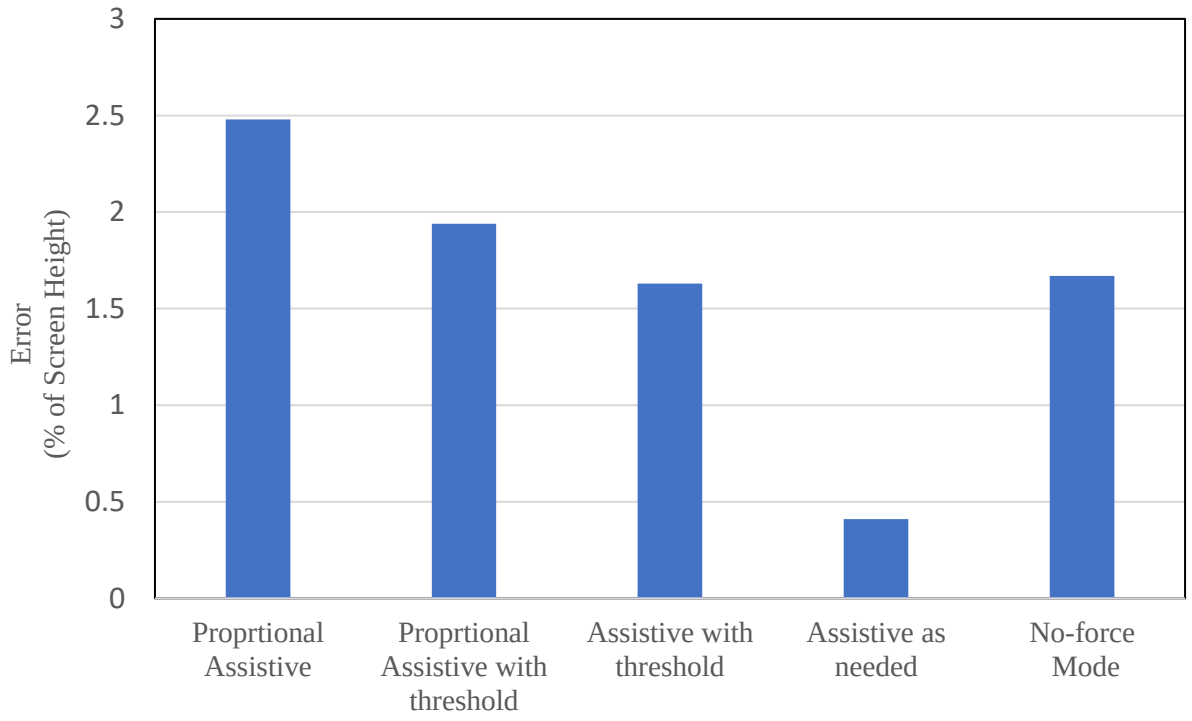

Figure 79: Average absolute error in assistive modes – joint 3 – radial deviation.

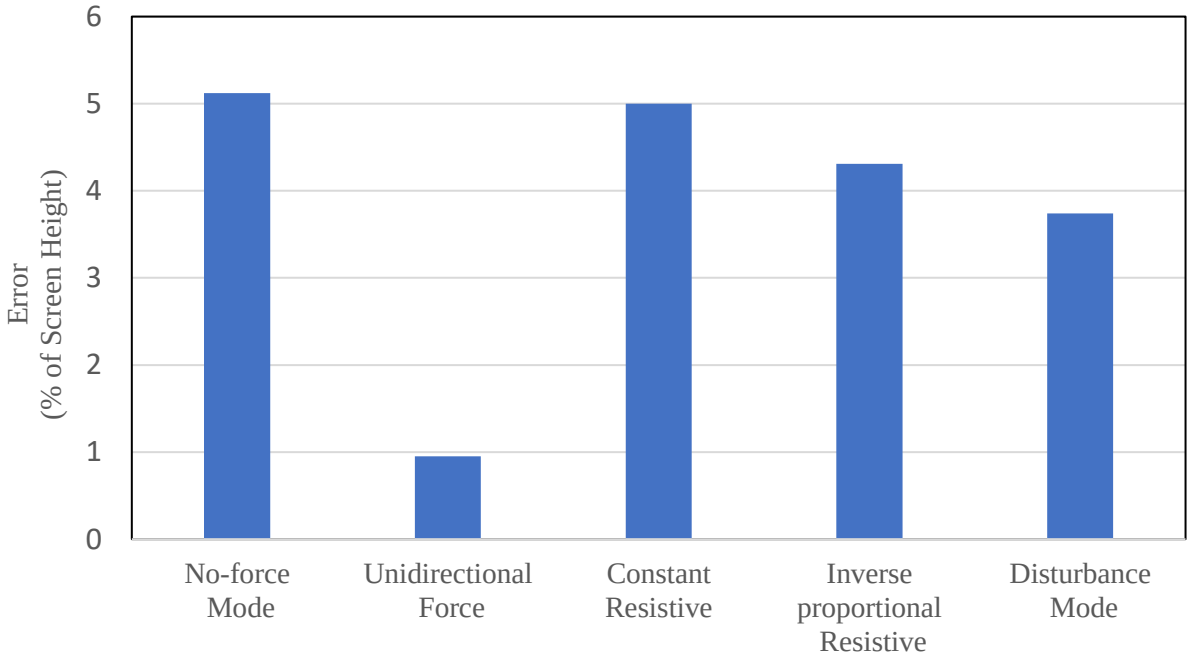

Figure 80: Average absolute error in resistive modes – joint 3 – ulnar deviation.

In Figure 79, for the reasons mentioned previously, the average absolute error is the largest in the proportional assistive mode for radial deviation. It is smaller in the proportional assistive with threshold mode, even smaller in the assistive with threshold mode. It is the minimum for the assistive-as-needed mode.

The same pattern in Figure 74 can be seen in Figure 80; the unidirectional force improved the user's performance and resulted in the smallest average absolute error between the resistive modes. The other resistive modes have a significantly larger average absolute error in ulnar deviation.

5.2.3 ANOVA Analysis

The comparison of average values across different groups should be interpreted with caution, as statistical significance is crucial for drawing meaningful conclusions. A naive interpretation might involve looking at these averages and concluding that there are differences between the groups. However, just observing differences in averages does not necessarily mean those differences are statistically significant. Simply observing differences in means does not guarantee the presence of true group effects.

To establish the reliability of these differences, it is advisable to perform an analysis of variance (ANOVA) test, which assesses whether the observed variations are statistically significant or could have occurred by chance. Without such rigorous statistical testing, any observed differences in averages may not carry substantive meaning. In other words, without performing an ANOVA or a similar statistical test, it is not possible to confidently determine whether the observed differences in group averages are meaningful. Differences could simply be due to random variability rather than actual differences in the underlying populations.

Analysis of variance (ANOVA) is a statistical test that compares the means of two or more groups to determine if there are statistically significant differences among them. It helps to quantify whether the observed differences in averages are likely to be reflective of true differences in the populations or if they could have occurred by random chance [49]. A two-way ANOVA test was conducted on the data of all subjects, considering various actuation modes and directions. The aim was to investigate the impact of two key factors: actuation mode and direction of movement, on

the success rate and absolute error of the computer game controlled by a robotic device. The following hypotheses guide the inquiry:

Null Hypotheses (H0):

- There is no significant effect of actuation mode on the success rate of the game.
- There is no significant effect of direction of movement on the success rate of the game.
- There is no interaction effect between actuation mode and direction of movement on the success rate of the game.

Alternative Hypotheses (Ha):

- There is a significant effect of at least one actuation mode on the success rate of the game.
- There is a significant effect of at least one direction of movement on the success rate of the game.
- There is a significant interaction effect between actuation mode and direction of movement on the success rate of the game.

These hypotheses provide a structured framework for exploring and analyzing the potential influence of actuation mode, direction of movement, and their interaction on the success rate of the computer game. The alternative hypotheses open avenues for discovering significant effects, allowing for a deeper understanding of the factors contributing to variations in game performance. Similar hypotheses can be written to investigate the effect of actuation modes and direction of movement on other features including absolute movement error. Table 2 illustrates the ANOVA parameters for success rate of the typical game using joint 3 in different actuation modes as an example.

In the context of a two-way ANOVA table, the term Source refers to the different sources of variation in the dataset. It includes the factors being analyzed (in this case, Actuation Mode and Movement Direction), their Interaction, the Error, and the Total. Actuation Mode and Movement Direction are independent variables in the study. Interaction refers to the combined effect of the two independent variables (Actuation Mode and Movement Direction) on the dependent variable. It examines whether the effect of one independent variable on the outcome varies by the levels of the other independent variable. Error represents the variability that cannot be explained by the independent variables. Total represents the overall variability in the dependent variable across the

entire dataset. It includes both the variability explained by the independent variables (and their interaction) and the unexplained variability (error).

The Sum of Squares (SS) quantifies the total variation for each source. It measures how much the data points deviate from the mean. The Degrees of Freedom (DF) indicates the number of independent values within a factor, calculated as the number of levels minus one. Mean Square (MS) is the SS divided by its corresponding DF. For Actuation Mode, Movement Direction, and Interaction, it represents the average variance explained by each factor or interaction. For Error, it is the average variance within groups.

The F-value (F) is the ratio of the MS of a source to the MS of the Error. It indicates how much the variance among the group means exceeds the variance within the groups, providing a basis for testing the null hypothesis. The P-value assesses the probability of observing an F-value as extreme as, or more extreme than, the one calculated if the null hypothesis were true. A low P-value (typically < 0.05) suggests that the observed data are unlikely under the null hypothesis, leading to its rejection.

Table 2: Two-way ANOVA test parameters for success rate in assistive modes – joint 2 – wrist flexion/extension

Source	SS	DF	MS	F	P-value
Actuation Mode	4.0585e+03	4	1.0146e+03	3.6082	0.0089
Movement Direction	661.1121	1	661.1121	2.3510	0.1287
Interaction	527.9396	4	131.9849	0.4694	0.7581
Error	2.5308e+04	90	281.2042	-	-
Total	3.0556e+04	99	-	-	-

In Table 2, the last column, referred to as the p-value, indicates a value of 0.0089 for the actuation mode. A p-value below 0.05 is commonly used to determine statistical significance. In this case, with this small p-value, there is strong evidence to reject the null hypothesis. The null hypothesis has stated that there is no difference in success rates among different actuation modes. Therefore, the alternative hypothesis is true; there is a significant effect of at least one actuation mode on the success rate of the game.

On the other hand, the large p-value of 0.1287 indicates that the direction of movement (wrist flexion or extension) does not have a significant impact on success rates. Moreover, the lack of significance in the interaction p-value suggests that the combined effect of actuation mode and direction of movement is not significantly influencing the users' performance. This reinforces the notion that the primary driver of success rates is the actuation mode applied.

Two-way ANOVA test has been done on success rate and absolute error dataset for each joint and all assistive or all resistive modes separately. The tables presenting the resulting parameters of the ANOVA tests are shown in the Appendix.

The p-value of less than 0.05 for actuation mode in Tables 8, 10, 12 for assistive modes and Tables 5, 7, 11, 13 and 15 for resistive modes suggest that there is a significant effect of at least one actuation mode on the game performance. The ANOVA test for the assistive mode in pronation/supination, as presented in Table 4, shows a large actuation mode p-value. This result affirms the rather small difference of success rate between proportional assistive and free mode in Figure 71. However, Table 5 with small p-value, shows that there is a significant difference for success rate between resistive mode and passive mode for joint 1, pronation/supination movements. This substantial difference can be observed in Figure 81.

This analogy extends to absolute movement error for joint 1, pronation/supination movements. Tables 6 and 7 show large and small p-values respectively; meaning, the assistive mode made no meaningful difference, but the resistive mode influenced the absolute movement error. Also, Figure 82 illustrates a slightly different absolute movement error between the proportional assistive and free mode and a substantial difference between proportional resistive and free mode. Therefore, for joint 1, pronation/supination movements, the proportional resistive mode greatly influenced the game performance leading to worse results, lower success rate and greater absolute error. While the proportional assistive mode made no meaningful difference.

For the second joint, wrist flexion/extension, Tables 8 and 9 show a small and a large actuation mode p-value respectively. Meaning the assistive modes help the users to make a meaningful difference in success rate, but the resistive modes lead to insignificant difference in success rate. As seen in Figure 73, the assistive as needed actuation mode improved the success rate the most followed by the assistive with threshold as the second most influencing assistive

actuation mode. For resistive modes, the inverse proportional and constant resistive led to the lowest success rate subsequently as seen in Figure 74.

Tables 10 and 11 both represent small p-values for assistive and resistive modes respectively. Proving the actuation modes were effectively influencing the absolute error. Similar to success rate, the assistive as needed mode resulted in lowest absolute error while the largest absolute error was associated with inverse proportional and constant resistive modes according to Figure 75 and Figure 76. Therefore, for joint 2, wrist flexion/extension, assistive as needed and assistive with threshold were the most helpful, while inverse proportional resistive and constant resistive were the most challenging actuation modes.

For the third joint, ulnar/radial deviation movements, Tables 12 and 13 both have small p-values for assistive and resistive modes respectively. Proving the actuation modes were effectively influencing the success rate. As seen in Figure 77, the assistive as needed actuation mode improved the success rate the most. For resistive modes, the inverse proportional and constant resistive led to the lowest success rate subsequently according to Figure 78.

Tables 14 and 15 show a large and a small actuation mode p-value respectively. Meaning at least one resistive mode challenged the users making a meaningful difference in absolute error, but the assistive modes lead to insignificant difference in absolute error. Similar to success rate, the assistive as needed mode resulted in lowest absolute error (see Figure 79) while the largest absolute error was associated with constant and inverse proportional resistive modes (see Figure 80). Therefore, for joint 3, ulnar/radial deviation, assistive as needed has been the most helpful, while inverse proportional resistive and constant resistive were the most challenging actuation modes.

In most tables the rather large p-values for direction indicates that the direction of movement does not have a significant impact on neither success rate nor absolute error. Except for Tables 5 and 7 for pronation/supination and Table 11 for wrist extension/flexion, showing small p-value for direction of movement.

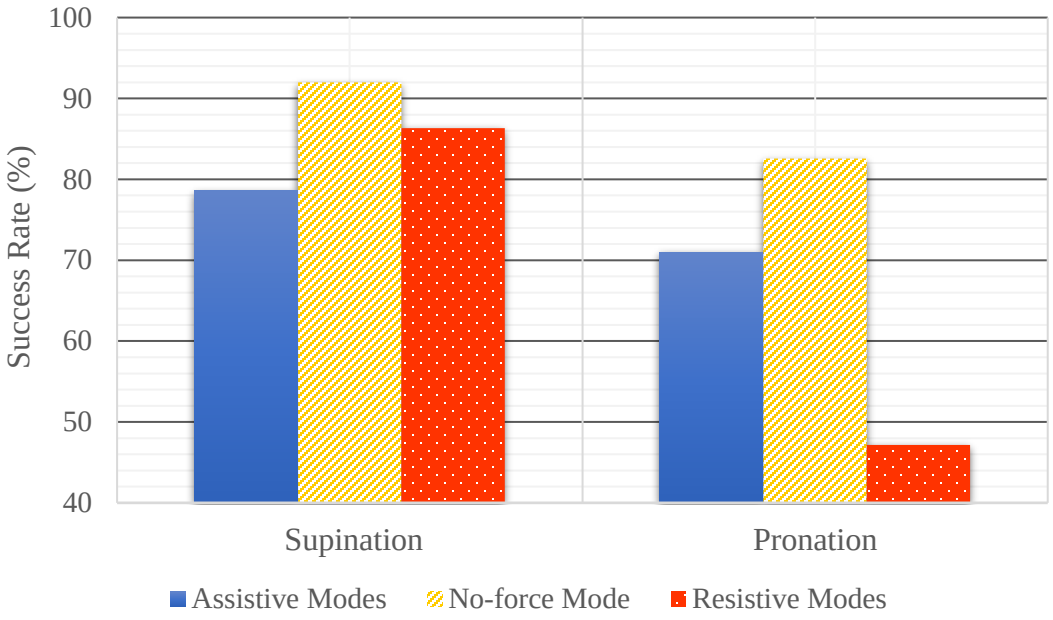

Figure 81: Average success rate – joint 1 – pronation/supination.

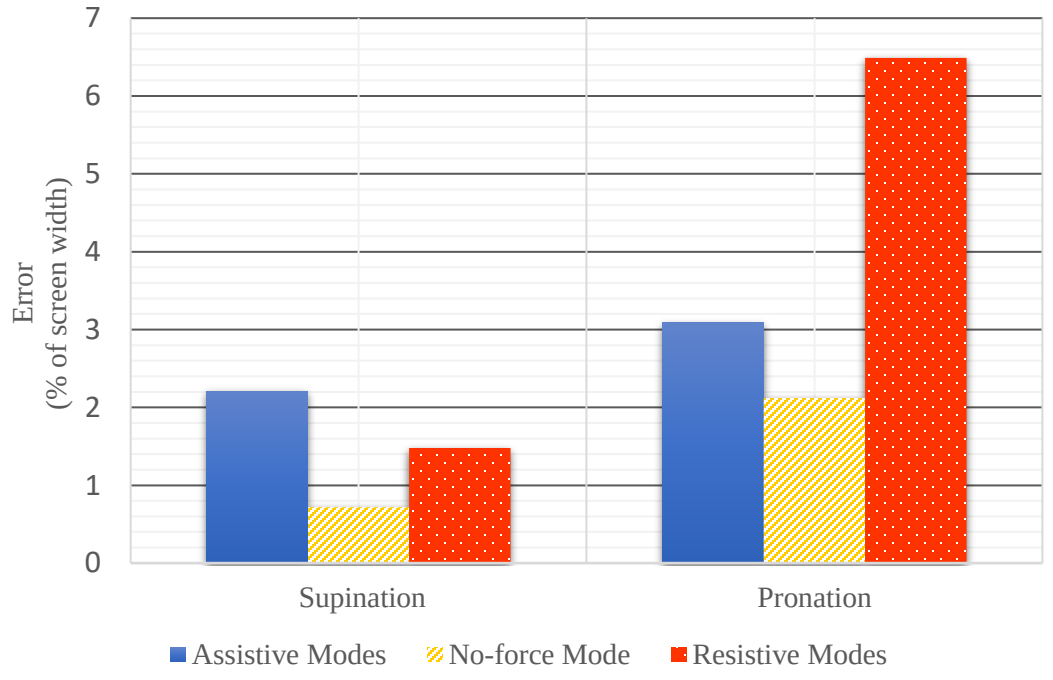

Figure 82: Average absolute error – joint 1 – pronation/supination.

Figure 81 shows the considerable success rate difference in resistive mode between supination and pronation. This almost %40 gap conforms with small p-value for direction of the movement in table 5. Also, Figure 82 illustrates the absolute error has a huge difference between pronation and supination. Therefore, in the resistive mode of joint 1 the subjects performed better at supination compared to pronation.

By observing the resistive modes absolute error in Figure 83, it can be noted that the average absolute error is significantly lager for wrist flexion compared to wrist extension in resistive modes. In this figure actuation codes were used instead of their names to allow all modes to be displayed on a single graph. The corresponding name of each actuation mode is shown in Table 3. Apart from these exceptions, the majority of the ANOVA tables suggest the user performance is not affected by the direction of movement in all three movements.

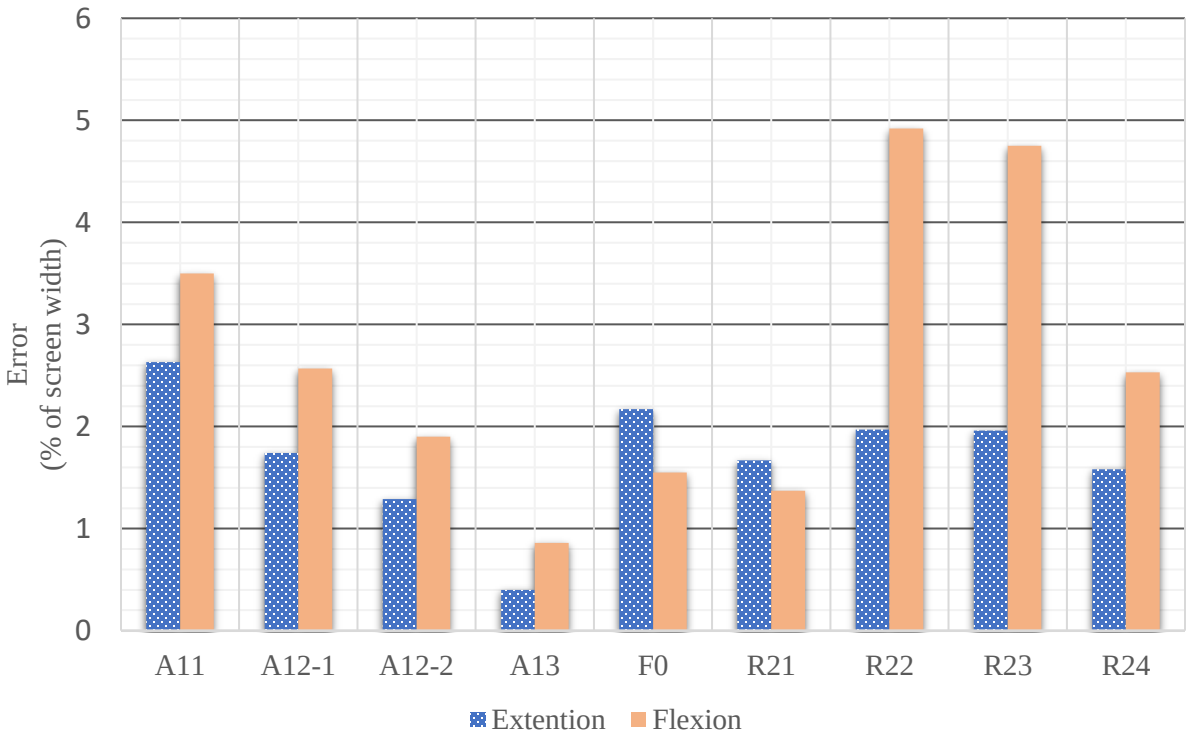

Figure 83: Average absolute error – joint 2 – wrist flexion/extension.

Table 3: Actuation modes names.

Assistive Modes	A11	A12-1	A12-2	A13
	Proportional Assistive	Proportional Assistive with threshold	Assistive with threshold	Assistive as needed
Passive Mode	F0	-	-	-
	Passive Mode	-	-	-
Resistive Modes	R21	R22	R23	R24
	Unidirectional Force	Constant Resistive	Inverse proportional Resistive	Disturbance Mode

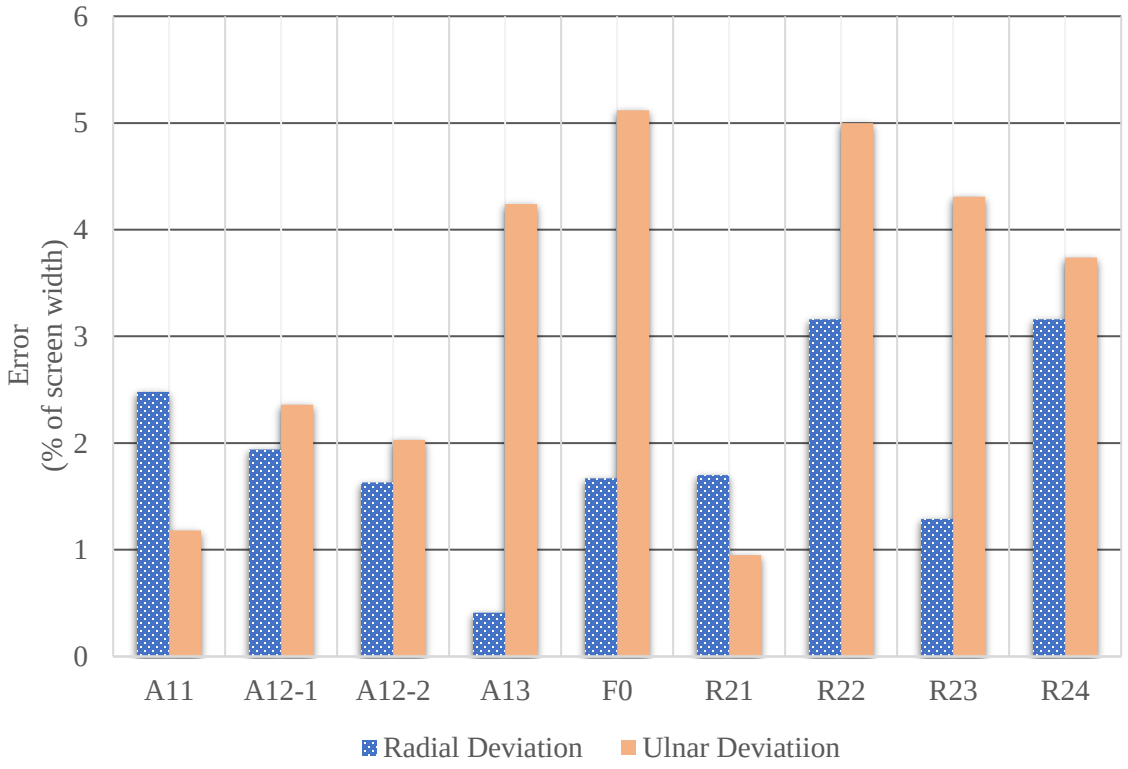

Figure 84: Average absolute error – joint 3 – ulnar/radial deviation.

For most cases the great interaction p-value in tables 4, 5, 6 for pronation/supination, tables 8, 9, 10 for wrist extension/flexion and tables 12, 13 and 15 for ulnar/radial deviation suggest that

there is no combined effect of actuation mode and direction of movement on success rate and absolute error. In other words, actuation mode and direction of movement impact the user's performance independently. The impact of direction of movement also has been rejected for most cases. Therefore, the actuation mode is the only factor influencing the game performance.

Only one of the ANOVA tests for each joint (Tables 7, 11 and 14) show the combined effect of actuation mode and direction of movement because of the small interaction p-value. This exception can be seen in Figure 83 and Figure 84. For a few actuation modes ulnar deviation and wrist flexion had lower error, while for most actuation modes subjects performed better in radial deviation and wrist extension. The other 9 tables had large p-values confirming the null hypothesis. Therefore, in general there is no interaction effect found between the actuation modes and direction of movement on the game performance.

5.3 User Suggestions

During the testing of the prototype device, participants made several comments as possible improvements or adjustments that could be made to improve the performance, usability, or overall usefulness of the developed devices in future implementation into clinical neurological rehabilitative assessments and exercises. Several valuable comments were collected during the evaluation phase, each contributing to the refinement of the system. Some of the noteworthy suggestions included:

- Forearm Support Height: Participants recommended lowering the forearm support height, especially when using the system while seated on a chair.
- Handle Diameter: Users suggested increasing the diameter of the handle to improve the overall comfort of gripping.
- Mouse Sensitivity: Adjusting the mouse sensitivity was proposed to address concerns about users not feeling at ease utilizing the full range of motion in their wrist and forearm during gameplay.
- Inertia Reduction: There was a consensus on the need to reduce the inertia of the mechanism, particularly in the first joint during forearm rotations.

- Applied Force Magnitude: Participants recommended decreasing the magnitude of the applied force, particularly for resistive modes.
- Game Speed and Target Frequency: Users expressed a preference for reducing the speed of the game and the frequency of target appearance. The absence of a time interval between the disappearance of one target and the appearance of a new one was highlighted as a challenging aspect.

  These insights serve as valuable input for further system enhancements and future steps.

5.4 Summary

The robotic rehabilitation device has been tested in conjunction with the RTP game and the associated game interface. Multiple subjects used the device to both verify the usability as well as to uncover any shortcomings.

The study demonstrated that assistive modes generally led to improvements in response and movement times compared to a passive mode, while resistive modes resulted in increased times for both metrics. Specifically, the "assistive as needed" and "assistive with threshold" modes significantly enhanced performance by increasing the success rate and reducing errors. In contrast, the "constant resistive" and "inverse proportional resistive" modes negatively impacted performance, decreasing success rate and increasing error.

To validate these findings, a two-way ANOVA test was applied to the data. This analysis predominantly confirmed the notable effects of the different actuation modes on performance and showed that the direction of movement or the combination of these factors did not significantly affect the game performance of the participants.

User data comments were also recorded and considered for the current and future version of the developed device.

VI. CONCLUSIONS

6.1 Contributions Made in This Thesis

This thesis introduces an advancement in neurological rehabilitation technology through the creation and evaluation of a robotic device compatible with fMRI. This device is specially designed to support the movements of the forearm and wrist, adhering to the strict operational standards required for use in MRI environments. Utilizing 3D printing, pneumatic actuation, and fiber optic sensors, the design successfully navigates the constraints posed by MRI's strong magnetic field.

The motion and force analysis, carried out using MATLAB Simulink Simscape Multibody, confirms that the developed device meets crucial specifications for assisting patients effectively, including necessary ranges of motion and torque. Integration with the RTP game, alongside a custom-developed interface, represents an innovative rehabilitation approach, enhancing engagement and adaptability to individual user needs. The device's smart assistive and resistive features based on real-time performance data, offer a personalized rehabilitation experience poised to significantly improve recovery outcomes for neurological rehabilitation patients.

Empirical testing involved ten healthy participants engaging with the RTP game through the manipulandum using different actuation modes, with data collected to assess performance across various assistive and resistive modes. Analysis of the game's performance metrics revealed that, on average, assistive modes led to improvements in user performance. Notably, the “assistive as needed” and “assistive with threshold” modes were the most effective. On the other hand, the resistive modes challenged the users on average with “constant resistive” and “inverse proportional resistive”, identified as the most challenging modes. Two-way ANOVA tests on performance features confirmed the significant effect of these actuation modes on user performance, while movement direction did not significantly influence the outcomes for these healthy participants.

This robotic device represents a significant shift from conventional rehabilitation methods by providing smart assistance (or resistance) leading to tailor rehabilitation activities to the patient's level of impairment and progress. By integrating the RTP game, this approach has the potential to set a new standard in therapeutic strategies. Additionally, this device ensures safety

and functionality in the MRI room, paving the way for brain scanning during neurological rehabilitation.

6.2 Future Work

Over the course of this project, issues and shortcomings of the design were identified. While many of these were dealt with, potential future additions, improvements and objectives include:

- Add a user-friendly method such as an LCD display and a button to the device to facilitate the adjustment of the control parameters. This includes modifying control modes, adjusting force magnitude and thresholds, selecting the active joint, and fine-tuning mouse sensitivity within the game interface.
- Enhance communication between the RTP game and the game interface by extending the transmitted information beyond just the position difference. This includes details of the game level and settings in the data sent to the wrist manipulandum's controller for dynamic adjustments of control parameters in real-time.
- Use heuristic approaches to dynamically adapt game settings and control parameters in response to user performance, enhancing the personalized gaming experience.
- Determine the threshold used in control algorithms based on key performance indicators such as player success rates, game session duration, and feedback loops from test sessions.
- Strengthen the device's reliability to accommodate individuals with injuries, broadening its applicability.
- Incorporate insights from user feedback obtained during device testing to ensure optimal user comfort and satisfaction.
- Develop more entertaining games while maintaining a high standard of features for thorough data analysis and interaction with the device.

REFERENCES

[1] S. S. Virani, A. Alonso, E. J. Benjamin, M. S. Bittencourt, C. W. Callaway, A. P. Carson, A. M. Chamberlain, A. R. Chang, S. Cheng, F. N. Delling, L. Djousse, M. S. Elkind, J. F. Ferguson, M. Fornage, S. S. Khan, B. M. Kissela, K. L. Knutson, T. W. Kwan, D. T. Lackland, T. T. Lewis, J. H. Lichtman, C. T. Longenecker, C. W. Tsao, L. B. VanWagner, D. L. Tirschwell, A. Stokes, N. L. Spartano, C. M. Shay, S. H. Shah, E. B. Schroeder, G. M. Satou, U. K. Sampson, G. A. Roth, W. D. Rosamond, A. M. Perak, M. E. Mussolino, A. E. Moran, K. Matsushita, S. S. Martin, P. L. Lutsey and M. S. Loop, "Heart Disease and Stroke Statistics—2020 Update: A Report From the American Heart Association," The American College of Cardiology Foundation and the American Heart Association, Inc, Circulation, New York, 2020.

[2] S. James, J. Ziviani, R. S. Ware and R. N. Boyd, "Relationships between activities of daily living, upper limb function, and visual perception in children and adolescents with unilateral cerebral palsy," *Developmental Medicine & Child Neurology,* vol. 57, no. 9, pp. 852-857, 2015.

[3] H. T. Hendricks, J. V. Limbeek, A. C. Geurts and M. J. Zwarts, "Motor Recovery After Stroke: A Systematic Review of the Literature," *Physical Medicine and Rehabilitation,* vol. 83, no. 11, pp. 1629-1637, 2002.

[4] K. B. Lee, S. H. Lim, K. H. Kim, K. J. Kim, Y. R. Kim, W. N. Chang, J. W. Yeom, Y. D. Kim and B. Y. Hwang, "Six-month functional recovery of stroke patients: a multi-time-point study," *International Journal of Rehabilitation Research,* vol. 38, no. 2, p. 173–180, 2015.

[5] J. Biernaskie and D. Corbett, "Enriched Rehabilitative Training Promotes Improved Forelimb Motor Function and Enhanced Dendritic Growth after Focal Ischemic Injury," *The Journal of Neuroscience,* vol. 21, no. 14, p. 5272–5280, 2001.

[6] B. n. Johansson, "Brain plasticity and stroke rehabilitation : The Willis lecture," *Stroke* , vol. 31, no. 1, pp. 223-230, 2000.

[7] J. W. Krakauer, S. T. Carmichael, D. Corbett and G. F. Wittenberg, "Getting Neurorehabilitation Right: What Can Be Learned From Animal Models?," *Neurorehabilitation and neural repair,* vol. 26, no. 8, pp. 923-931, 2012.

[8] K. Klingels, H. Feys, G. Molenaers, G. Verbeke, S. V. Daele, J. Hoskens, K. Desloovere and P. D. Cock, "Randomized Trial of Modified Constraint-Induced Movement Therapy With and Without an Intensive Therapy Program in Children With Unilateral Cerebral Palsy," *Neurorehabilitation and Neural Repair,* vol. 27, no. 9, pp. 799-807, 2013.

[9] M. U. Farooq and S. Y. Ko, "A Decade of MRI Compatible Robots: Systematic Review," *IEEE Transactions on Robotics,* vol. 39, no. 2, pp. 862 - 884, 2022.

[10] Digital Rehab Research Inc., *Neuro-Function Evaluation Software,* Winnipeg: Digital Rehab Research Inc., 2017.

[11] Y. M. Senturk and V. Patoglu, "Design and control of an MRI compatible series elastic actuator," in *International Conference on Robotics and Biomimetics (ROBIO)*, Qingdao, China, 2016.

[12] Subcommittee F04.15 on Material Test Methods, ASTM F2503-23e1: Standard Practice for Marking Medical Devices and Other Items for Safety in the Magnetic Resonance Environment, vol. 13.02, West Conshohocken: ASTM, 2023.

[13] V. Groenhuis, F. Siepel and S. Stramigioli, "Dual-Speed MR Safe Pneumatic Stepper Motors," in *Robotics: Science and Systems*, Pittsburg, US, 2018.

[14] G. S. Fischer, G. Cole and H. Su, "Approaches to creating and controlling motion in MRI," in *nnual International Conference of the IEEE Engineering in Medicine and Biology Society*, Boston, MA, USA, 2011.

[15] R. Gassert, A. Yamamoto, D. Chapuis, L. Dovat, H. Bleuler and E. Burdet, "Actuation methods for applications in mr environments," *Concepts in Magnetic Resonance Part B,* vol. 39B, pp. 191-210, 2006.

[16] D. Stoianovici, A. Patriciu, D. Petrisor, D. Mazilu and L. Kavoussi, "A New Type of Motor: Pneumatic Step Motor," *IEEE/ASME Transactions on Mechatronics,* vol. 12, no. 1, pp. 98-106, 2007.

[17] W. H. Organization, "Rehabilitation," World Health Organization, 26 October 2020. [Online]. Available: https://www.who.int/news-room/fact-sheets/detail/rehabilitation. [Accessed Dec 2023].

[18] J. H. Medicine, "Neurological Rehabilitation," John Hopkins Medicine, 2021. [Online]. Available: https://www.hopkinsmedicine.org/health/treatment-tests-and-therapies/neurological-rehabilitation. [Accessed Dec 2023].

[19] E. Clayton, S. Kinley-Cooper, R. Weber and D. Adkins, "Brain stimulation: Neuromodulation as a potential treatment for motor recovery following traumatic brain injury," *Brain Research,* vol. 1640, no. Part A, pp. 130-138, 2016.

[20] L. Coletta, P. Avesani, L. Zigiotto, M. Venturini, L. Annicchiarico, L. Vavassori, S. Ng, H. Duffau and S. Sarubbo, "Integrating direct electrical brain stimulation with the human connectome," *Brain,* vol. 147, no. 3, pp. 1100-1111, March 2024.

[21] F. Khan, B. Amatya, M. P. Galea, Mary P, R. Gonzenbach and J. Kesselring, "Neurorehabilitation: applied neuroplasticity," *Journal of Neurology,* vol. 264, no. 4, pp. 603-615, 2016.

[22] "Effects of Stroke," Better Health, [Online]. Available: https://www.betterhealth.vic.gov.au/health/conditionsandtreatments/effects-of-stroke. [Accessed 27 Mar 2024].

[23] V. L. Feigin, M. Brainin, B. Norrving, S. Martins, R. L. Sacco, W. Hacke, M. Fisher, J. Pandian and P. Lindsay, "World Stroke Organization (WSO): global stroke fact sheet 2022," *International Journal of Stroke,* vol. 17, no. 1, pp. 18-29, 2022.

[24] S. Bhujel and S. Hasan, "A comparative study of end-effector and exoskeleton type rehabilitation robots in human upper extremity rehabilitation," *Human-Intelligent Systems Integration,* vol. 5, pp. 11-42, 2023.

[25] M.-A. Choukou , S. Mbabaali, J. B. Hani and C. Cooke, "Haptic-Enabled Hand Rehabilitation in Stroke Patients: A Scoping Review," *Applied sciences,* vol. 11, no. 3712, 2021.

[26] S. M. Hatem, G. Saussez, M. Della Faille, V. Prist, X. Zhang, D. Dispa and Y. Bleyenheuft, "Rehabilitation of Motor Function after Stroke: A Multiple Systematic Review Focused on Techniques to Stimulate Upper Extremity Recovery," *Frontiers in human neuroscience,* vol. 10, no. 442, 2016.

[27] R. Ocampo and M. Tavakoli, "Improving User Performance in Haptics-Based Rehabilitation Exercises by Colocation of User's Visual and Motor Axes via a Three-Dimensional Augmented-Reality Display," *IEEE robotics and automation letters,* vol. 4, no. 2, pp. 438-444, 2019.

[28] A. Basteris, S. Contu, T. K. Plunkett, C. W. Kuah and I. J. Konczak, "Robot-Aided Bimanual Assessment of Wrist Proprioception in People with Acute Stroke," in *IEEE International Conference on Biomedical Robotics and Biomechatronics (Biorob)*, Enschede, Netherlands, 2018.

[29] A. C. Alarcón-Aldana, M. Callejas-Cuervo and A. P. L. Bo, "Upper Limb Physical Rehabilitation Using Serious Videogames and Motion Capture Systems: A Systematic Review," *Sensors 2020,* vol. 20, no. 21, p. 5989, 2020.

[30] M. Vieux, "Invictus Fitness," Invictus Fitness, 10 May 2015. [Online]. Available: https://www.crossfitinvictus.com/blog/simple-solutions-for-poor-wrist-mobility/. [Accessed 13 January 2024].

[31] J. A. Martinez, P. Ng, S. Lu, M. S. Campagna and O. Celik, "Design of Wrist Gimbal: A forearm and wrist exoskeleton for stroke rehabilitation," in *IEEE International Conference on Rehabilitation Robotics*, 2013.

[32] E. Pezent, C. G. Rose, A. D. Deshpande and M. K. O'Malley, "Design and Characterization of the OpenWrist: A Robotic Wrist Exoskeleton," in *IEEE International Conference on Rehabilitation Robotics :*, London, UK, 2017.

[33] J. Oblak, I. Cikajlo and Z. Matjačić, "Universal haptic drive: A robot for arm and wrist rehabilitation," in *IEEE transactions on neural systems and rehabilitation engineering*, 2009.

[34] S. J. Spencer, J. Klein, K. Minakata, V. Le, J. E. Bobrow and D. J. Reinkensmeyer, "A low cost parallel robot and trajectory optimization method for wrist and forearm rehabilitation using the Wii," in *2nd IEEE RAS & EMBS International Conference on Biomedical Robotics and Biomechatronics*, Scottsdale, AZ, USA, 2008.

[35] M. A. Ergin and V. Patoglu, "Assiston-se: A self-aligning shoulderelbow," in *IEEE International Conference on Robotics and Automation*, Saint Paul, MN, USA, 2012.

[36] B. Manzella, "Hackmotion," Hackmotion, [Online]. Available: https://hackmotion.com/understanding-wrist-graphs-by-brian-manzella/. [Accessed 20 3 2024].

[37] LiteGait, "TherapyMouse," Litegait, [Online]. Available: https://litegait.com/product/therapy-mouse. [Accessed 14 Mar 2024].

[38] Igus, "Igus Canada," Igus, [Online]. Available: https://www.igus.ca/product/174?artNr=KCLM-05. [Accessed 14 Mar 2024].

[39] Micronor, "Micronor Sensors," Micronor, [Online]. Available: https://micronor.com/product/mr348/. [Accessed 24 Mar 2024].

[40] Airpot, "Airpel," Airpot, [Online]. Available: https://www.airpot.com/product-category/product-lines/pneumatic-actuation/airpel-anti-stiction-air-cylinders/. [Accessed 14 Mar 2024].

[41] SMC, "SMCUSA," SMC, [Online]. Available: https://www.smcusa.com/products/itv00-compact-electro-pneumatic-regulator~72497. [Accessed 18 Mar 2024].

[42] Garosa, "PWM-to-Voltage Module," Garosa, [Online]. Available: https://www.amazon.ca/Voltage-Module-Voltage-Converter-Digital-Analog/dp/B07WZNV1V2/ref=asc_df_B07WZNV1V2/?tag=googleshopc0c-20&linkCode=df0&hvadid=579148679207&hvpos=&hvnetw=g&hvrand=1513242382506281387&hvpone=&hvptwo=&hvqmt=&hvdev=c&hvdvcmdl=&hvlocint=&. [Accessed 18 Mar 2024].

[43] Raspberry Pi, "Raspberry Pi Pico and Pico W," Raspberry Pi , 2024. [Online]. Available: https://www.raspberrypi.com/documentation/microcontrollers/raspberry-pi-pico.html. [Accessed 27 Mar 2024].

[44] J. Soucie, C. Wang, A. Forsyth, S. Funk, M. Denny and K. Roach, "Range of motion measurements: reference values and a database for comparison studies," *Haemophilia,* vol. 17, no. 3, pp. 500-507, 2011.

[45] G. H. Brigstocke, A. Hearnden, C. A. Holt and G. M. Whatling, "The functional range of movement of the human wrist," *Journal of Hand Surgery (European Volume),* vol. 38, no. 5, pp. 554-556, 2013.

[46] R. F. Pitzalis, D. Park, D. G. Caldwell, G. Berselli and J. Ortiz, "State of the Art in Wearable Wrist Exoskeletons Part I: Background Needs and Design Requirements," *Machines,* vol. 11, no. 4, p. 458, 2023.

[47] S. T. Parmar, A. Kanitka, N. Sepehri, S. Bhairannawar and T. Szturm, "Computer Game-Based Telerehabilitation Platform Targeting Manual Dexterity: Exercise Is Fun. “You Are Kidding—Right?”," *Sensors,* vol. 21, no. 17, p. 5766, 2021.

[48] W. Kinsner, Microcontroller, Microprocessor and Microcomputer Interfacing for Real-Time Systems, Winnipeg, MB: OCO Research {ISBN: 978-0-9939347-5-9, eBook}, Sep 2020, p. 973.

[49] R. J. Winter, A Crash Course in Statistics, Thousand Oaks: SAGE Publications, Incorporated, {ISBN: 9781544307046, ebook}, 2017, pp. 47,61-67.

[50] M. Lorenzo, C. Maura, G. Psiche, S. Giulio and M. Pietro, "Performance adaptive training control strategy for recovering wrist movements in stroke patients: a preliminary, feasibility study," *Journal of NeuroEngineering and Rehabilitation*, vol. 6, no. 44, 2009.

Appendix

ANOVA Test Tables

The results of two-way ANOVA test are shown in the following tables for each joint to examine the effect of actuation mode and movement direction on success rate and average absolute error.

Table 4: Two-way ANOVA test parameters for success rate in assistive modes – joint 1 – pronation/supination

Source	SS	DF	MS	F	P-value
Actuation Mode	557.3945	1	557.3945	2.0458	0.1681
Movement Direction	565.2871	1	565.2871	2.0747	0.1652
Interaction	9.2045	1	9.2045	0.0338	0.8560
Error	5.4493e+03	20	272.4642	-	-
Total	6.5812e+03	23	-	-	-

Table 5: Two-way ANOVA test parameters for success rate in resistive modes – joint 1 – pronation/supination

Source	SS	DF	MS	F	P-value
Actuation Mode	1.5625e+03	1	1.5625e+03	6.9075	0.0161
Movement Direction	2.5057e+03	1	2.5057e+03	11.0773	0.0034
Interaction	859.3742	1	859.3742	3.7991	0.0654
Error	4.5240e+03	20	226.2020	-	-
Total	9.4516e+03	23	-	-	-

Table 6: Two-way ANOVA test parameters for absolute error in assistive modes – joint 1 – pronation/supination

Source	SS	DF	MS	F	P-value
Actuation Mode	9.2504e-04	1	9.2504e-04	2.5204	0.1281
Movement Direction	8.0504e-04	1	8.0504e-04	2.1934	0.1542
Interaction	3.5042e-05	1	3.5042e-05	0.0955	0.7605
Error	0.0073	20	3.6703e-04	-	-
Total	0.0091	23	-	-	-

Table 7: Two-way ANOVA test parameters for absolute error in resistive modes – joint 1 – pronation/supination

Source	SS	DF	MS	F	P-value
Actuation Mode	0.0040	1	0.0040	18.6037	3.3827e-04
Movement Direction	0.0061	1	0.0061	28.9175	2.9041e-05
Interaction	0.0019	1	0.0019	9.1497	0.0067
Error	0.0042	20	2.1247e-04	-	-
Total	0.0163	23	-	-	-

Table 8: Two-way ANOVA test parameters for success rate in assistive modes – joint 2 – wrist flexion/extension

Source	SS	DF	MS	F	P-value
Actuation Mode	4.0585e+03	4	1.0146e+03	3.6082	0.0089
Movement Direction	661.1121	1	661.1121	2.3510	0.1287
Interaction	527.9396	4	131.9849	0.4694	0.7581
Error	2.5308e+04	90	281.2042	-	-
Total	3.0556e+04	99	-	-	-

Table 9: Two-way ANOVA test parameters for success rate in resistive modes – joint 2 – wrist flexion/extension

Source	SS	DF	MS	F	P-value
Actuation Mode	3.0161e+06	4	7.5402e+05	1.0051	0.4092
Movement Direction	7.0081e+05	1	7.0081e+05	0.9342	0.3364
Interaction	3.0176e+06	4	7.5440e+05	1.0056	0.4089
Error	6.7516e+07	90	7.5018e+05	-	-
Total	7.4251e+07	99	-	-	-

Table 10: Two-way ANOVA test parameters for absolute error in assistive modes – joint 2 – wrist flexion/extension

Source	SS	DF	MS	F	P-value
Actuation Mode	0.0063	4	0.0016	3.2654	0.0151
Movement Direction	2.0164e-04	1	2.0164e-04	0.4212	0.5180
Interaction	8.0346e-04	4	2.0086e-04	0.4196	0.7941
Error	0.0431	90	4.7874e-04	-	-
Total	0.0503	99	-	-	-

Table 11: Two-way ANOVA test parameters for absolute error in resistive modes – joint 2 – wrist flexion/extension

Source	SS	DF	MS	F	P-value
Actuation Mode	0.0064	4	0.0016	3.1750	0.0173
Movement Direction	0.0033	1	0.0033	6.4487	0.0128
Interaction	0.0056	4	0.0014	2.7675	0.0321
Error	0.0457	90	5.0736e-04	-	-
Total	0.0610	99	-	-	-

Table 12: Two-way ANOVA test parameters for success rate in assistive modes – joint 3 – ulnar/radial deviation

Source	SS	DF	MS	F	P-value
Actuation Mode	2.0074e+03	4	501.8523	4.7501	0.0016
Movement Direction	18.5356	1	18.5356	0.1754	0.6763
Interaction	471.1379	4	117.7845	1.1148	0.3545
Error	9.5086e+03	90	105.6516	-	-
Total	1.2006e+04	99	-	-	-

Table 13: Two-way ANOVA test parameters for success rate in resistive modes – joint 3 – ulnar/radial deviation

Source	SS	DF	MS	F	P-value
Actuation Mode	2.4589e+03	4	614.7362	3.9344	0.0055
Movement Direction	8.7226	1	8.7226	0.0558	0.8138
Interaction	469.2136	4	117.3034	0.7508	0.5601
Error	1.4062e+04	90	156.2478	-	-
Total	1.6999e+04	99	-	-	-

Table 14: Two-way ANOVA test parameters for absolute error in assistive modes – joint 3 – ulnar/radial deviation

Source	SS	DF	MS	F	P-value
Actuation Mode	0.0014	4	3.5036e-04	0.4192	0.7944
Movement Direction	2.0736e-04	1	2.0736e-04	0.2481	0.6196
Interaction	0.0119	4	0.0030	3.5452	0.0098
Error	0.0752	90	8.3573e-04	-	-
Total	0.0887	99	-	-	-

Table 15: Two-way ANOVA test parameters for absolute error in resistive modes – joint 3 – ulnar/radial deviation

Source	SS	DF	MS	F	P-value
Actuation Mode	0.0130	4	0.0032	4.5892	0.0020
Movement Direction	0.0011	1	0.0011	1.5291	0.2195
Interaction	0.0036	4	9.0574e-04	1.2795	0.2840
Error	0.0637	90	7.0790e-04	-	-
Total	0.0814	99	-	-	-